Integrated Microbioreactors for Rapid Screening and Analysis of Bioprocesses

by

ANDREA ZANZOTTO

Bachelor of Engineering, Chemical Engineering
McGill University, 1997

Submitted to the Department of Chemical Engineering
in partial fulfillment of the requirements for the degree of

DOCTOR OF PHILOSOPHY IN CHEMICAL ENGINEERING

at the

MASSACHUSETTS INSTITUTE OF TECHNOLOGY

February 2005

Signature of Author: _____
Department of Chemical Engineering
January 24, 2005

Certified by: _____
Klavs F. Jensen
Lammot du Pont Professor of Chemical Engineering and
Professor of Materials Science and Engineering
Thesis Advisor

Accepted by: _____
Daniel Blankschtein
Professor of Chemical Engineering
Chair, Committee for Graduate Students

Integrated Microbioreactors for Rapid Screening and Analysis of Bioprocesses

by

Andrea Zanzotto

Submitted to the Department of Chemical Engineering on January 24, 2004,
in partial fulfillment of the requirements for the degree of
Doctor of Philosophy in Chemical Engineering

Abstract

This thesis presents the design, fabrication, and characterization of a batch microbioreactor with integrated, automated sensors and aeration through a permeable polymer membrane as a step towards establishing high-throughput bioprocessing platforms. In particular, the thesis demonstrates the feasibility of culturing bacterial cells in microliter volumes and obtaining reproducible results similar to those shown at larger scales. A microbioreactor designed to provide sufficient oxygen to a growing culture is fabricated out of PDMS and glass. Models are developed to understand oxygen transport and consumption as well as the kinetics of growth within the microbioreactor. Sensors are integrated to measure the growth parameters optical density (OD), dissolved oxygen (DO), and pH. Based on these measurements as well as cell morphology and total and viable cell counts, reproducibility is established and comparisons to bench-scale bioreactors are made. It is demonstrated that the behavior of bacteria at the two scales is very similar. It is further demonstrated that off-line analysis of the medium can be carried out by serial sacrifice of microbioreactors operating under identical conditions. The test case of HPLC analysis of the fermentation medium to measure glucose consumption and organic acid production is used. Additional sensing capabilities in the form of *in situ* measurements for luminescence and fluorescence are demonstrated, and a potential glucose sensor is modeled to explore feasibility.

Once reproducibility in fabrication, experimental protocol, and experimental results is established, the microbioreactor is used for several applications. The ability to monitor luminescence and fluorescence on-line enables the use of bacterial reporter strains to characterize the bioreactor environment. The ability to reproducibly sacrifice microbioreactors mid-run is exploited to demonstrate the feasibility of linking microbioreactors to genome-wide expression studies using DNA microarrays. The potential of the microbioreactor for investigating different growth conditions is confirmed by comparing bacterial growth, as evaluated by the measured parameters, under conditions of different medium and oxygen concentration. It is shown that statistical differences can be observed, and that these differences are similar to those observed at a larger scale.

The demonstrated functionality of the microbioreactor could potentially have a large impact in the numerous fields in which fermentations are used. In bioprocess development, the batch microbioreactor could be used to select strains at all stages of metabolic engineering and to explore and optimize growth conditions during scale-up. The microbioreactor could also be an effective tool in screening applications ranging from toxicology studies that use bacterial reporter strains, to studies that attempt to elucidate metabolic pathways, to intensification of genome-

wide expression profiling using either direct links to DNA microarrays or screens of libraries carrying transcription reporters.

Thesis Supervisor: Klavs F. Jensen
Title: Lammot du Pont Professor of Chemical Engineering and Professor of Materials and Engineering

Acknowledgements

First and foremost, I would like to extend my gratitude to my thesis advisor, Klavs Jensen. This thesis would never have come together without his continuous guidance and support from the earliest days of the "microfermentor" project. I would also like to thank the members of my thesis committee – Professors Charles Cooney, Martin Schmidt, and Anthony Sinskey – whose input and guidance, both technically and professionally, have been invaluable. In particular, Prof. Sinskey's many helpful suggestions and generously-offered insights have done much to shape this thesis.

Many people have contributed to the work in this thesis, and I extend my thanks to all. Nicolas Szita, in particular, has been both a mentor and a friend. We have worked closely these past years, and he has taught me a tremendous amount about everything from the proper ergonomics of office furniture to the finer points of academic writing. Paolo Boccazzi has also provided advice and support in many different areas, especially with his significant contribution to the microarray work. His expertise in all things bio has been invaluable. Other past and present members of the DMA team that deserve special mention are Nathalie Gorret, who guided my early forays into the world of plate streaking and cell counting; Philip Lessard, whose extensive knowledge of microbiology is surpassed only by his patience with explaining it to the uninitiated; Harry Lee, whose ready counsel on optical sensing and generous lending of equipment have been an indispensable help; and Ben Zhang, to whom I throw the torch - be his to hold it high. Thanks also go to Rebecca Jackman, who helped me get started in the lab and cleanroom, and to Hang Lu, who continually provided much-needed advice and guidance.

The UROPs that have worked on this project deserve mention: Vincent Chen for his help with automation, Daniel Mun for his work on the HPLC experiments, and Yelena Gorlin for her contribution to the glucose modeling work. All three also ran their fair share of fermentations and became well-acquainted with the properties of PDMS.

I would like to thank the Dupont-MIT Alliance for the funding that has made this project possible. I would also like to acknowledge the input that the DuPont team has provided through many stimulating discussions. In particular, I thank Tina Van Dyk for her collaboration on the luminescence sensing work.

I also feel a deep appreciation for the friends that have made my grad school experience so unforgettable: Chelsey, my cubicle buddy, for her staunch support in all areas of life and for having her feet firmly on the ground; Melissa for the insights shared during a myriad activities and for always being up for anything; Nuria for the many conversations about the past, present, and future; Thomas for always lending a sympathetic ear and for supporting initiatives to improve the office dress code; Axel for his quick wit and unique outlook; Jamil for his quick wit and equally-unique outlook; Sameer for the steady flow of Onion articles; and Tamara for the late-night office breaks.

Finally, I would like to thank my family for their love and support, and John for everything.

Table of Contents

List of Figures

List of Tables

Chapter 1. Introduction

1.1. Background and Motivation

1.1.1. Microbial fermentation

The term 'fermentation' as applied to microbial processes at one time referred to microbial growth in the absence of oxygen. More recently it has been expanded to include any microbial process during which cells are maintaining viability. The term 'bioreaction' can be applied interchangeably. For the purpose of this work we will therefore define a microbial fermentation or bioreaction as a process whereby bacteria are cultured in a suitable medium and utilize substrate within the medium to grow and metabolize. Along the way they produce measurable products that are either (1) useful in and of themselves, (2) indicative of a response to the cellular environment (thus enabling the cell to act as a sensor), or (3) indicative of some aspect of cellular function under investigation, thus providing clues to the inner workings of the cell.

1.1.1.1. Cells as producers of useful products

Microbial fermentations are important sources of biological products used in the pharmaceutical, food, and chemical industries.[1,2] These products include primary and secondary metabolites, enzymes, recombinant proteins,[3,4] vaccines, and the cells themselves (e.g. yeast). A characteristic common to a majority of commercial fermentation processes has been an attempt to increase the production of industrial products through improvement of microbial strains.[5,6] In addition to the classical method of incremental improvement through sequential strain selection, several methods of mutagenesis are now commonly used to introduce changes to the DNA sequence. Mutation, which uses chemical or physical agents to alter the microbial DNA, is a

random method that results in slow, incremental changes. Genetic recombination and genetic engineering are both used to make more substantial changes to the bacterial genome in a single generation, the first of these methods being random and the second targeted. These techniques are frequently used in combination with each other to reach the desired goal. Currently, improved strains are selected using an iterative cycle of three basic principles: mutation, screening, and assay. Strain improvement relies on knowledge of microbial physiology as well as pathway regulation and control. Strain improvement also requires familiarity with the fermentation process for each bacterial strain, and the ability to optimize the fermentation conditions.

1.1.1.2. Cells as sensors

Light emission from luminescent and fluorescent bacteria (and more recently, yeast) created to act as reporters for various environmental conditions is finding application in several areas of biology, including toxicity assays for environmental pollutants, chemical detection, and gene expression profiling.[7-12]

For example, for nonspecific environmental reporting the *lux*[13-16] or *gfp*[17-20] cassette is fused to a stress response promoter that responds to a number of environmental and chemical stresses. For instance, the heat shock response is activated whenever environmental conditions cause changes in protein structure, and the SOS regulatory circuit is activated in response to DNA damage.

1.1.1.3. Cells as sources of biological information

Small-scale fermentations are used to identify and screen biocatalysts,[21] design new pathways,[22] and identify a variety of unique biological organisms from various sources.

Additionally, fermentation and cell culture can play a critical role in the elucidation of gene function in other organisms. The most common method involves the cloning and expression of a genome in a suitable host, such as *E. coli* or yeast, followed by fermentation in a bioreactor. The fermentation allows the identification of conditions that regulate gene expression, as well as production optimization of the protein that is then expressed. In particular, the recent completion of the human genome sequence provides an especially labor-intensive challenge in this area.[23]

1.1.2. Methods of obtaining information

The type and amount of information required in each of the above-mentioned areas can approximately be separated into two broad categories: screening and scale-up. In screening processes, a limited amount of information about a large number of experimental conditions is generally required. During scale-up, operating conditions are optimized and a large amount of information about a small number of experimental conditions is required. In both cases, it is desirable to obtain fast and accurate analytical information that can be used to evaluate rapidly the interactions between biological systems and bioprocess operations.

1.1.2.1. Screening

Screening operations are typically carried out in shake flasks, test tubes, Petri dishes, or microtiter plates. During the screening phase, only limited control of environmental parameters is possible and endpoint data are generally obtained to gauge the performance of cells. Efforts have been made to overcome this limitation. In microtiter plates, on-line measurements of dissolved oxygen[24,25] or pH[26] during fermentation have been demonstrated. On-line measurements of dissolved oxygen[27-30] and pH[31] in shake flasks during fermentation have also been reported. However, these screening approaches have the fundamental limitation that the

effort involved largely continues to scale with the number of individual cultures involved, meaning that experiments with more cultures become more demanding both technically and mechanically. This is exacerbated by the difficulty of integrating culture steps that precede and follow the fermentation itself.

1.1.2.2. Scale-up

Scale-up refers to the process of increasing the volume in which a bioreaction takes place. The objective is to increase the scale of the bioprocess without sacrificing the yield obtained at a smaller scale. Often this proves difficult due to the engineering limitations that occur as the size of the bioreactor increases. For example, mixing increasingly deviates from 'ideal', and problems with adequate aeration and environment homogeneity become more pronounced. As a result, during the process of scaling-up a particular bacterial strain to fermentation in industrial-sized bioreactors (100-300,000 ℓ), it is necessary to consider any environmental changes that the new strain will encounter in the larger reactor.

The method of scale-up to larger-volume fermentations has historically been centered on an attempt to maintain the same physical environment for the growing cells. Scale-up is typically based on maintaining one or more of the following: equal shear stress through a constant impeller tip speed, constant agitation power per unit volume of fermentation medium, constant mixing time, or constant rate of oxygen mass transfer through the maintenance of a constant k_La value.[5]

Efforts towards process scale-up are currently limited by the time, expense, and labor-intensiveness of the required experiments. Thus, only a limited number of operating conditions can be investigated, with the result that true optimization is frequently not possible because of limited probing of the experimental space.

1.2. Types of Bioreactors

Bioreactors can be classified into one of three general modes of operation: batch or fed-batch, semi-continuous (also called semi-batch), and continuous. Batch culture is characterized by the introduction of cells and medium at the beginning of the batch cycle and the removal of product at the end. In fed-batch culture, nutrients are added either continuously or periodically throughout the batch cycle. During semi-continuous operation, a bioreactor is inoculated with cells that are then allowed to grow for a period of time, often until the culture is approaching early stationary phase. A large fraction of the cell culture broth is then harvested and the bioreactor is replenished with fresh medium, at which point the cycle is repeated. Continuous culture is characterized by the continuous addition and removal of medium. In a chemostat, cells are continuously removed and a steady-state is maintained inside the bioreactor, while in a perfusion culture the cells are retained within the reactor while a cell-free sidestream is removed.[32]

1.3. Microfabrication Technology

As seen from the discussion of screening and scale-up in previous sections, a need exists for a bioprocessing platform that would allow high-throughput, parallel, automated processing of a variety of bacterial strains under a variety of controlled conditions, with integrated sensors yielding real-time data on process parameters. Microfabrication provides the tools needed to reach this objective.

Microfabrication techniques that allow parallel processing were initially developed for the electronics industry to enable the rapid manufacturing of large numbers of identical devices. Over the last three decades these fabrication techniques have been applied to the fabrication of

microelectromechanical systems (MEMS). With feature sizes on the order of microns, the first demonstrations of MEMS were fabricated in silicon and used as sensors and actuators (e.g. airbag accelerometers).[33,34] The field has since grown to include a wide range of materials and microfabrication methods and has been extended to chemistry and biology,[35,36] where microfabrication is used to fabricate microchemical reaction systems[37] and chemical analysis devices called micro-total-analysis-systems (μTAS).[38]

The suite of materials that is used in the fabrication of microdevices has grown to encompass glass, plastics, and ceramics in addition to silicon. Techniques have been developed that provide a way to transfer patterns into these unconventional materials, onto nonplanar surfaces, and into three-dimensional structures.[39,40] These techniques are collectively described as soft lithograpic techniques and they use poly(dimethylsiloxane) (PDMS), a deformable and moldable elastomer, as a stamp, mold, or substrate. A rapid-prototyping technique has also been developed that uses high-resolution transparencies as masks for photolithography to significantly reduce the fabrication time of new devices.[41-43]

1.4. Microbioreactor Requirements

Bench-scale bioreactors are generally 0.5-5 ℓ in volume. They are typically equipped with temperature and pH controllers, as well as a dissolved oxygen sensor. Most other measurements are made off-line, including the determination of optical density, cell number, dry weight, and concentration of chemicals of interest (both substrates and products). Attempts are being made to integrate on-line measurements of some of these attributes, particularly at the production scale where contamination is frequently a concern (especially during continuous culture).[44-46] The oxygenation of laboratory bioreactors is generally accomplished by sparging, and agitation is

achieved with the use of an impeller.

A microbioreactor appropriate for high-throughput applications will ideally retain the functionality of larger bioreactors in a miniaturized form, while allowing the integration of additional sensors and the automation of the fermentation process. The following criteria will therefore need to be met: biocompatibility of the chosen material, adequate aeration, temperature control, sensing of biomass, sensing of dissolved oxygen, and sensing of pH.[44,47] In addition, it is desirable to have added sensing capabilities in the form of *in situ* glucose sensing, as well as the sensing of small light intensities such as may be produced by luminescent or fluorescent bacterial cultures. Finally, it is desirable that the medium can be removed from the microbioreactor for off-line analysis during a fermentation run. This is necessary for linking the microbioreactor to existing technology such as microarrays or instruments used for analysis.

1.4.1. Material biocompatibility

The primary requirement of any material used for bioprocess applications is that the material be biocompatible. There are two main considerations for defining the biocompatibility of a particular material: surface properties that affect cell adherence and cytotoxicity. PDMS has been used extensively in medical implants and biomedical devices because of its low toxicity.[48-51] The relatively short time that batch experiments with quickly-growing bacterial strains typically last (<12 hours) allows the use of PDMS as a fabrication material. Longer experiments would eventually require surface modifications to prevent the adhesion of cells.

1.4.2. Aeration

Aeration of the cell culture is required to provide oxygen to the cells and to remove produced gases, primarily carbon dioxide. In current industrial cell culture, oxygen demand is generally

met in one of three ways as illustrated in Figure 1-1.

The first method of aeration commonly used is surface aeration, in which mass transfer occurs through the surface of the liquid only. In order to increase the mass transfer, a surface or subsurface impeller can be added. This impeller can act either by increasing the surface area of the medium in contact with the gas, or additionally by entraining bubbles. Uncontrolled entrainment of bubbles into the culture can, however, be detrimental to cell health.

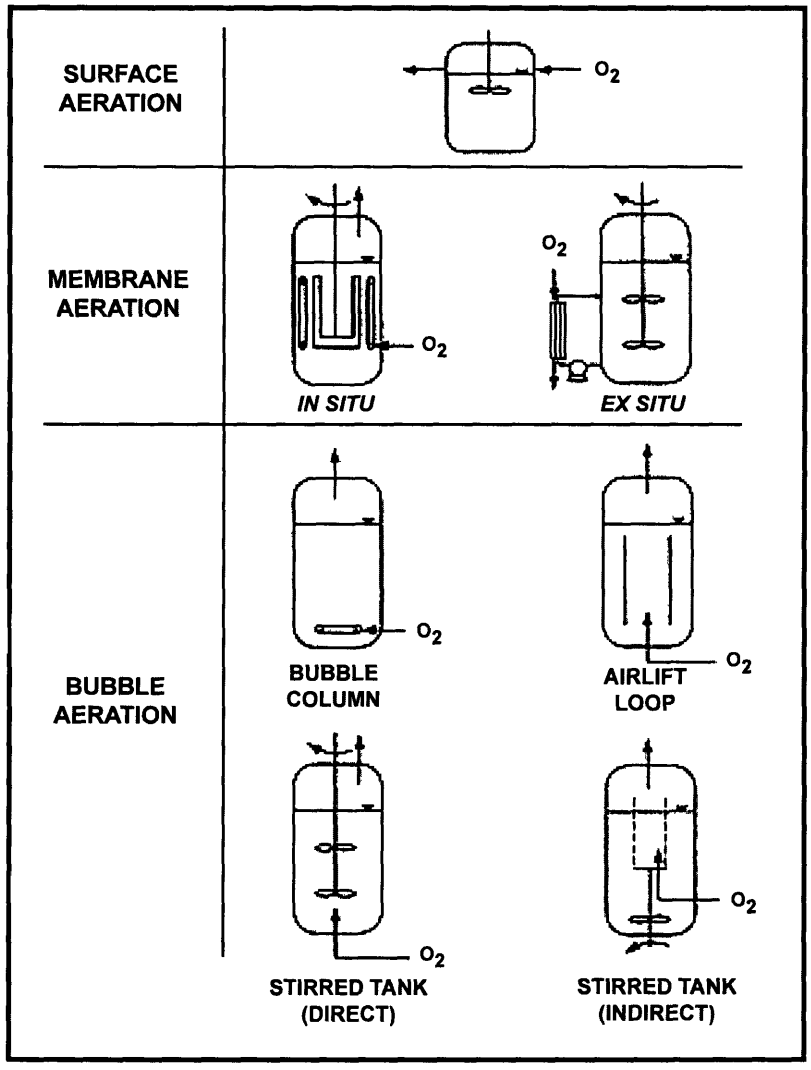

Figure 1-1. Common methods of oxygen supply to cell cultures.[52]

The second aeration method in use is bubble aeration, in which oxygen is bubbled into the medium through a sparger at the bottom of the bioreactor. The sparging can be combined with a subsurface mechanical impeller. Alternatively, sparging can be used to create an airlift loop, in which the gas bubbles themselves circulate the medium in addition to delivering oxygen. Bioreactors with high aspect ratios are used for this purpose.

The third aeration method in use is membrane aeration, in which the oxygen demand of the cell culture is met by the diffusion of oxygen through an oxygen-permeable membrane. This process can occur either *in situ*, where the medium that the cells are in is oxygenated directly, or *ex situ*, where the medium is continuously removed from the bioreactor, aerated, and returned.

Due to their high oxygen demand, microbial cell cultures generally employ one or both of the first two aeration methods outlined above (surface and bubble aeration). Conversely, mammalian cells, which have a much lower oxygen demand and greater frailty because of their lack of a cell wall, are generally oxygenated through a membrane or through impeller-less surface aeration.

One of the unique advantages of microsystems is the reduced mixing times that result from small diffusion lengths. Thus, although membrane aeration is not generally feasible for industrial or lab-scale microbial cultures, this method of aeration can be employed within the microbioreactor.

1.4.3. Temperature control

Prokaryotes are classified by the temperature range in which they grow. Mesophiles, including *Escherichia coli*, can grow between 10-47°C, and have as their optimal range 30-45°C.[53] The generation time of a cell culture, also referred to as the doubling time, is the time needed for the population to double in number. Figure 1-2 shows the generation time of an *E. coli* culture as a function of temperature, illustrating the importance of temperature control in

generating meaningful, reproducible data from the microbioreactor.

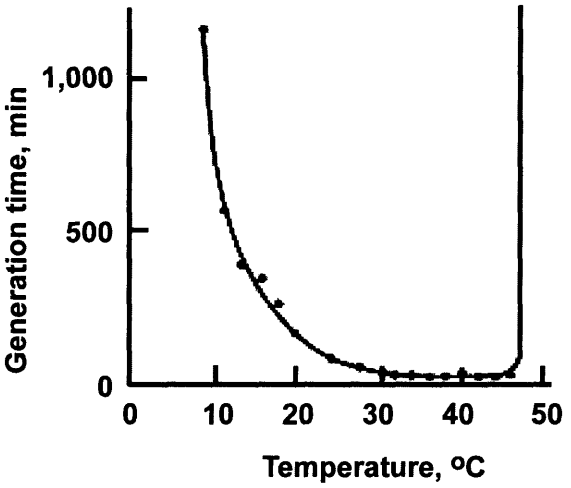

Figure 1-2. Effect of temperature on the generation time of *E. coli*.[53]

1.4.4. Sensing of optical density, dissolved oxygen, and pH

The three parameters that are most commonly monitored during fermentations are optical density (OD), dissolved oxygen (DO), and pH.

Optical density, calculated using a transmittance measurement through the culture medium, provides an estimation of biomass and is commonly measured at or close to 600 nm. The optical transparency of PDMS allows this measurement to be made through the body of the microbioreactor.

Oxygen concentration in bioreactors is conventionally monitored with the use of a Clark electrode. This electrode, however, consumes oxygen as part of its operation. Conversely, optical DO sensors are attractive for our application as they do not have this requirement. The majority of optical and fiber-optic sensors are based on absorption and fluorescence methods. In practice, optical oxygen sensing is most commonly based on the collisional quenching of a fluorophore embedded in a support matrix.[54-56]

Because protein configuration and activity are pH dependent, cellular transport processes, reactions, and growth rates depend on pH (Figure 1-3). Bacterial growth rates generally reach a maximum in the pH range of 6.5-7.5.[57] Typically, negligible growth results from a change in 1.5 to 2.0 pH units above or below the optimal pH. As with dissolved oxygen sensing, optical measurements using fluorescence can be used to measure pH.[58,59]

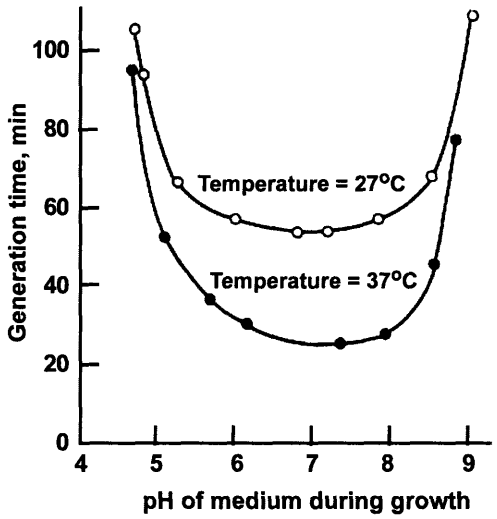

Figure 1-3. Effect of pH and temperature on the generation time of *E. coli*.[60]

1.4.5. Sensing of glucose

In bioprocessing, control of glucose levels in fermentation medium is crucial in both fed-batch and continuous systems when glucose is used as the carbon source. Effective control requires the ability to monitor glucose levels quickly and accurately. In addition, knowledge of glucose consumption is needed to close the carbon balance as well as for metabolic studies and medium optimization, making glucose monitoring crucial for batch systems as well.

1.4.6. Sensing of luminescence and fluorescence

As discussed previously, light emission from luminescent and fluorescent bacteria and yeast created to act as reporters for various environmental conditions is finding application in several areas of biology, including toxicity assays for environmental pollutants, chemical detection, and gene expression profiling.[7-12] The ability to monitor light emission would greatly expand the functionality of the microbioreactor.

1.4.7. Off-line analysis

Although efforts are continually being made to integrate into bioreactors as many on-line measurement techniques as possible,[44,46] it is sometimes necessary to remove samples during the course of a fermentation for off-line analysis, for example using high performance liquid chromatography (HPLC) or gas chromatography (GC). Medium must also be removable to enable global gene expression analysis using DNA microarrays, a technique widely applied in general biological research and in specific fields such as drug screening, environmental testing, and clinical diagnosis.[61,62]

1.5. Microbial Bioreactors

Strong interest exists in developing small-scale bioreactors.[63] Kim and Lee[64] developed a silicon microfermentor chip that makes use of electrodes to measure cell density, dissolved oxygen, pH, and glucose. However, cell growth was not reported. Kostov et al.[65] described a 2 mℓ microbioreactor that consists of a cuvette equipped with optical sensors for the continuous measurement of optical density, dissolved oxygen, and pH, in which aeration is accomplished by sparging the medium with air. Maharbiz et al.[66,67] developed a bioreactor built using microtiter plate wells, integrated with an aeration system in which oxygen is generated beneath a silicone

membrane using hydrolysis. Biomass was measured optically and pH was monitored using a solid-state pH sensor chip. Oxygen input rates were also monitored. The volume of this bioreactor is around 250 μℓ. Lamping et al.[68] recently reported on a miniature bioreactor machined from Plexiglas with a working volume of 6 mℓ. Oxygenation in this bioreactor is achieved by sparging, and mixing is achieved by means of an impeller. Measurements of cell density, dissolved oxygen, and pH are performed optically.

1.6. Thesis Objective

The purpose of this thesis is to design, fabricate, and characterize a batch microbioreactor with integrated sensors as a step toward establishing high-throughput screening bioprocessing platforms. The microbioreactor should meet the requirements described previously (biocompatibility of materials, oxygen delivery, temperature sensing and control, biomass sensing, oxygen sensing, and pH sensing), and should demonstrate reproducibility. It is also desirable to have a method of performing off-line analysis of the culture medium to maintain flexibility in analytical techniques. Finally, it is necessary to understand the similarities and differences in bacterial behavior at different size scales. *E. coli* will be used as the model organism for this study.

1.7. Thesis Outline

The work in this thesis covers three major categories: (1) fabrication and control of the microbioreactor, (2) analysis of performance, including uncertainty and scale comparisons, (3) applications.

Chapter Two describes the design, fabrication, and characterization of a 5 μℓ batch

microbioreactor with integrated sensors for OD, DO, and pH. Reproducibility of the system is investigated under several different conditions, and results at various size scales are compared. Since one of the main concerns with a system of this size is the potential difficulty with sampling, off-line HPLC analysis using the microbioreactor contents is presented. Modeling of oxygen transport is also carried out to obtain insight into the growth and oxygenation of bacteria.

Chapters Three and Four present additional applications of the microbioreactor technology. Chapter Three describes sensing capabilities that allow *in situ* measurements of bacterial luminescence and fluorescence. These measurements enable the cells to act as environmental sensors. Chapter Four describes the linking of microbioreactors to DNA microarrays. A technique is described that allows microarray experiments to be run using only 500 ng of total RNA. This increased sensitivity enables DNA microarrays to be used to analyze genome-wide gene expression changes during microbioreactor fermentations.

Chapter Five presents a model of a potential glucose sensor. The feasibility of miniaturizing and integrating this sensor is explored by investigating the characteristics of the sensor under various operational assumptions.

Chapter Six summarizes the work presented in this thesis and lists recommendations for future work.

Chapter 2. A Membrane-Aerated Microbioreactor for High-Throughput Bioprocessing

2.1. Introduction

The number and variety of products obtained through microbial fermentation today is large and growing quickly. These products include, among others, primary metabolites, secondary metabolites, enzymes, therapeutic proteins, vaccines, and gums.[2] Each new product is the result of a development process that begins at the screening stage.[22,69] During this phase many potential bacterial strains are screened to identify those that have the most favorable yield of the desired product. Criteria at this stage may be a high yield on a specific substrate, or high production under certain growth conditions. The screening phase may be combined with strain optimization using techniques of metabolic engineering, in which case strain creation and screening are carried out iteratively.[5,70] Experiments at the screening phase are typically carried out using a combination of Petri dishes, microtiter plates, and shake flasks. Once a likely microbial candidate has been identified, the strain is transferred to the development phase. At this stage the physiology of the strain is characterized in more detail, and the growth conditions of the strain are determined. These experiments are generally carried out in bioreactors with volumes of 0.5-10 ℓ. From here, development proceeds as the process is gradually scaled up in bioreactor volume until production scale is reached (100-300,000 ℓ).

Significant limitations in data generation currently exist at every stage of microbial and process development. During the screening phase, only limited control of environmental parameters is possible and endpoint data are generally obtained to gauge the performance of cells. Efforts have been made to overcome this limitation. In microtiter plates, on-line

measurements of dissolved oxygen[24,25] and pH[26] during fermentation have been demonstrated. On-line measurements of dissolved oxygen[27-30] and pH[31] in shake flasks during fermentation have also been reported. However, these screening approaches have the fundamental limitation that the effort involved largely continues to scale with the number of individual cultures involved, meaning that experiments with more cultures become more demanding both technically and mechanically. This is exacerbated by the difficulty of integrating culture steps that precede and follow the fermentation itself. During the process development phase that follows, the prohibitive time, expense, and labor involved in running experiments limits the number of strains and conditions that can be tested. At each stage, therefore, decisions are made with incomplete and insufficient data sets. A need clearly exists for a bioprocessing platform that would allow high-throughput, parallel, automated processing of a variety of bacterial strains under a variety of controlled conditions, with integrated sensors yielding real-time data on process parameters.

Efforts in this area have been made. Kim and Lee[64] developed a silicon microfermentor chip that makes use of electrodes to measure cell density, dissolved oxygen, pH, and glucose. However, cell growth was not reported. Kostov et al.[65] described a 2 mℓ microbioreactor that consists of a cuvette equipped with optical sensors for the continuous measurement of optical density, dissolved oxygen, and pH, in which aeration is accomplished by sparging the medium with air. Maharbiz et al.[66,67] developed a bioreactor using microtiter plate wells, integrated with an aeration system in which oxygen is generated beneath a silicone membrane using hydrolysis. Biomass is measured optically and pH is monitored using a solid-state pH sensor chip. Oxygen input rates are also monitored. The volume of this bioreactor is around 250 μℓ. Lamping et al.[68] reported on a miniature bioreactor machined from Plexiglas with a working volume of 6 mℓ.

Oxygenation in this bioreactor is achieved by sparging, and mixing is achieved by means of an impeller. Measurements of cell density, dissolved oxygen, and pH are performed optically.

We have developed a membrane-aerated microbioreactor with a volume as low as 5 μℓ. The size and design of the microbioreactor are compatible with microfabrication techniques, which enable fast and inexpensive scale-out through multiplication of devices. A microfabricated bioprocessing platform also allows integration of sensors as well as automation of liquid handling and process control. In this work we describe the design and fabrication of the microbioreactor. We compare results from microbioreactor fermentations with *Escherichia coli* in which OD, DO, and pH are monitored continuously and compare these with results obtained in 500 mℓ bench-scale bioreactors. We present the results of off-line analysis of the medium to determine organic acid production and substrate utilization. We also present data on two different operating conditions within the microbioreactor to demonstrate the feasibility of obtaining statistically significant growth data from our system. Finally, we use modeling to understand the oxygen transfer characteristics of our microbioreactor, and demonstrate that we can predict times for oxygen depletion and oxygen recovery based on growth characteristics of our model organism.

2.2. Materials and Methods

2.2.1. Microbioreactor fabrication

The microbioreactor (Figure 2-1) was fabricated out of poly(dimethylsiloxane) (PDMS) and glass. PDMS was used for the body of the fermentor, the bottom layer into which the sensors were embedded, and the aeration membrane. This polymer was selected for its biocompatibility, optical transparency in the visible range, and high permeability to gases (including oxygen and

carbon dioxide).[71] The base support of the bioreactor was made of glass, which provided the necessary rigidity as well as optical access. The typical volume of the microbioreactor was 5-50 μℓ, depending on the diameter used. The surface area-to-volume ratio was kept constant to ensure adequate oxygenation. The depth of the well was 300 μm, and the thickness of the aeration membrane was 100 μm. Of the experiments discussed below, those using complex medium were carried out in a volume of 5 μℓ, while those using defined medium were carried out in a volume of 50 μℓ to allow for off-line analysis of the medium.

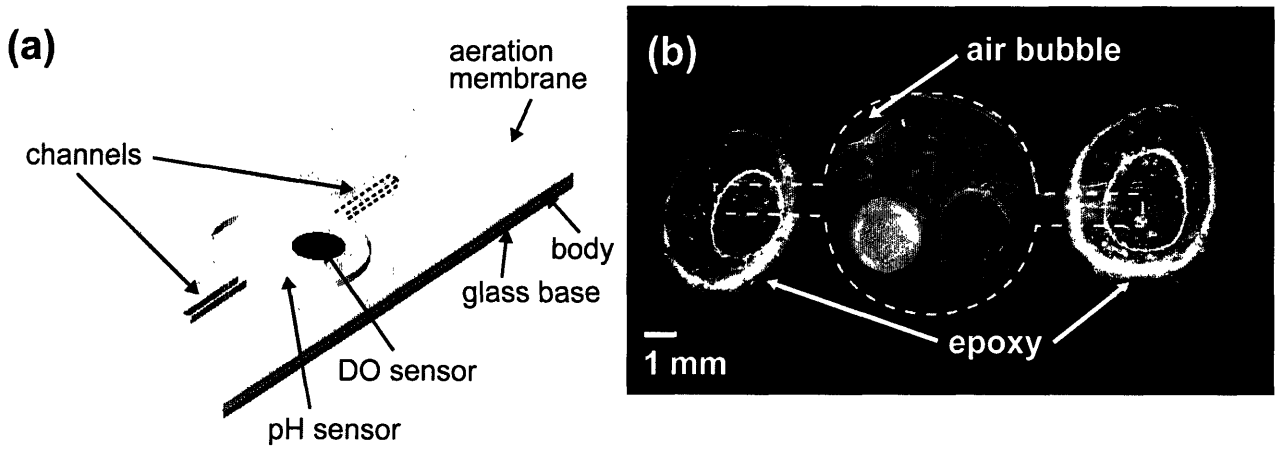

Figure 2-1. Microbioreactor built from three layers of PDMS on top of a layer of glass. (a) Solid model drawn to scale; (b) photograph of microbioreactor at the end of a fermentation run.

The three PDMS layers were obtained by spincoating PDMS (Sylgard 184 Silicone Elastomer Kit, Dow Corning) onto silanized silicon wafers to the required thickness. The PDMS was then cured for two hours at 70°C, and the appropriate shapes were cut out of each layer. The bottom layer was 280 μm thick and contained two round holes into which two sensor foils were inserted, one for dissolved oxygen and one for pH as described in the following section. Each sensor was 2 mm in diameter and 150-220 μm in height. The sensors were held in place with

silicone vacuum grease. Recessing the foils in this way allowed the tops to be flush with the bottom of the microbioreactor, which is especially critical for the dissolved oxygen foil as a result of the oxygen gradient that develops in the medium during fermentations (see Results and Discussion). The 300 μm middle layer, which made up the body of the microbioreactor, consisted of a round opening of the desired diameter and channels for inoculation. The top layer was the 100 μm polymer aeration membrane. These layers were attached to each other and to the glass using an aquarium-grade silicone adhesive (ASI 502, American Sealants, Inc.) and allowed to cure overnight. Figure 2-1b shows a filled microbioreactor at the end of a fermentation run.

2.2.2. Analytical methods

Optical sensing methods were selected to monitor biomass, dissolved oxygen, and pH. The major advantage of optical sensors is that the bulk of the cost and complexity of the sensing infrastructure can be kept outside of the microbioreactor, keeping the microbioreactor simple to fabricate and inexpensive, and thus disposable.

Optical density, calculated from a transmission measurement at 600 nm, was used to monitor biomass. Light from an orange LED (Epitex L600-10V, 600nm) was passed through the microbioreactor, collected by a collimating lens (F230SMA-A, Thorlabs), and sent to a photodetector (PDA55, Thorlabs). The optical density was calculated using Equation 2-1.

$$OD = 33.33 \log_{10}\left(\frac{I_{reference}}{I_{signal}}\right) \qquad (2\text{-}1)$$

In this equation I_{signal} is the intensity of the signal and $I_{reference}$ is the intensity of the first measurement for a given experiment. Intensity readings were corrected for intensity fluctuations

of the light source using a reference signal. The multiplication factor of 33.33 in Equation 2-1 is a normalization for the pathlength of 300 μm in the microbioreactor which enables direct comparisons with results from conventional cuvettes with pathlengths of 1 cm. This adjustment is only strictly valid if the absorption and light scattering by the cell culture are in the linear region. Calibration data from the microbioreactor using known concentrations of *E. coli* show that the measurements are within the linear region, i.e. before saturation is reached. It is important to note that this measurement is very sensitive to both the path length and to any curvature of the PDMS aeration membrane.

Fluorescence from oxygen- and pH-sensitive dyes was selected for the measurement of dissolved oxygen[54-56] and pH,[58,59] respectively, because of the high sensitivity and specificity of this measurement.[72] The fluorescence of these dyes could be monitored using either fluorescence intensity or fluorescence lifetime measurements.[73] There are several major advantages to using lifetime measurements. They are insensitive to background light, fluctuations of the excitation source and photodetector, changes in distance from the excitation source, bending of optical fibers, changes in medium turbidity, leaching of the indicator, and displacement of the sensing layer relative to the measurement setup.

Both dissolved oxygen and pH were monitored by phase-modulation lifetime fluorimetry using commercially available sensor foils from PreSens Precision Sensing GmbH (Regensburg, Germany). Dissolved oxygen was measured using a PSt3 sensor foil, while pH was measured using an HP2A sensor foil.

Figure 2-2 shows the experimental setup. Bifurcated optical fibers (custom-made, Romack) connected to LEDs and photodetectors led into the chamber from both the top and bottom. As described above, a transmission measurement was used to calculate the optical density. The DO

and pH sensors were excited with a square-wave modulated blue-green LED (NSPE590S, Nichia, 505 nm) and a blue LED (NSPB500S, Nichia, 465 nm), respectively. Exciter bandpass filters (XF1016 and XF 1014, Omega Optical) and emission longpass filters (XF 3016 and XF 3018, Omega Optical) separated the respective excitation and emission signals and minimized cross-excitation. Data switches (8037, Electro Standards Laboratories) multiplexed the output signal and the input signal of the function generator (33120A, Agilent Technologies) and the lock-in amplifier (SR830, Stanford Research Systems), respectively. The lock-in amplifier measured and output the phase shift, which is directly related to the fluorescence lifetime, between the excitation and emission signals for the DO and pH measurement. All instruments were PC-controlled under a LabVIEW software routine, which allowed for automated and on-line measurement of the three parameters OD, DO, and pH. Readings of these parameters were taken every 10 minutes.

To determine the dissolved oxygen, the measured phase shift of the oxygen signal was related to the oxygen concentration using a modified Stern-Volmer equation.[74,75] An eleven-point calibration between 0% and 100% oxygen was carried out to confirm the validity of the equation and to calculate a Stern-Volmer constant. It was found that a better fit was obtained for low oxygen concentrations when the calibration range included in the model fit was limited to 0-21% oxygen. Therefore, data from experiments with air as the contacting gas were processed using that range, while data from experiments using pure oxygen were processed using the full range of calibration.

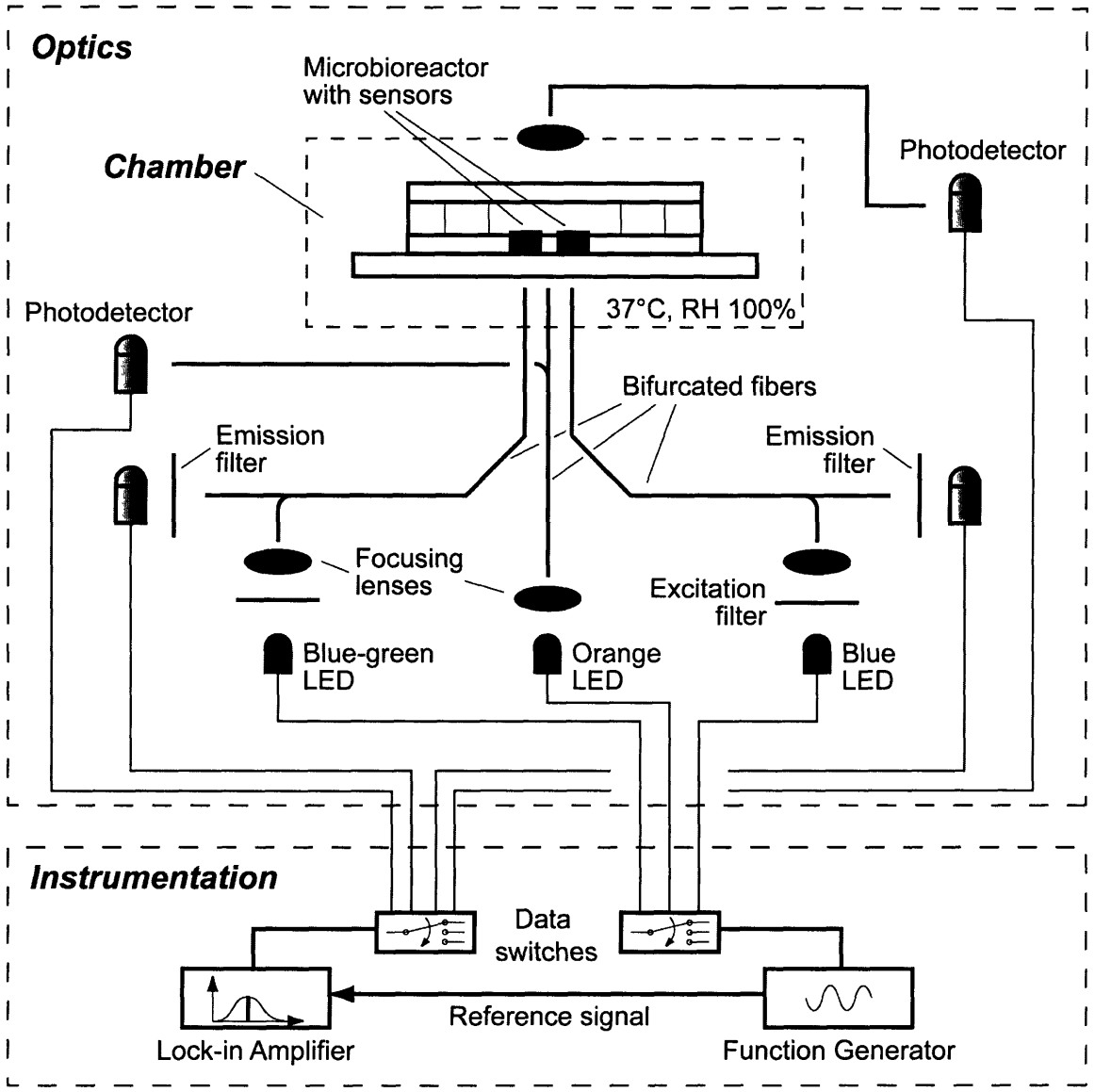

Figure 2-2. Schematic of the experimental setup. The chamber is kept at 100% humidity and 37°C. The microbioreactor is placed inside and the chamber is sealed. Three optical fibers carry three different wavelengths of light to the bottom of the microbioreactor for the three measurements: OD, DO, and pH. Photodetectors collect the transmitted or emitted light and send it to a lock-in amplifier where the signal is detected and analyzed.

The measured phase shift of the pH sensor fluorescence was related to the pH by fitting to the sigmoidal Boltzmann curve.[76] A six-point calibration was carried out between pH 4 and pH 9 using colorless buffers (VWR).

2.2.3. Microbioreactor experimental setup

Experiments were carried out in an airtight, aluminum chamber (Figure 2-2). The chamber provided a means for controlling the humidity and the composition of the gas above the microbioreactor membrane. It also provided a large thermal mass for holding the temperature at the desired set point. The interior of the chamber had an area of 11.5 cm by 6.5 cm, and a height of 2.5 cm. This volume was large compared to the volume of the microbioreactor to ensure that gaseous oxygen was in large excess compared to the oxygen consumed by the cells during a fermentation. As a result, the chamber could be sealed for the duration of a run once it had been flushed with the desired gas. Temperature was controlled with a water bath that flowed water at the desired setpoint through the chamber base. Temperature was monitored using a thermocouple.

In addition to controlling environmental parameters, the chamber provided optical isolation and optical access for the desired measurements. Optical access was from the top and bottom of the chamber, directly above and below the microbioreactor, respectively, as shown in Figure 2-2.

2.2.4. Biological methodology

2.2.4.1. Organism and medium

Escherichia coli FB21591 (*thi*C::Tn*5* -pKD46, Kan^R) was used in all experiments and purchased from the University of Wisconsin. Stock cultures were maintained at -80°C in 20% (vol/vol) glycerol. Prior to fermentation experiments, single colonies were prepared by streaking out the frozen cell suspension onto LB plates containing 2% (wt/vol) agar and 100 μg/mℓ of kanamycin. The plates were incubated overnight at 37°C to obtain single colonies, and subsequently stored at 4°C for up to a week or used immediately to inoculate precultures.

Luria-Bertani medium had the following composition: 10 g/ℓ tryptone (Difco Laboratories), 5 g/ℓ yeast extract (Difco Laboratories), and 5 g/ℓ NaCl. The solution was autoclaved for 40 minutes at 120°C and 150 kPa. The LB medium was supplemented with 10 g/ℓ glucose (Mallinckrodt), 100 mM MES buffer at pH 6.9 (2-(N-Morpholino)-ethanesulfonic acid)) (Sigma), and 100 μg/mℓ of kanamycin (Sigma). The glucose stock solution was autoclaved for 20 minutes at 120°C and 150 kPa, and the MES and kanamycin stock solutions were filtered through 0.2 μm filters (Millipore).

The defined medium had the following composition: K_2HPO_4 [60 mM], NaH_2PO_4 [35 mM], $(NH_4)_2SO_4$ [15 mM], NH_4Cl [70 mM], $MgSO_4 \cdot 7H_2O$ [0.8 mM], $Ca(NO_3)_2 \cdot 4H_2O$ [0.06 mM], $FeCl_3$ [20 mM], MES [100 mM], glucose [10 g/ℓ], thiamine [100 μM], kanamycin [100 μg/mℓ], $(NH_4)_6Mo_7O_{24} \cdot 4H_2O$ [0.003 μM], H_3BO_3 [0.4 μM], $CuSO_4 \cdot 5H_2O$ [0.01 μM], $MnCl_2 \cdot 4H_2O$ [0.08 μM], $ZnSO_4 \cdot 7H_2O$ [0.01 μM]. Glucose, MES, kanamycin, and thiamine were added to the medium as stock solutions.

2.2.4.2. Precultures

For experiments using LB medium, 5 mℓ of sterile medium were transferred into test tubes and each was inoculated with a single colony of *E. coli* FB21591 from an LB-kanamycin agar plate. These cultures were incubated on a roller at 60 rpm and 37°C. Samples were removed periodically and measured for optical density (600 nm). When the optical density of the cultures reached OD = 1 ± 0.1, medium was removed from each test tube and transferred to a 500 mℓ baffled shake flask containing 30 mℓ of fresh medium to a starting optical density of 0.05. The inoculated shake flasks were incubated on shakers (150 - 200 rpm) at 37°C. Samples were withdrawn periodically until the optical density within the flasks reached OD = 1. At this point

the culture was used to inoculate either the bench-scale bioreactors or a microbioreactor.

Precultures for experiments using defined medium were carried out as above, except that the shake flasks into which the cultures from the test tubes were transferred contained defined medium.

2.2.4.3. Bench-scale bioreactor

Batch cultures were grown in 500 mℓ SixFors bioreactors (Infors, Switzerland) with a starting medium volume of 450 mℓ. Dissolved oxygen probes (405 DPAS-SC-K8S/200, Mettler Toledo) were calibrated with nitrogen gas (0% DO) and air (100% DO) prior to each run. pH probes (InPro 6100/220/S/N, Mettler Toledo) were calibrated with buffer at pH 7.0 and 4.0 (VWR).

The bioreactors were inoculated to a starting optical density of 0.05. The aeration rate of gas was set to 1 VVM (volume of gas per volume of medium per minute) and the impeller speed was set to 500 rpm. This combination of stirring and sparging was selected to match the estimated k_La of the microbioreactor. The k_La was measured using the well-known method of "dynamic gassing out".[77] The temperature of the vessels was maintained at 37°C for all fermentations. Dissolved oxygen and pH were not controlled, so as to simulate the batch microbioreactor. The time courses of temperature, dissolved oxygen, and pH were recorded every 10 minutes throughout all fermentations. Biomass was monitored by removing samples from the bioreactor at defined time intervals and measuring the optical density at 600 nm on a spectrophotometer (Spectronic 20 Genesys, Spectronic Instruments).

2.2.4.4. Microbioreactor

Inoculation of the medium for the microbioreactor was carried out outside of the bioreactor.

Ten milliliters of fresh medium were transferred to a Falcon conical tube, and to this was added the preculture medium from a shake flask for a starting optical density of 0.05. This inoculated medium was then introduced into the microbioreactor by injecting the liquid via channels (Figure 2-1).

Sterility was maintained through the use of the antibiotic kanamycin in the medium. Other methods of sterilizing, such as autoclaving and UV radiation, were not feasible due to the incompatibility of either the DO sensor or the pH sensor with each of these methods. Gamma radiation was tested as an alternative technique. Ethanol could also be used as a means of sterilization. However, for the present studies we found that using a fast-growing, antibiotic-resistant strain was sufficient for preventing contamination.

To ensure the flatness of the PDMS membrane, excess liquid was squeezed out of the chamber by applying a uniformly distributed pressure from the top. A bulge in the membrane would change the path length for the calculation of optical density, as well as change the distance over which diffusion of oxygen occurred, thus changing the mass transfer characteristics of the microbioreactor. After injection of the inoculated medium, the needle holes created in the channels were sealed with epoxy (Figure 2-1). This was to prevent evaporation at these injection sites. Although PDMS self-seals to a large extent, we have noticed that needle holes increase the rate of evaporation and provide sites for the growth of air bubbles.

Once the microbioreactor was filled with medium it was placed inside the chamber and secured to the base. Open reservoirs of water were placed inside the chamber to provide humidity. Keeping the atmosphere within the chamber at high humidity minimizes evaporative losses through the PDMS membrane. The chamber was then closed and continuous readings were started. When fermentations were performed with pure oxygen in the chamber headspace,

oxygen was passed through the chamber prior to the start of the readings.

The time between inoculation of fresh medium and placement of the filled microbioreactor in the chamber was 20 minutes. During this time the medium was kept at room temperature to minimize cell growth. The time between placement of the bioreactor in the chamber and the first reading was 10 minutes. During this time the bioreactor and cells warmed up to 37°C.

2.2.4.5. Cell counts

Estimates of cell number from the microbioreactor and the bench-scale bioreactor were obtained using two methods. Direct cell counts were carried out using a Petroff-Hausser counting chamber and standard counting methodology. Viable cell counts were carried out using the technique of plating serial dilutions.[78]

2.2.4.6. Medium analysis

A series of experiments in defined medium was carried out to provide samples for off-line analysis of organic acids and glucose in both the bench-scale bioreactor and the microbioreactor.

During fermentations in the bench-scale bioreactors, samples of the medium were periodically removed, filtered, and frozen for later analysis.

Samples from the microbioreactors were obtained by sacrificing their entire volume. In order to obtain a sufficient volume of medium for analysis, the microbioreactors were fabricated to contain a volume of 50 $\mu\ell$. This allowed for volume loss during filtering and transfers, and provided sufficient filtered volume to meet the requirements of the HPLC protocol (5 $\mu\ell$). The medium samples were collected over several days. Each day three microbioreactors were inoculated and allowed to run in parallel while process parameters were measured. All three were then sacrificed at a common, predetermined time, and their contents were removed, filtered,

and frozen. This process was repeated daily over the course of five days, such that microbioreactor data was obtained at five time points.

An Agilent 1100 Series HPLC equipped with an organic acid analysis column (Aminex HPX-87H Ion Exclusion Column, Bio Rad) was used for off-line medium analysis. Samples were prepared by filtration through a 0.2 μm membrane (Pall Gelman Laboratory). Calibration was carried out by running standards at two concentrations for each of the organic acids assayed, and four different standards for glucose. A linear fit through the origin was obtained for all of the concentration ranges used.

2.3. Results and Discussion

2.3.1. Modeling of oxygen transport and consumption

The design of the microbioreactor was based on preliminary modeling of the oxygen transfer through the PDMS membrane and the medium using the simulation software FEMLAB (parameters used are listed in Table 2-1, variables used are listed in Table 2-2). Monod growth[79] of homogeneously-dispersed cells with oxygen as the limiting substrate was assumed. The Monod constant was approximated by using the critical oxygen concentration for *E. coli*.[57] R_V was zero within the membrane.

$$\frac{\partial C}{\partial t} = D\frac{\partial^2 C}{\partial x^2} - R_V \qquad (2\text{-}2)$$

$$R_V = OxygenUptakeRate = -Y_{O/x}\frac{dN}{dt} \qquad (2\text{-}3)$$

$$\frac{dN}{dt} = N\mu \qquad (2\text{-}4)$$

$$\mu = \frac{\mu_{max} C}{K_S + C} \qquad (2\text{-}5)$$

Table 2-1. List of parameters used in models.

Parameter	Definition	Value	Reference
S_{PDMS}	†Solubility of O_2 in PDMS	0.18 cm^3(STP)/cm^3•atm	71
D_{PDMS}	†Diffusivity of O_2 in PDMS	3.4 x 10^{-5} cm^2/s	71
S_{H2O}	†‡Solubility of O_2 in water	7.36 mg/ℓ	80
D_{H20}	†‡Diffusivity of O_2 in water	2.5 x 10^{-5} cm^2/s	80
K	†‡PDMS-H_2O partition coefficient	0.135	Calculated
$Y_{O/X}$	Yield of biomass on oxygen	1 g_{O2} consumed/g_{DCW} (Dry Cell Weight) produced	81
N_0	Initial number of cells	3.8 x 10^7 cells/mℓ	Experiment
t_d	Doubling time	30 min	Experiment
μ_{max}	Maximum specific growth rate	0.0231 min^{-1}	Experiment
	Conversion	5.5 x 10^{-13} g_{DCW}/*E.coli* cell	Experiment
K_s	*Monod constant	0.26 mg/ℓ	Calculated
k	Logistic model constant	0.025	Model fit
β	Logistic model constant	2.5 x 10^{-16} m^3/cell	Model fit
C*	Percent oxygen at saturation	100%	Definition

† At 35°C, in equilibrium with 0.21 atm of oxygen
‡ Values for pure water were used since only 10 g/ℓ of glucose was present in the medium
* Critical oxygen concentration = 0.0082 mmol/ℓ (~ 3.6 % of air saturation)[57]

Table 2-2. List of variables used in models.

Variable	Description
C	Concentration of oxygen
D	Diffusivity of O_2 in each phase
R_V	Volumetric accumulation term
N	Number of cells
μ	Specific growth rate of cells
k_La	Oxygen transfer coefficient

We determined that a depth of 300 μm allowed sufficient oxygenation to reach a final cell number ~ 10^9 cells/mℓ. It was found that the major resistance to mass transfer occurs in the medium rather than the membrane, a result of the low solubility of oxygen in water. From the model it is also evident that a concentration gradient exists within the medium as oxygen is gradually depleted. Oxygen depletion occurs first at the bottom and moves gradually up the microbioreactor. This is shown in the cross-sectional view of Figure 2-3, which shows oxygen concentration as a function of depth at increasing time.

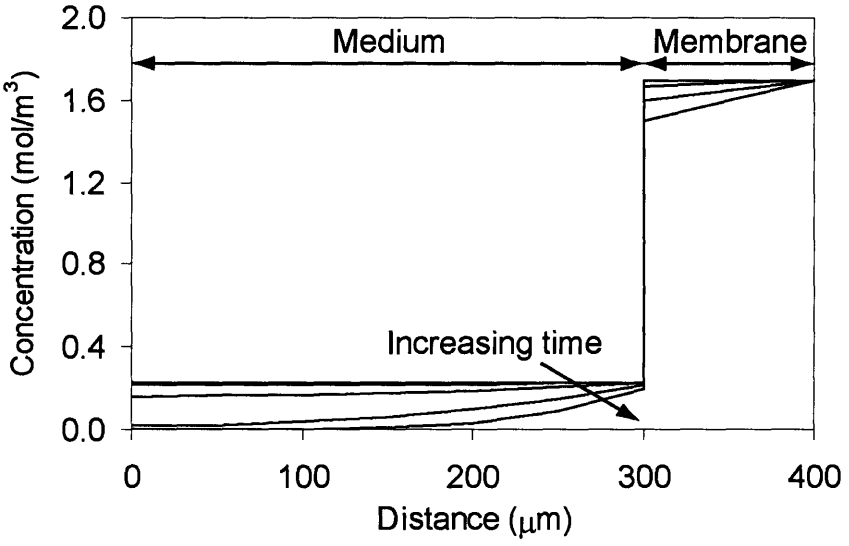

Figure 2-3. Modeled oxygen gradient within the medium and the membrane of the microbioreactor when Monod growth is assumed. Oxygen concentrations are shown at t = 0, 0.5, 1, 1.5, and 2 hours.

Because of the presence of the oxygen gradient, the height of the dissolved oxygen sensor foil is critical to the measurements obtained. If the sensor is raised above the height of the microbioreactor bottom or is somehow at an angle, it will take longer to be reached by the zero-dissolved-oxygen zone during depletion, and will register dissolved oxygen earlier during

reoxygenation of the medium. Depending on its height, it may never show oxygen depletion. Thus the oxygen sensor must be positioned such that its entire surface is exposed to the same oxygen concentration. In this case the gradient is perpendicular to the bottom of the fermentor, and the foil must therefore be positioned horizontally (i.e. along the bottom of the chamber), rather than on the side where readings would be ambiguous. In terms of microbioreactor fabrication, adequate positioning can be achieved by viewing the bioreactor from the side before the aeration membrane is put into place. The sensor should appear planar with the PDMS bottom, without any protruding edges. This step is especially critical.

Oxygen depletion occurs after approximately 3 hours at the bottom of the microbioreactor (Figure 2-4). Experimental data show a similar trend. The model has also been used to successfully predict dissolved oxygen curves for *E. coli* growing in defined medium. During bacterial growth, the oxygen depletion phase typically corresponds to the period of biomass increase as measured by optical density. After some time the cells enter stationary phase, at which time metabolism shifts from growth to maintenance. Oxygen demand drops significantly, allowing oxygen levels to recover.

To model this oxygen recovery observed in experiments, the logistic curve (Equation 2-6) was fit to experimental growth data and substituted for N in Equation 2-3. This model was developed by Verhulst[82] to describe population growth and includes cell concentration-dependent inhibition. As in the case of the Monod model, this simple model is both unstructured (balanced growth approximation) and unsegregated ("average cell" approximation). It is useful when the limiting nutrient is unknown, or when multiple factors affect cellular growth as is the case here. To take these multiple factors into account would necessitate the removal of the balanced-growth assumption listed above and a move towards structured models, which is not

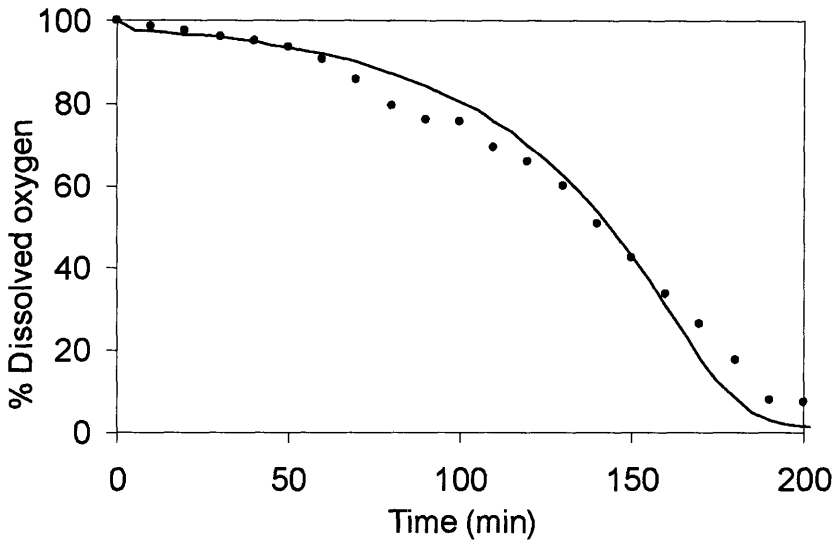

Figure 2-4. Oxygen concentration at the bottom of the microbioreactor as a function of time during a fermentation with a doubling time of 30 minutes. Model (-) uses Monod growth to predict oxygen depletion, experimental data (•) are for a fermentation run with a resulting doubling time of 30 minutes.

the major focus of this paper. The logistic model is therefore used despite its limitations. The fit to the curve is shown in Figure 2-5a.

$$N = \frac{N_O e^{kt}}{1 - \beta N_O (1 - e^{kt})} \qquad (2\text{-}6)$$

Modeling of the oxygen concentration within the microbioreactor using this fit is shown in Figure 2-5b. The difference between the predicted and measured curves in Figure 2-5 may be attributed to the limitations of the model used, as discussed above.

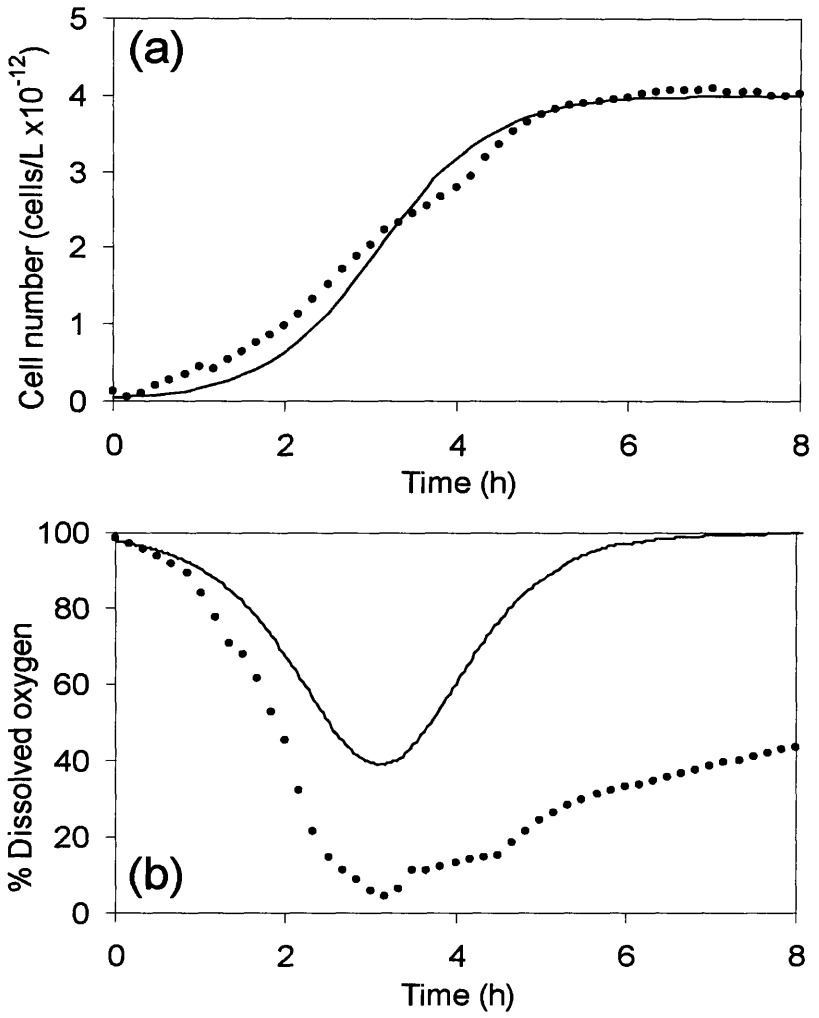

Figure 2-5. (a) Logistic curve (–) fit to experimental data (•) with k = 0.025, $\beta = 2.5 \times 10^{-16}$ m^3/cell. Experimental data are an average of three fermentations. (b) Oxygen concentration at the bottom of the microbioreactor as a function of time during a fermentation. Theoretical curve (–) uses a logistic model for cell growth, experimental data (•) are an average of three fermentations.

2.3.2. Mass transfer coefficient

To allow the comparison of results obtained with the microbioreactor and the bench-scale reactor, a k_La was measured in the microbioreactor and the operating conditions of the larger bioreactor were set so that its k_La would be comparable. The calculation of the k_La in the

microbioreactor was based on a kinetic experiment (at 37°C) in which the medium was allowed to come to equilibrium with nitrogen (0% DO) in the chamber headspace, at which time the headspace was flushed with air (100% DO) and continuous readings of the dissolved oxygen at the bottom of the microbioreactor were taken. Except for the absence of active stirring, this technique is similar to that of the dynamic "gassing-out" method that is commonly used for stirred bioreactors, during which the k_La is extracted as a first-order rate constant using Equation 7. The technique has previously been used to find the k_La of a stagnant system.[83]

$$\frac{dC}{dt} = k_L a(C^* - C) \qquad (2\text{-}7)$$

The first-order approximation of Equation 2-7 is applicable if mass transfer is slow relative to the response time of the sensor. If the time response of the sensor is potentially significant relative to that of the entire system, a second order fit can be used as in Equation 2-8, where τ_1 is the time constant of the sensor and τ_2 is the time constant of mass transfer.

$$C(t) = 100\left(1 - \frac{\tau_1 e^{\frac{-t}{\tau_1}} - \tau_2 e^{\frac{-t}{\tau_2}}}{\tau_1 - \tau_2}\right) \qquad (2\text{-}8)$$

Experimentally we found the time constant of our sensor to be ~ 5 s. When response curves of our system were fit to Equation 2-8, we calculated an average k_La of ~ 60 h^{-1}. This is within the range of values measured in shake flasks[29,30,84] and shaken microtiter plates.[24,85]

We carried out a dynamic simulation of the experimental setup and procedure using

FEMLAB. In the simulation we modeled the two-level microbioreactor inside the chamber, through which air flowed at the measured flow rate starting at $t = 0$. The initial conditions imposed were 0% oxygen concentration within the medium and in the membrane. The resulting oxygen curve yielded $k_La \sim 170\ h^{-1}$ ($\tau \sim 21$ s). The flowrate of air through the chamber was high enough that the boundary layer formed at the air-membrane interface was negligible.

The discrepancy between the measured and theoretical time constants for this system may be a result of assumptions made about the permeability of the PDMS membrane. It can be shown that any decrease in the solubility or diffusivity of oxygen in PDMS that is used in the model will have a large impact on the calculated k_La, which is extracted from a fast process (time scale of tens of seconds), while having little impact on the oxygen transfer during a fermentation, which is a slow process (time scale of hours) during which the PDMS presents relatively little transport resistance. This difference in the permeability could either be due to experimental conditions, such as the age of the membrane or the presence of oil or dust on the surface, or simply a difference between the PDMS used in experiments and that reported in literature (such as degree of cross-linking).

It should also be noted that the method of fitting a curve to the oxygen concentration on the bottom of the microbioreactor to estimate a k_La provides a lower bound for the measurement, since this is where the lowest concentration of oxygen is found at every time point. The extracted k_La will be larger if, for example, a space-average of the oxygen concentration is used. For the case of the simulation, with which $\tau \sim 21$ s ($k_La \sim 170\ h^{-1}$) was calculated using the bottom DO level, taking a space-average of the DO and finding the time constant of the resulting response curve yields $\tau \sim 14$ s ($k_La \sim 250\ h^{-1}$).

2.3.3. Fermentations with air

Experiments in defined medium were carried out in both the microbioreactors and the bench-scale bioreactors. MES buffer was added to provide some stabilization for the pH, since pH control was not implemented. The objectives were to establish the reproducibility of the microbioreactor relative to the bench-scale, and to demonstrate the feasibility of time-point sacrificing of the microbioreactors in order to carry out off-line analysis of the bioreactor medium throughout a fermentation. Three microbioreactors were sacrificed at each time point, and the medium was analyzed for glucose consumption and mixed-acid fermentation products using HPLC. In basic research or scale-up applications, this type of analysis would be necessary if an *in situ* sensor was not available for an analyte of interest.

The three measured parameters within the microbioreactor and the bench-scale bioreactor are shown in Figure 2-6. Each curve represents a separate run. A comparison of Figure 2-6a and Figure 2-6b shows that the optical density in both bioreactor types displays a similar trend, and results in a similar final OD of ~ 6. Figure 2-6c and Figure 2-6d show the dissolved oxygen as a function of time in the microbioreactor and the bench-scale bioreactor, respectively. Again, it can be seen that the trend in both bioreactors is similar – even though the Sixfors chambers are mixed. This result is consistent with the similar values of oxygen mass transfer (k_La) for the two systems. Oxygen levels deplete during the exponential growth of cultures and eventually recover as the bacteria reach stationary phase. The variation in the microbioreactor runs appears slightly larger than in the bench-scale bioreactor runs. As discussed earlier, this is most likely due to the sensitivity of the oxygen measurements in the microbioreactor to the positioning of the dissolved oxygen foil. Specifically, if any or all of the DO foil is raised above the floor of the microbioreactor, the time to depletion and the time at depletion will change due to the oxygen

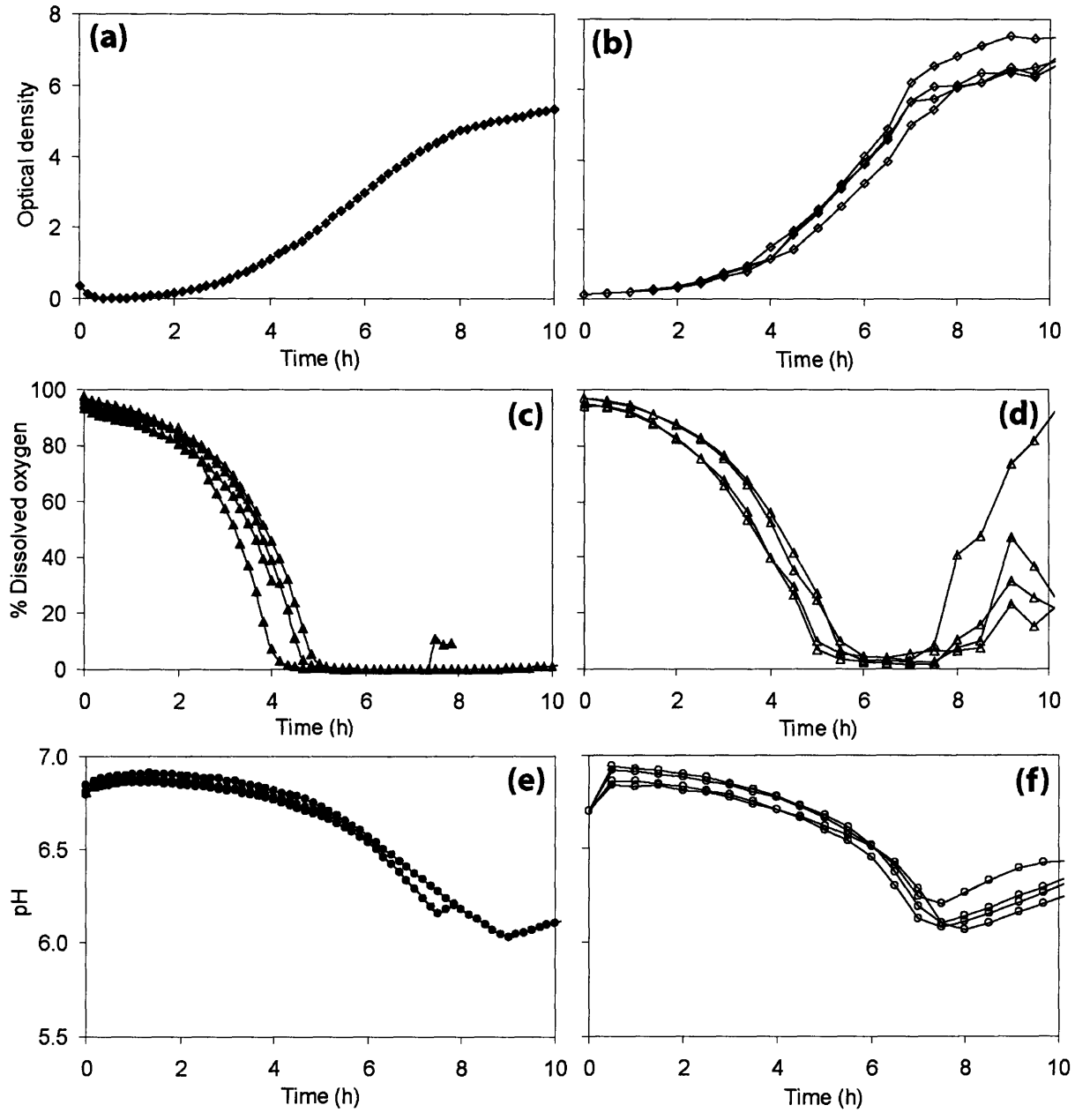

Figure 2-6. Replicate fermentations with *E. coli* in defined medium in the microbioreactor and a bench-scale bioreactor. (a) OD in microbioreactor (b) OD in bench-scale bioreactor (c) DO in microbioreactor (d) DO in bench-scale bioreactor (e) pH in microbioreactor (f) pH in bench-scale bioreactor. Experiments in the microbioreactor were performed on successive days, and microbioreactors were sacrificed each day at a predetermined time. The medium was harvested for HPLC analysis. Each data series represents a single run.

gradient that exists within the medium.

The trends for pH variations over time within both bioreactor types are again very similar. It appears that this measurement exhibits less variation between runs in the microbioreactor than the DO measurement. This is most likely due to the insensitivity of the pH measurement to the positioning of the pH sensor, suggesting that a pH gradient does not exist within the microbioreactor and the bioreactor can be considered well-mixed with respect to protons.

This hypothesis was confirmed experimentally by placing the pH sensor at the top of the chamber during a fermentation run. The pH curve showed the same time profile as those from fermentations in which the sensor was at the bottom. This result is consistent with the analysis of the reaction and diffusion times within the microbioreactor. An estimate of the reaction time can be obtained by converting the pH versus time curve to an $[H_3O^+]$ versus time curve. The steepest slope on this curve can be used to find the largest $d[H_3O^+]/dt$ ($\sim 5 \times 10^{-9}$ M/min). Normalizing this slope with the concentration of H_3O^+ at that time point ($\sim 5 \times 10^{-7}$ M) gives a $t_{rxn} \sim 100$ min. Note, this is not the time scale for the acid-base reaction, which is very rapid, but the time scale for the pH change as a result of the growth. The diffusion time of the system with respect to protons can be estimated as L^2/D. Using $D_{H^+} = 9.311 \times 10^{-5}$ cm^2/s (at 25°C)[86] gives $t_{diff} \sim 0.2$ min. Thus, $t_{rxn} >> t_{diff}$ implying that a pH gradient would not be expected, and the pH sensor would not be affected by its location in the microbioreactor – as observed experimentally.

When bacteria were viewed at the end of fermentation runs, the morphology of all cultures looked normal, with no stress-induced elongation visible. Final direct cell counts in both bioreactor types were carried out, and the concentration of cells in each was found to be on the order of 10^9 cells/mℓ. It is difficult to get an exact count using this method, since the depth of field on the microscope is less than the 0.02 mm depth of the counting chamber, and the small

size of the bacteria results in individual cells coming in and out of focus as the focus is adjusted. However, the estimate is consistent with the numbers obtained from viable cell counts, which yielded counts of 1-4 x 10^9 CFU/mℓ in both sizes of bioreactor.

Figure 2-7 shows concentration curves for the analytes measured using HPLC. The glucose uptake in the microbioreactor (Figure 2-7a) corresponds closely with that in the larger bioreactor. Additionally, Figure 2-7b shows that concentrations of the *E. coli* mixed-acid fermentation products acetate, formate, and lactate show similar trends in both bioreactor systems (succinate was not found in either bioreactor type). Acetate in particular is produced in significant amounts as the fermentation proceeds.

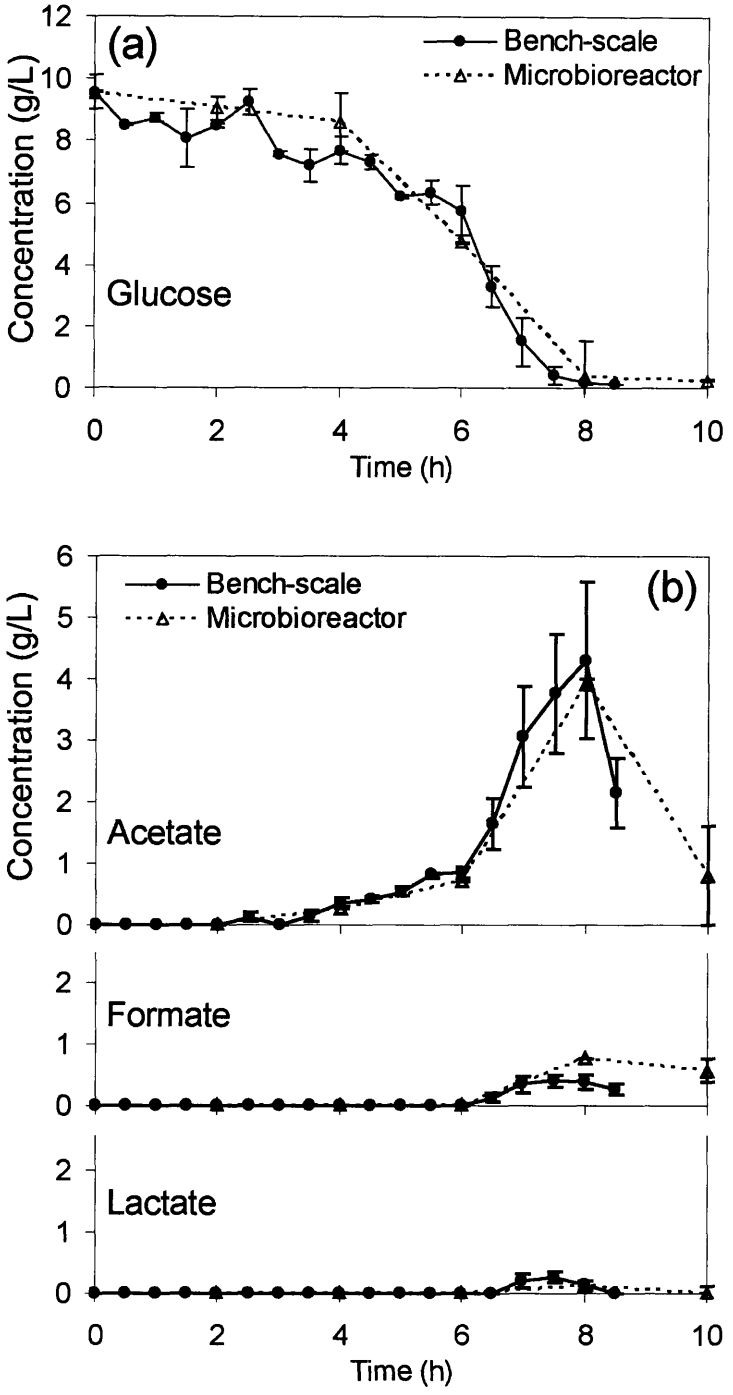

Figure 2-7. (a) Glucose uptake during fermentations with *E. coli* in defined medium in a bench-scale bioreactor (*n=2*) and a microbioreactor (*n=3*). Data are averaged over *n* runs, error bars report standard error. (b) Organic acid production during fermentations of *E. coli* in defined medium in a bench-scale bioreactor *(n=4)* and a microbioreactor *(n=3)*. Data are averaged over *n* runs, error bars report standard error.

2.3.4. Fermentations with pure oxygen

Additional experiments were carried out in LB medium, with air as well as 100% oxygen in the headspace of the chamber (above the aeration membrane) to determine whether a difference could be observed in bacterial growth characteristics. Supplying a partial pressure of 1 atm of oxygen above the microbioreactor instead of the 0.21 atm found in air leads to an approximately five-fold increase in the solubility of oxygen in the medium, as defined by Henry's law. This approach is commonly used in large-scale fermentations to avoid oxygen limitations. An extensive literature exists on the effects of total and partial oxygen pressure on microorganisms, including *E. coli*.[81,87,88] The general consensus appears to be that partial pressures of oxygen higher than those found in air are toxic to microorganisms and inhibit their growth, but that this effect is less pronounced in a robust organism such as *E. coli*. Growth inhibition has been noted in *E. coli* in the presence of pure oxygen when minimal medium is used. It is thought that the absence of CO_2 contributes to this inhibition.[89] Although it is known that CO_2 can inhibit microbial growth, some CO_2 may be needed by a culture growing in minimal medium for the biosynthesis of essential compounds. In a complex medium these compounds may already be present. Alternatively, fermentation of substrates within the complex medium may provide sufficient CO_2 to meet the needs of the cells. In either case, the lack of CO_2 is not inhibitory. As a result, *E. coli* grown in complex medium under pure oxygen conditions does not seem to show inhibited growth. The focus of the present microbioreactor study was the effect of increased oxygen levels on *E. coli* growth.

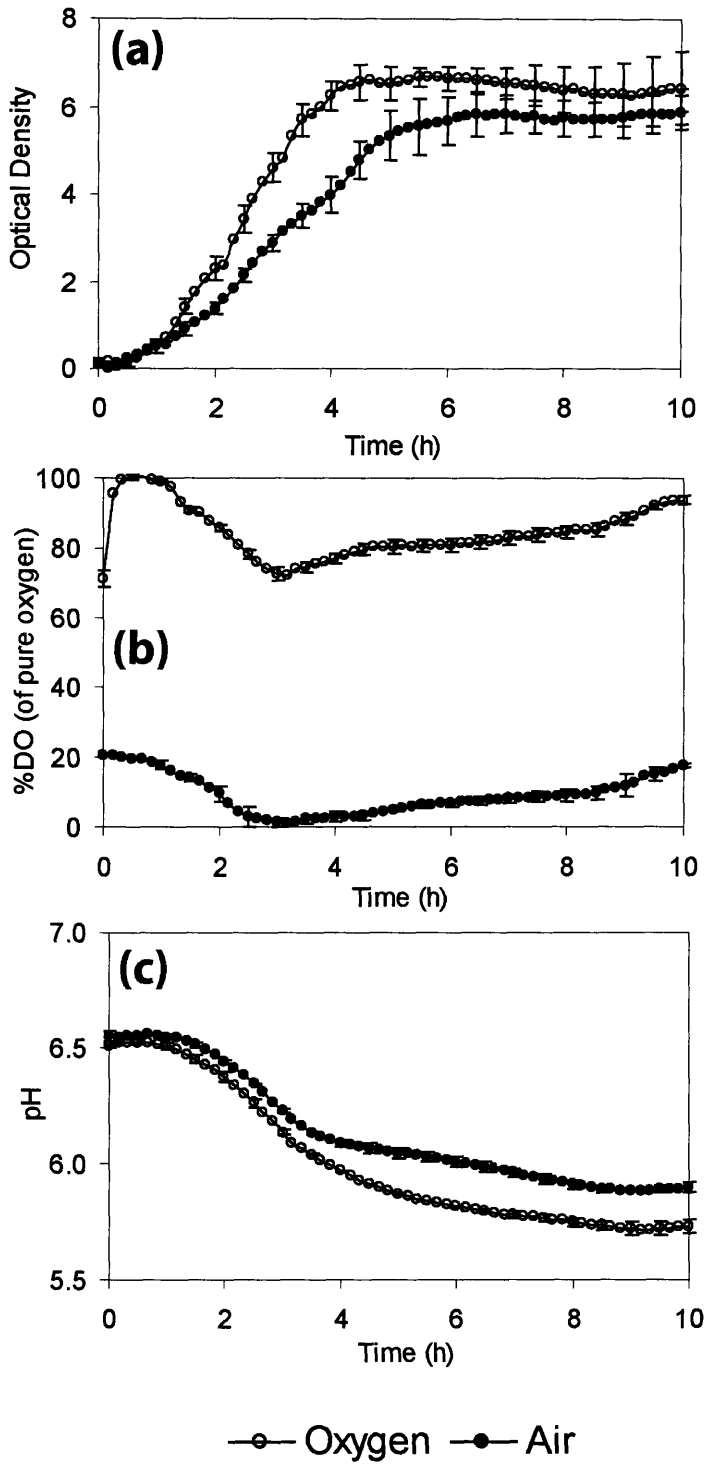

Figure 2-8. Comparison of (a) optical density, (b) dissolved oxygen, and (c) pH with *E. coli* grown in LB medium in a microbioreactor with air (*n=3*) and oxygen (*n=3*) in chamber headspace. Data are averaged over *n* runs, error bars report standard error.

In the presence of pure oxygen the initial maximum growth rate (Figure 2-8a) does not appear to be different than the growth rate in the presence of air, but the bacteria are able to maintain it for a longer period of time. This is supported by the calculated doubling time in each case. With air in the headspace $t_d = 28 \text{ min} \pm 3$ min, and with oxygen in the headspace $t_d = 24 \text{ min} \pm 6$ min. The overlapping error bars indicate that the difference in the mean is not statistically significant (at one standard error). The maximum optical density (and thus cell count) is somewhat higher when pure oxygen is used compared to air. As stationary phase progresses, however, the optical density of cells under pure oxygen decreases until the curve coincides with the air curve. This effect could possibly be attributed to higher rates of cell lysis under pure oxygen conditions.

When pure oxygen is contacted with the aeration membrane (Figure 2-8b), the oxygen within the medium shows a minimum but never depletes entirely. The lowest oxygen level that the bacteria encounter is approximately 70%. This oxygen level is still three times higher than the maximum oxygen level with air as the contacting gas. In the case of the pH time course within the microbioreactor (Figure 2-8c) the error bars, representing standard error, do not show overlap at any time point beyond the beginning of the fermentation. The curves show that the pH experiences a sharper drop in the presence of oxygen than in the presence of air. This is consistent with the higher growth observed in the OD curve in the presence of pure oxygen. Since the major source of protons in the medium comes from the protons that are excluded as ammonia (existing as NH_4^+ in the medium) crosses the cell membrane and is internalized as NH_3,[90] more growth would be expected to lead to a higher rate of proton generation, and subsequently a lower pH. At the end of fermentation runs with oxygen, bacteria exhibit normal morphology.

2.4. Conclusion

We have demonstrated the operation of a microbioreactor with a volume as low as 5 $\mu\ell$ containing integrated, automated sensors for the measurement of OD, DO, and pH. We have shown that results from the microbioreactor are reproducible in both complex medium (LB) and defined medium, and that we are able to understand the oxygen transfer characteristics of the microbioreactor and effectively model growth and oxygen consumption of the bacteria during a fermentation. We have also shown that it is possible to sequentially sacrifice microbioreactors that are running in parallel to carry out off-line analysis using traditional techniques. Finally, we have shown that results obtained from the microbioreactor correspond closely with results obtained in bench-scale volumes. This suggests that our microbioreactor can effectively bridge the gap between current high-throughput processes that yield little data, such as microtiter plates, and scale-up to increasingly large fermentors that approach production scale. In effect, microbioreactors have the potential to provide much of the data and functionality that a large bioreactor system makes available while offering the advantages of high-throughput processes, in terms of labor, time, and cost.

Future work on the microbioreactor bioprocessing platform will need to address integration and streamlining of the fluid handling. In particular, the incubation and preculture stages are both time- and labor-intensive. The ability to go from inoculation with cells from a plate to a completed fermentation run on a single device would greatly reduce both the effort involved in preparing for and running fermentations, as well as sources of error associated with current transfers between stages. Future efforts should also involve the integration of additional sensors into the microbioreactor. In particular, a sensor for the measurement of CO_2 is desirable.[91] The ability to measure the level of CO_2 in the medium as well as in the off-gas would allow the

closing of the carbon balance on the system. This would enable experiments such as isotopic studies and flux analyses to be carried out on a large scale with minimal quantities of reagent.

Chapter 3. *In Situ* Measurement of Bioluminescence and Fluorescence in an Integrated Microbioreactor

3.1. Introduction

Light emission from luminescent and fluorescent bacteria (and more recently, yeast) created to act as reporters for various environmental conditions is finding application in several areas of biology, including toxicity assays for environmental pollutants, chemical detection, and gene expression profiling.[7-12]

The importance of bioluminescence as a marker for gene expression was first recognized by Engebrecht,[92] who used a DNA fragment from the marine bacteria *Vibrio fischeri* to construct recombinant *Escherichia coli* strains that produced light in response to transcriptional activation of a specific gene. This practical application was established while the biochemistry of luminescence was being elucidated.[93-95] The use of green fluorescent protein (GFP) as a gene expression marker was first described by Chalfie,[96] the properties of GFP having been described by Shimomura[97] and later by Morin[98] and Morise.[99]

There are three major areas in which luminescent and fluorescent reporters are being used. The first is for nonspecific environmental reporting. For these applications, the *lux*[13-16] or *gfp*[17-20] cassette is fused to a stress response promoter that responds to a number of environmental and chemical stresses. For instance, the heat shock response is activated whenever environmental conditions cause changes in protein structure, and the SOS regulatory circuit is activated in response to DNA damage. A second area is that of monitoring for specific substances in the environment. Examples include reporters for metals[100,101] and organic compounds.[102-104] Finally, libraries of strains have been developed in which *lux* and *gfp* fusions representing large portions

of the bacterial genome can be used as an alternative to microarray technology[105] and for clarifying metabolic pathways.[106-109] Similar examples of these applications exist with yeast as the model organism.[110-112]

The choice between the use of luminescence and fluorescence is application-specific. The advantages of the *lux* system are a faster response time[13,113] and a lower limit of detection due to the lack of interference that cellular autofluorescence causes when *gfp* is used.[113] The advantages of *gfp* include the fact that *gfp* has not been found to be a self-regulator like *lux*,[114] and that the response of autofluorescent *gfp* is independent of substrate concentrations in the medium as is the case with *lux*.

For all of the applications discussed, it is clearly desirable to have the ability to carry out multiple fermentations in parallel. Currently, high-throughput experiments with fluorescent and luminescent bacteria are generally carried out on agar plates,[115] or in microtiter plates[109] or shake flasks. These approaches yield limited data since many growth parameters cannot be measured on-line in such systems. Alternatively, when growth data is needed, bioreactors are used.[116,117] However, this approach is both costly and time-consuming. Furthermore, because the fluorescent/luminescent response is frequently used as an indicator for gene expression, the very nature of the experimental design dictates that a large number of experiments are needed.

The ability to measure the fluorescent/luminescent response in integrated, multiplexed microbioreactors would allow an experimenter to run multiple small-scale experiments in parallel, thus greatly decreasing the resources needed per experiment, as well as increasing the number of experiments that could be run. In addition, the use of a microbioreactor with integrated sensors allows the collection of additional data that are not generally available when shake flasks and microtiter plates are used, such as growth kinetics, dissolved oxygen over time,

and pH over time. The microbioreactor system that we have previously described could potentially provide the needed platform (Chapter Two of this thesis).[118]

Our model system for measurements of luminescence is a collection of *E. coli* strains provided by DuPont Company. These strains have been created using transcriptional fusions of the *luxCDABE* operon to bioluminesce in response to specific environmental stresses.[14,105,119] We have shown that we can induce and detect bioluminescence in microbioreactors by exposing the bacteria to a known stress (e.g. lack of nutrient), and we have compared the results to those obtained in bench-scale bioreactors under similar conditions. Experiments in which fluorescence was measured were carried out with an *E. coli* strain that carried a constitutive promoter fused to *gfp*. These experiments were also repeated at a larger scale, in shake flasks.

3.2. Materials and Methods

3.2.1. Microbioreactor

Fermentations were carried out in 50 μℓ poly(dimethylsiloxane) microbioreactors in which oxygenation occurred through a gas-permeable membrane (Figure 3-1). The depth of the microbioreactor well was 300 μm, and the thickness of the aeration membrane was 100 μm. Sensors for dissolved oxygen and pH were embedded in the bottom of the well. During experiments, the microbioreactor was housed in a chamber that controlled temperature and maintained high humidity. Additional details on fabrication and sensor placement may be found in Zanzotto et al.[118]

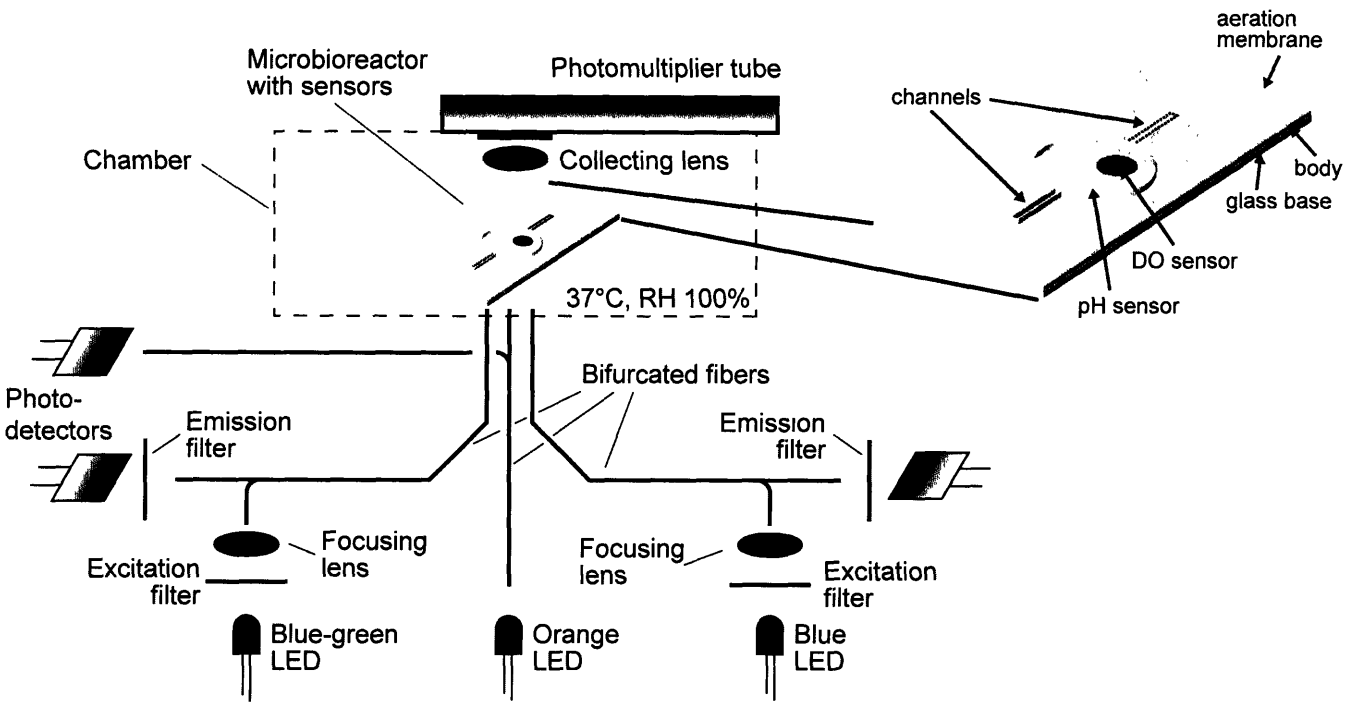

Figure 3-1. Schematic of the microbioreactor and experimental setup. Both the DO sensor and the pH sensor are used during luminescence measurements. Only the DO sensor is used during fluorescence measurements because of the overlap between the excitation and emission spectra between green fluorescent protein (GFP) and the pH sensor.

3.2.2. Analytical methods

3.2.2.1. Dissolved oxygen

Dissolved oxygen (DO) was measured using fluorescence lifetime.[54-56] The DO sensor (PSt3, PreSens, Germany), located at the bottom of the microbioreactor, was excited with a square-wave modulated blue-green LED (NSPE590S, Nichia, 505 nm). An exciter bandpass filter (XF1016, Omega Optical) and an emission longpass filter (XF3016, Omega Optical) separated the excitation and emission signals and minimized cross-excitation. Data switches (8037, Electro Standards Laboratories) multiplexed the output signal and the input signal of the function

generator (33120A, Agilent Technologies) and the lock-in amplifier (SR830, Stanford Research Systems), respectively. The lock-in amplifier measured and output the phase shift between the excitation and emission signals for the DO measurement, which were correlated to a dissolved oxygen concentration.

3.2.2.2. pH

During experiments in which luminescence was followed, pH was measured using fluorescence lifetime.[58,59] The pH sensor (HP2A, PreSens, Germany), located at the bottom of the microbioreactor, was excited with a square-wave modulated blue LED (NSPB500S, Nichia, 465 nm). An exciter bandpass filter (XF1014, Omega Optical) and an emission longpass filter (XF3018, Omega Optical) separated the excitation and emission signals and minimized cross-excitation. The signal was collected and analyzed using the same procedure as for the DO measurement. pH measurements were not made during runs in which GFP fluorescence was measured due to the overlap between the excitation and emission spectra of GFP and the pH sensor. (GFP absorbs light at two wavelengths: 395 nm and 470 nm. We found a stronger emission intensity when the excitation wavelength of 470 nm was used. The maximum intensity of the resulting emission signal was at 510 nm).

3.2.2.3. Optical measurements using a photomultiplier tube

A photomultiplier tube (R928, Hamamatsu) located directly above the microbioreactor was used to measure luminescence, fluorescence, and optical density. Initial experiments used a hand-held multimeter (Fluke 189, Fluke) to take direct current measurements. In later experiments, the current was passed to a low-noise current preamplifier (Model SR570, Stanford Research Systems) that converted the signal to a voltage (at a sensitivity setting of 20 μA/V) that

was then passed to an automated multimeter (Fluke 45, Fluke). Luminescence was measured continuously and readings for optical density were taken every 10 minutes. Operational characteristics of the PMT were determined to ensure correct numerical analysis. The PMT was found to have an anode luminous sensitivity of 1419 A/lm and an anode dark current of 0.03 nA. The signal-to-noise of the PMT with a dark chamber was approximately 30 (after sufficient warm-up time for the PMT, approximately one hour), and the calculated minimum detectable luminescence signal was approximately 100 photons/second (two standard deviations above the mean background signal).

3.2.2.3.1. Luminescence

Light was collected above the microbioreactor using a plano-convex lens (LA1131-A, Omega) and passed to the PMT. Luminescence was measured as the total signal minus the background, in the absence of all other light. Measurements of luminescence light intensity are presented in arbitrary units. For figures in which luminescence appears with other measurements, it was scaled to fit on an existing axis. For the analysis of reproducibility, the luminescence signals were adjusted to match their maximum signal amplitudes. This was done to compensate for the positioning of each microbioreactor within the chamber. Because the microbioreactors are not necessarily centered beneath the collecting lens, the absolute magnitude of the luminescence signal varies somewhat between experiments. The relative signal intensity over time is the critical factor.

3.2.2.3.2. Fluorescence

Excitation light from a blue LED (NSPB500S, Nichia, 465 nm) was passed through a collimating lens, a bandpass filter (XB78, Omega), and a collecting lens before being split using

a bifurcated cable. Half of the light was sent to a photodetector to monitor the excitation intensity, and the other half was passed inside the chamber, directly beneath the microbioreactor. The emitted light (maximum intensity at 510 nm) was collected using a plano-convex lens (LA1131-A, Omega) and passed through a longpass filter (XF3092, Omega) before it was collected by the PMT. Measurements of fluorescence intensity were scaled for the purpose of graphing, and are presented in arbitrary units.

3.2.2.3.3. Optical density

Optical density, calculated from a transmission measurement at 600 nm, was used to monitor biomass. Light from an orange LED (Epitex L600-10V, 600nm) was passed through the microbioreactor, collected by a plano-convex lens (LA1131-A, Omega), and sent to the PMT. During experiments with luminescent bacteria, the optical density was calculated from the total measured signal minus the magnitude of the signal due to luminescence and background. During experiments with fluorescent bacteria, the measured signal was not corrected for alternate sources of light. The optical density was calculated using Equation 3-1.

$$OD = 33.33 \log_{10}\left(\frac{I_{reference}}{I_{signal}}\right) \qquad (3\text{-}1)$$

In this equation I_{signal} is the intensity of the signal and $I_{reference}$ is the intensity of the first measurement for a given experiment. The multiplication factor of 33.33 in Equation 3-1 is a normalization for the pathlength of 300 μm in the microbioreactor which enables direct comparisons with results from conventional cuvettes with pathlengths of 1 cm. Calibration data from the microbioreactor using known concentrations of *E. coli* show that the measurements are

within the linear region.

3.2.3. Biological methodology

3.2.3.1. Organisms and medium

Experiments involving bioluminescence were carried out using *Escherichia coli* strains DPD2276 and DPD2417 obtained from DuPont Company. Plasmids pDEW257 and pDEW657 are members of a collection of plasmids containing random *Escherichia coli* genomic fragments fused to a *Photorhabdus luminescens luxCDABE* reporter that has been described previously.[105] Plasmid pDEW257 contains the *gyrA* promoter region, *E. coli* nucleotides 2336048 to 2337993,[120] joined to the *luxCDABE* reporter in the appropriate orientation. Plasmid pDEW657 contains the *nirB* promoter region, *E. coli* nucleotides 3490135 to 3491711.[120] DPD2276 and DPD2417 are the transformants of *E. coli* strain DPD1675[119] containing plasmid pDEW257 and pDEW657, respectively. Initial characterization of DPD2276 revealed that it produced very bright, essentially constitutive bioluminescence. By contrast, the bioluminescence of strain DPD2417 was dramatically increased under oxygen limiting conditions, due to the regulation of *nirB* expression by the anaerobic regulatory protein Fnr.[121] Both of these *E. coli* strains contain an ampicillin resistance marker on the plasmid.

Experiments involving fluorescence were carried out using an *Escherichia coli* strain that constitutively expresses green fluorescent protein. We used strain JM83 {F^-ara Δ(lac-proAB) rpsL (Str^r) [ϕ80dlacΔ(lacZ)M15]},[122] transformed with plasmid pCF56. This plasmid was constructed by cloning *gfp* under the control of the constitutive promoter CP25,[123] into plasmid pKAN,[124] which carries kanamycin and ampicillin resistance cassettes.

Stock cultures were maintained at -80°C in 20% (vol/vol) glycerol. Prior to fermentation

experiments, single colonies were prepared by streaking out the frozen cell suspension onto LB plates containing 2% (wt/vol) agar and either 100 μg/mℓ of ampicillin (DPD2276 and DPD2417) or 100 μg/mℓ of ampicillin and 100 μg/mℓ of kanamycin (JM83). The plates were then incubated overnight at 37°C to obtain single colonies, and subsequently stored at 4°C for up to a week or used immediately to inoculate precultures.

For all fermentations we used Luria-Bertani medium, which contained: 10 g/ℓ tryptone (Difco Laboratories), 5 g/ℓ yeast extract (Difco Laboratories), and 5 g/ℓ NaCl. The solution was autoclaved for 40 minutes at 120°C and 150 kPa.

3.2.3.2. Precultures

For all experiments, 5 mℓ of sterile LB medium were transferred into test tubes. The appropriate antibiotics were added and each tube was inoculated with a single colony of *E. coli*. These cultures were incubated on a roller at 60 rpm and 37°C. Once the cultures reached an OD of 1, medium was removed from each test tube and transferred to a 500 mℓ baffled shake flask containing 35 mℓ of fresh medium to a starting optical density of 0.05. The inoculated shake flasks were incubated on shakers (150 - 200 rpm) at 37°C and grown to OD = 1. The medium was then used to inoculate bench-scale bioreactors, shake flasks, or microbioreactors to a starting OD of 0.05.

3.2.3.3. Bench-scale bioreactor

Batch cultures were grown in 500 mℓ SixFors bioreactors (Infors, Switzerland) with a starting medium volume of 450 mℓ. Dissolved oxygen probes (405 DPAS-SC-K8S/200, Mettler Toledo) were calibrated with nitrogen gas (0% DO) and air (100% DO) prior to each run. pH probes (InPro 6100/220/S/N, Mettler Toledo) were calibrated with buffer at pH 7.0 and 4.0

(VWR).

The aeration rate of gas was set to 1 VVM (volume of gas per volume of medium per minute) and the impeller speed was set to 500 rpm. The temperature of the vessels was maintained at 37°C for all fermentations. Dissolved oxygen and pH were not controlled, so as to simulate the batch microbioreactor. The time courses of temperature, dissolved oxygen, and pH were recorded every 10 minutes throughout all fermentations. Biomass was monitored by removing samples from the bioreactor at defined time intervals and measuring the optical density at 600 nm on a spectrophotometer (Spectronic 20 Genesys, Spectronic Instruments). Luminescence was measured with an off-line luminometer (Optocomp I, MGM Instruments).

3.2.4. Shake flasks

Shake flasks with a volume of 500 mℓ, containing 35 mℓ of fresh medium, were inoculated to a starting optical density of 0.05. Between readings they were housed in an incubator at 37°C and 150 rpm. Samples were removed periodically to measure OD and fluorescence. Fluorescence intensity measurements were taken using a fluorimeter (Fluorescence Spectrophotometer, F-4500, Hitachi Instruments). An excitation wavelength of 470 nm was used with a slit width of 5 nm. Emission was measured at a wavelength of 510 nm with a slit width of 5 nm. The detector voltage was 700 V.

3.2.5. Microbioreactor

Inoculation of the medium for the microbioreactor was carried out outside of the bioreactor. Ten milliliters of fresh medium were transferred to a Falcon conical tube, and to this was added the preculture medium from a shake flask for a starting optical density of 0.05. This inoculated medium was then introduced into the microbioreactor by injecting the liquid via channels (Figure

3-1). The headspace of the chamber was filled with air for all experiments except for the fermentation of DPD2417 in which oxygen depletion was avoided by using pure oxygen.

3.3. Results and Discussion

The bioluminescence of *E. coli* DPD2276 is shown in Figure 3-2. *E. coli* DPD2276 contains a plasmid-borne *gyrA-luxCDABE* gene fusion resulting in strong, essentially constitutive bioluminescence. The total measured luminescence would therefore be expected to increase in proportion to biomass, as the figure demonstrates. Results indicate that luminescence is associated with cell growth and drops off as the culture reaches stationary phase. This is in agreement with previous studies which demonstrated that peak induction and the response time to peak bioluminescence are closely correlated with the growth rate, and that both maximum induction and the most rapid response time occur during mid-exponential phase.[14]

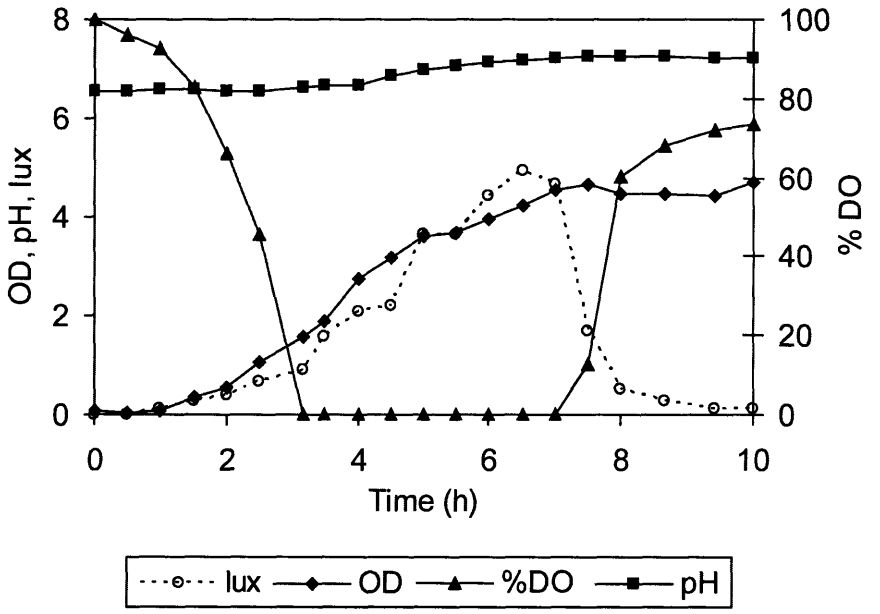

Figure 3-2. Total luminescence (lux), optical density (OD), dissolved oxygen (%DO), and pH in a microbioreactor for an *E. coli* strain constitutive for the expression of the *lux* operon.

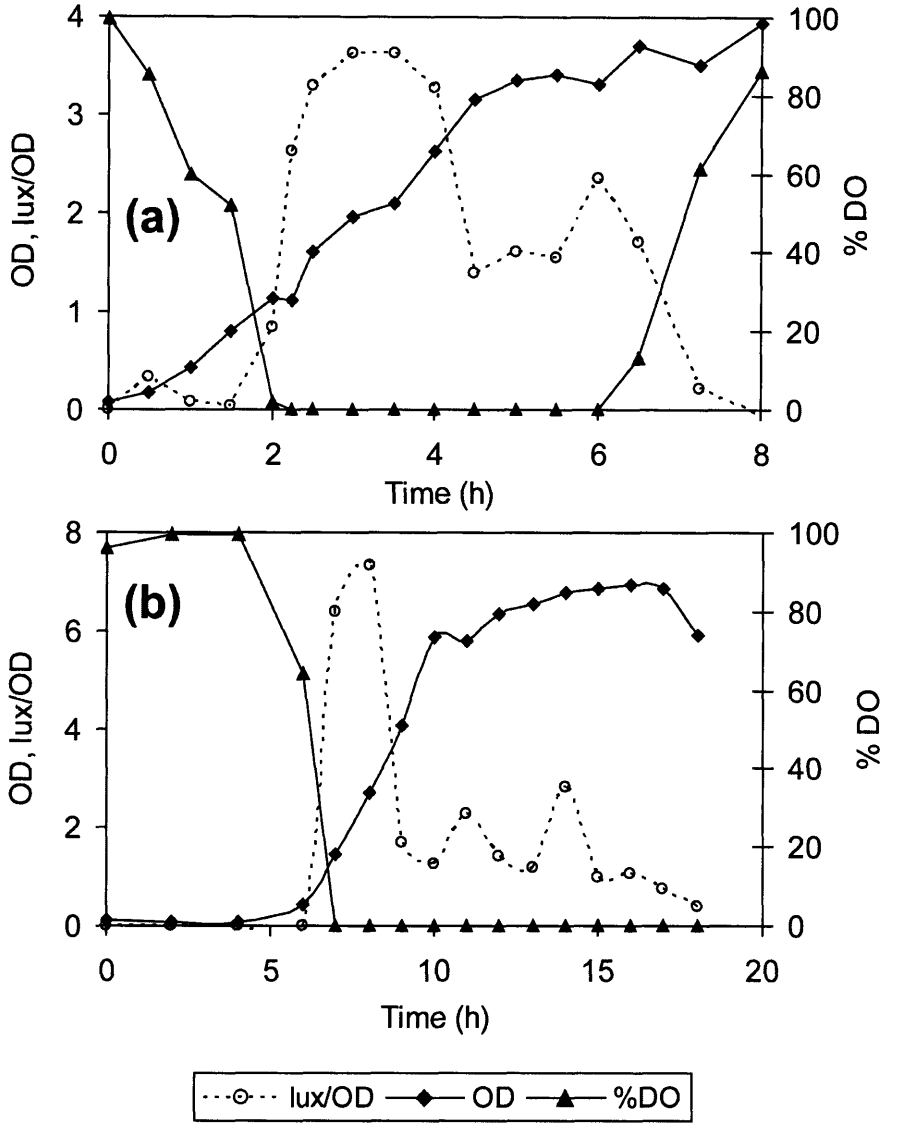

Figure 3-3. Specific bioluminescence (lux/OD), optical density (OD), and dissolved oxygen (%DO) for an anaerobiosis-sensitive strain of *E. coli* in (a) a microbioreactor and (b) a bench-scale bioreactor.

Fermentation of *E. coli* DPD2417 under oxygen limitation is shown in Figure 3-3. *E. coli* DPD2417 carries an anaerobically-regulated *nirB-luxCDABE* gene fusion that is expressed as the oxygen level in the medium drops. In a microbioreactor the strain experiences a sharp peak in specific luminescence (luminescence in arbitrary units/OD) when the dissolved oxygen in the medium depletes (Figure 3-3a). A similar response can be seen in a 500 mℓ bench-

scale bioreactor (Figure 3-3b). By contrast, when pure oxygen is supplied to the microbioreactor, no luminescence response is seen (Figure 3-4).

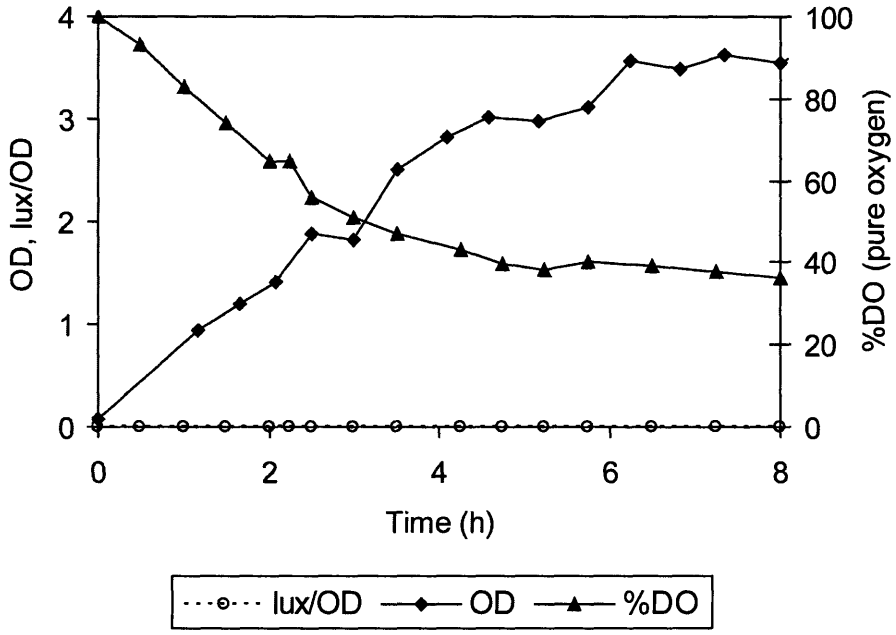

Figure 3-4. Specific bioluminescence (lux/OD), optical density (OD), and dissolved oxygen (%DO) for an anaerobiosis-sensitive strain of *E. coli* in a microbioreactor when oxygen is used as the contacting gas.

Replicates of the oxygen-level induction in the microbioreactor were performed to examine the reproducibility of the bioluminescence response and measurement (Figure 3-5). When the raw luminescence (a.u.) is plotted as a function of the oxygen level inside the microbioreactor (Figure 3-5a), a strong initial bioluminescence peak is seen as the oxygen level depletes. A secondary peak occurs as the oxygen level begins to recover. This is consistent with the growth association of the luminescence response. As stated previously, expression of the lux operon, as well as the different rates of synthesis and degradation of the five *lux* proteins, is closely correlated with the growth rate of the cell. In addition, oxygen is necessary for the luciferase-

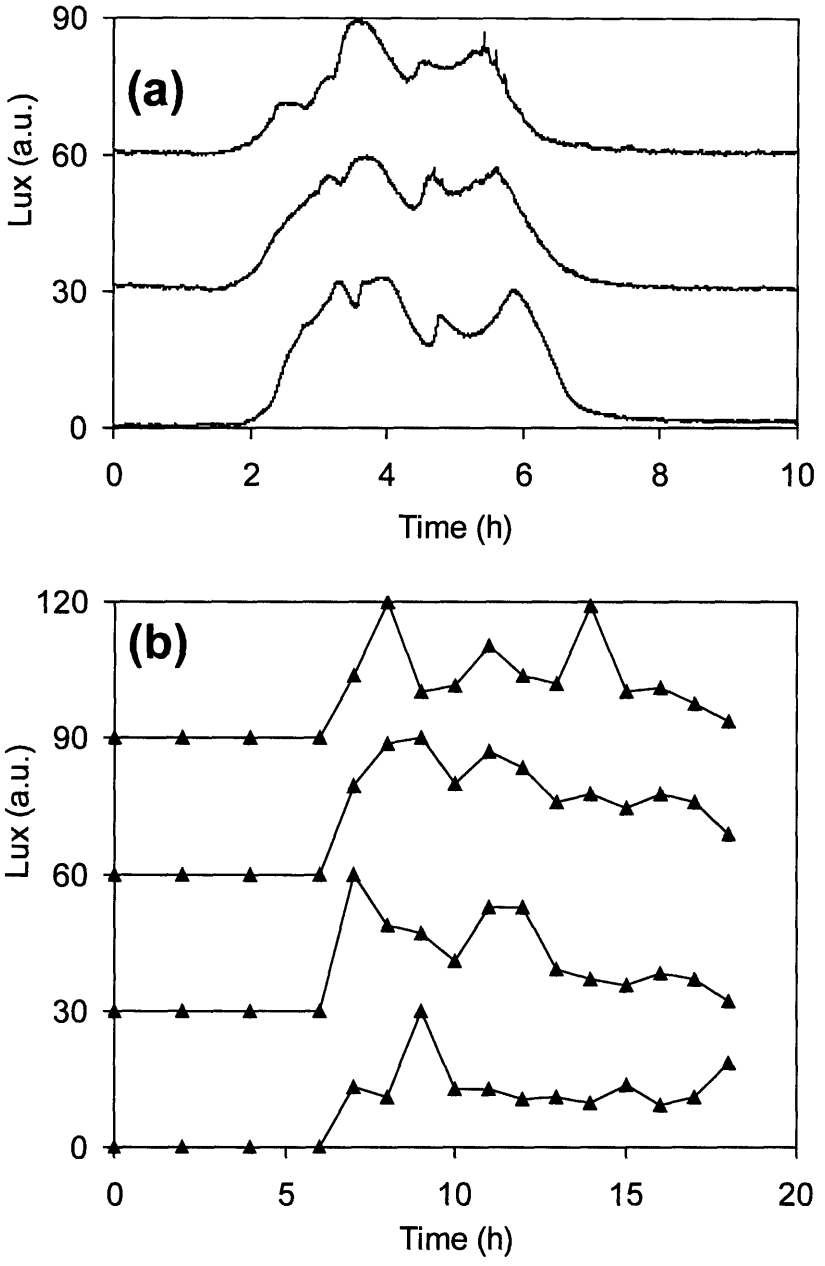

Figure 3-5. Luminescence measurements of an anaerobiosis-sensitive strain of *E. coli* during independent experiments in (a) a microbioreactor and (b) a bench-scale bioreactor. All curves were scaled to have the same luminescence intensity range. Curves on each plot are offset for clarity.

catalyzed reaction to occur. Therefore, it is expected that the bioluminescent signal would increase temporarily as oxygen levels in the microbioreactor begin to recover.

By contrast, in the Sixfors only the initial peak is seen to be reproducible (Figure 3-5b). One possible reason for this is the difficulty of obtaining accurate measurements of luminescence due to the Inner Filter Effect (IFE). The IFE occurs because while cells emit light (emission) they also absorb and scatter this emitted light (extinction), thereby diminishing the measured quantity. The IFE becomes more significant at higher cell densities and must be accounted for if the true level of bioluminescence is to be known. For example, it has been found that in a luminescing bacterial culture at an optical density of 40, the light is attenuated three- to four- fold.[125] The IFE also affects fluorescence readings made in turbid media. Researchers have presented data that suggest that extremely large errors appear at OD values close to 1.0.[126] Other researchers have shown that significant deviations have been found with OD values as low as 0.2.[127] When the IFE of bacterial bioluminescence has been studied, it was found that OD values above 0.3-0.6 caused a decrease in the measured luminescence.[125] In measurements of bioluminescence, the IFE can be compensated for in one of two ways. In direct, on-line measurements, an algorithm can be used to correct for the light attenuation.[125,126] The drawback is that a model must first be fit to existing data and validated, thus necessitating previous knowledge of bacterial behavior. Alternatively, samples can be removed, diluted to a sufficiently low cell concentration, and measured off-line in a luminometer. The difficulty with this approach, apart from the obvious increase in labor that this entails, is that the bioluminescence reaction is extremely sensitive. In particular, dilution of the culture fails to accurately represent the bioluminescence of the original solution. It is hypothesized that this may be caused by a decrease in the concentration of the bioluminescence reaction substrates, most probably the long-chain aldehyde. Therefore, there is no simple, accurate method with which to account for the IFE in a large bioreactor at high cell density.

On the other hand, the wide aspect ratio of the microbioreactor results in a much shorter pathlength that is "seen" by the measuring instrument. The result is that absolute optical densities (before a pathlength correction factor is applied) in the microbioreactor are typically below 0.5. Therefore the IFE is diminished, and accurate measurements of bioluminescence can be made allowing real-time gene expression measurements. In this way, one of the most promising features of gene expression reporters can be realized.

Detection of *E. coli* JM83 fluorescence is shown in Figure 3-6. It can be seen that in both microbioreactors and shake flasks, specific fluorescence (fluorescence/optical density) increases throughout the bacterial growth cycle. As with the measurement of bioluminescence, it is possible that in the microbioreactors the effects of high cell density on light attenuation are avoided as a result of the low levels of absolute optical density as calculated from transmittance measurements.

3.4. Conclusions

Real-time monitoring of bioluminescence and fluorescence of bioprocesses is an important tool as gene expression markers become widely used in toxicity assays, chemical detection, and gene expression profiling. In particular, the ability to link bioluminescence and fluorescence measurements to multiple, parallel studies of bacterial growth would provide great flexibility in applying these methods, particularly in the area of gene expression analysis where a large number of experiments must be run. We have demonstrated the measurement of both bioluminescence and fluorescence in a microbioreactor. We have used an *E. coli* strain sensitive to anaerobiosis to indicate the presence of oxygen depletion, and compared the response to a growth situation where oxygen limitation does not occur to demonstrate the feasibility of using reporter strains as environmental markers. We have also examined the reproducibility of the

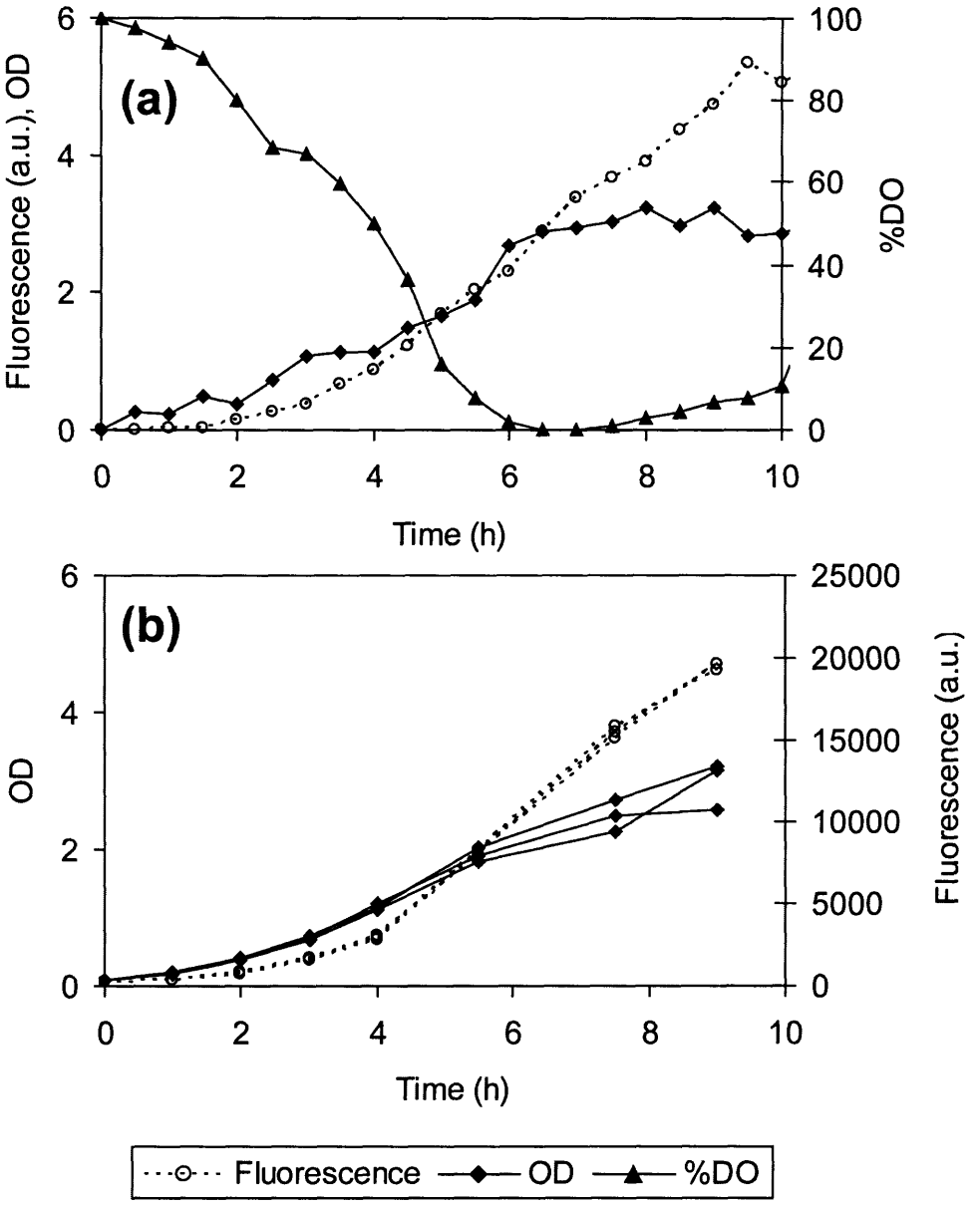

Figure 3-6. Optical density (OD), dissolved oxygen (%DO), and fluorescence for a strain of *E. coli* that expresses green fluorescent protein (GFP) constitutively in (a) a microbioreactor and (b) a shake flask.

luminescence response and compared it to the reproducibility achieved with off-line measurements from a bench-scale system. Our results suggest that the design and configuration of the microbioreactor allow a direct, on-line reading unhampered by the inner filter effect, and

thus more reliable and reproducible than measurements obtained with the necessity of off-line handling. One area in which this ability could have a great impact is that of genome-wide expression profiling. Currently, samples must be removed at set time points, and the data analyzed separately for each on a separate DNA microarray. The ability to monitor the expression of a gene in real-time (and, with parallel scale-out, potentially all of the genes for a given cell), would obviate the need for discrete analysis at different times and provide a true dynamic picture of cellular gene expression, where the kinetics of gene expression can be untangled and elucidated.

Chapter 4. Gene Expression Analysis of *Escherichia coli* Grown in Miniaturized Bioreactor Platforms

4.1. Introduction

Global gene expression analysis using DNA microarrays is a technique widely applied in general biological research and in specific fields such as drug screening, environmental testing, and clinical diagnosis.[61,62] The ability to combine global gene expression analysis and high-throughput screening of microbial growth parameters would allow the simultaneous rapid characterization of microbial strains at the physiological and molecular levels. The increasing availability of complete genomic sequences of microorganisms offers the unprecedented opportunity for detailed investigations of the functioning of these organisms. Genomic expression assays provide the ability to look at a single aspect of physiology, as well as to see the interaction of genes and operons with every other aspect of physiology.

To reach the goal of a rapid and informative high-throughput screening technology there remain two significant obstacles: first, as the techniques for DNA microarrays continue to be developed, an ongoing need persists for methods of performing microarrays on very small samples of bacterial cultures; second, of the many metabolic and genetic experiments that can now be designed and performed in bacteria, only a small fraction can be tested using standard culture systems. The number of culture conditions that can be tested using tubes, flasks and bench-scale bioreactors (with volumes between 0.5 and 10 liters) is limited due to the time required to obtain sufficient data, the effort required to obtain reproducible data, and the high costs of operation. In microbiological research there clearly exists a need for a biochemical platform with integrated sensors yielding real-time data on process parameters that would allow

high-throughput, parallel, and automated processing of a variety of microbial cultures under a variety of controlled conditions. Multidisciplinary efforts that link engineering and biology are generating novel miniaturized bioreactor platform devices that could allow the production of multiple disposable bioreactor units for high-throughput data analysis.[65,67,68,118,128,129] The 50 $\mu\ell$ bioreactor platform that was recently described by Zanzotto et al.[118] (Chapter Two of this thesis) is a step toward a system that can be economically scalable and can generate real-time data for optical density (OD), dissolved oxygen (DO), and pH, offering the advantages of high-throughput processes in terms of labor, time, reproducibility, and cost.

Zanzotto et al.[118] demonstrated that *E. coli* cultures grown in this microbioreactor platform exhibit reproducible growth characteristics in complex and minimal media; this included time curves of OD, DO, and pH as well as cell number and morphology, substrate uptake, and organic acid production. In these respects, growth of *E. coli* mimicked that seen in conventional culture conditions (e.g. shake flasks). We also demonstrated that serial harvest of microbioreactors was a feasible way to obtain samples for off-line analysis. The microbioreactor used to grow the cultures is fabricated using current bioMEMS and microfluidic technologies and is made out of poly(dimethylsiloxane) (PDMS) and glass and equipped with on-line measurements for OD, DO and pH. Aeration of cultures occurs through a gas-permeable PDMS membrane.

In the present study, we sought to determine whether cells grown in the microbioreactor format could be used in global gene expression studies using DNA microarrays as a step toward integrating high-throughput bacterial culture with high-throughput transcription profiling. To perform DNA microarray analysis for gene expression profiling we used Resonance Light Scattering (RLS) labeling technology. While microarray analysis is now well established, the technology continues to evolve, particularly toward more sensitive methods and the use of

amplification techniques.[130,131] Current protocols for prokaryotic DNA microarrays require 5 to 10 μg of total RNA as starting material; Bao et al.[132] reported high-sensitivity detection of DNA hybridization on microarrays of human genes using RLS technology which uses colloidal metal particles (between 40 and 120 nm in diameter) that efficiently scatter light for cDNA labeling. As detailed by Yguerabide and Yguerabide,[133] the light-emitting power of single RLS particle labels is an order of magnitude greater than fluorescent labels such as Cy3 and Cy5. More recently Francois et al.[134] have shown that it is possible to detect and identify bacterial pathogens with the RLS system from small culture volumes, starting with only 10 to 500 ng of total RNA. We performed global gene expression analysis with 500 ng of total RNA from *Escherichia coli* cultures grown in LB medium and in defined minimal medium in a 50 μℓ bioreactor, using the Genicon RLS system (Invitrogen, Carlsbad, CA) for cDNA labeling. The data compared favorably to similar microarray studies that have been conducted with bacterial cultures grown at larger scales. These growth conditions were chosen because two earlier studies compared gene expression analysis in *E. coli* grown in 50 mℓ volumes of the same media[135,136] and their findings could be used to validate our experiments.

4.2. Materials and Methods

4.2.1. Organism and growth conditions

All experiments were conducted using *Escherichia coli* FB21591 (*thi*C::Tn*5* -pKD46, Kan^R) obtained from the University of Wisconsin (www.genome.wisc.edu). Cultures were grown in Luria-Bertani medium (LB) or defined minimal medium (DM), both supplemented with 10 g/ℓ glucose.

The composition of LB is: 10 g/ℓ tryptone (Difco Laboratories, BD, Sparks, MD), 5 g/ℓ yeast

extract (Difco), and 5 g/ℓ NaCl. After sterilization, the medium was supplemented with final concentrations of 10 g/ℓ glucose (Mallinckrodt, Phillipsburg, NJ), 100 mM MES (pH 6.9) buffer (Sigma, St. Louis, MO), and 100 μg/mℓ kanamycin (Sigma). The 40% (w/v) glucose stock was autoclaved for 20 minutes at 120°F, 150 kPa; MES (2 M) and kanamycin (100 mg/mℓ) stocks were filter-sterilized.

The composition of the DM is: K_2HPO_4 [60 mM], NaH_2PO_4 [35 mM], $(NH_4)_2SO_4$ [15 mM], NH_4Cl [70 mM], $MgSO_4 \cdot 7H_2O$ [0.8 mM], $Ca(NO_3)_2 \cdot 4H_2O$ [0.06 mM], $FeCl_3$ [20 mM], $(NH_4)_6Mo_7O_{24} \cdot 4H_2O$ [0.003 μM], H_3BO_3 [0.4 μM], $CuSO_4 \cdot 5H_2O$ [0.01 μM], $MnCl_2 \cdot 4H_2O$ [0.08 μM], $ZnSO_4 \cdot 7H_2O$ [0.01 μM], glucose [10 g/ℓ], thiamine [100 μM], MES (pH 6.9) [100 mM], kanamycin [100 μg/mℓ]. Glucose, MES, and kanamycin were added to the medium as stock solutions (see above). Thiamine was also added as stock solution (100 mM), previously filter-sterilized.

For inoculum preparation the strain was first adapted to LB or DM as follows: for LB experiments, tubes with 5 mℓ of medium were inoculated with single colonies from overnight LB-kanamycin agar plates and incubated at 37°C on a roller drum at 60 rpm. When these cultures reached an optical density of 1 ± 0.1, the medium was used to inoculate 30 mℓ of fresh LB in 500 mℓ baffled shake flasks to an optical density of 0.05. The flasks were then incubated at 37°C on a horizontal rotary shaker at 150 - 200 rpm until the optical density reached 1. At this point the culture was transferred to fresh LB to an OD_{600} of about 0.05, and used to inoculate microbioreactors.

Precultures for inoculum preparation for DM experiments were carried out as described for LB, except that shake flasks and the inoculum contained defined minimal medium.

4.2.2. Microbioreactor fermentations

A microbioreactor fabricated from PDMS and glass[118] was used for all fermentations (Figure 4-1). A separate microbioreactor was fabricated for each experiment. PDMS formed the bottom layer (in which the sensors were embedded), the body of the fermentor, and the aeration membrane. The base support of the bioreactor was made of glass, which provided the necessary rigidity as well as optical access. The volume of the microbioreactor was 50 $\mu\ell$. The bottom layer of the microbioreactor contained two sensor foils (PreSens, Regensburg, Germany), one for dissolved oxygen and one for pH as described previously.[118] Experiments were carried out in an airtight, aluminum chamber (Figure 4-1). The chamber allowed control of humidity and gas composition above the microbioreactor membrane; it also provided a large thermal mass which stabilized the temperature at the desired set point of 37°C. Temperature was controlled by circulating water at 37°C through the chamber base.

Optical density was used to monitor biomass. It was calculated from a transmission measurement at 600 nm. Light from an orange LED (L600-10V, 600nm, Epitex, Kyoto, Japan) was passed through the microbioreactor, collected by a collimating lens (F230SMA-A, Thorlabs, Newton, NJ), and sent to a photodetector (PDA55, Thorlabs). The optical density was calculated using Equation 4-1.

$$OD = 33.33 \log_{10}\left(\frac{I_{reference}}{I_{signal}}\right) \qquad (4\text{-}1)$$

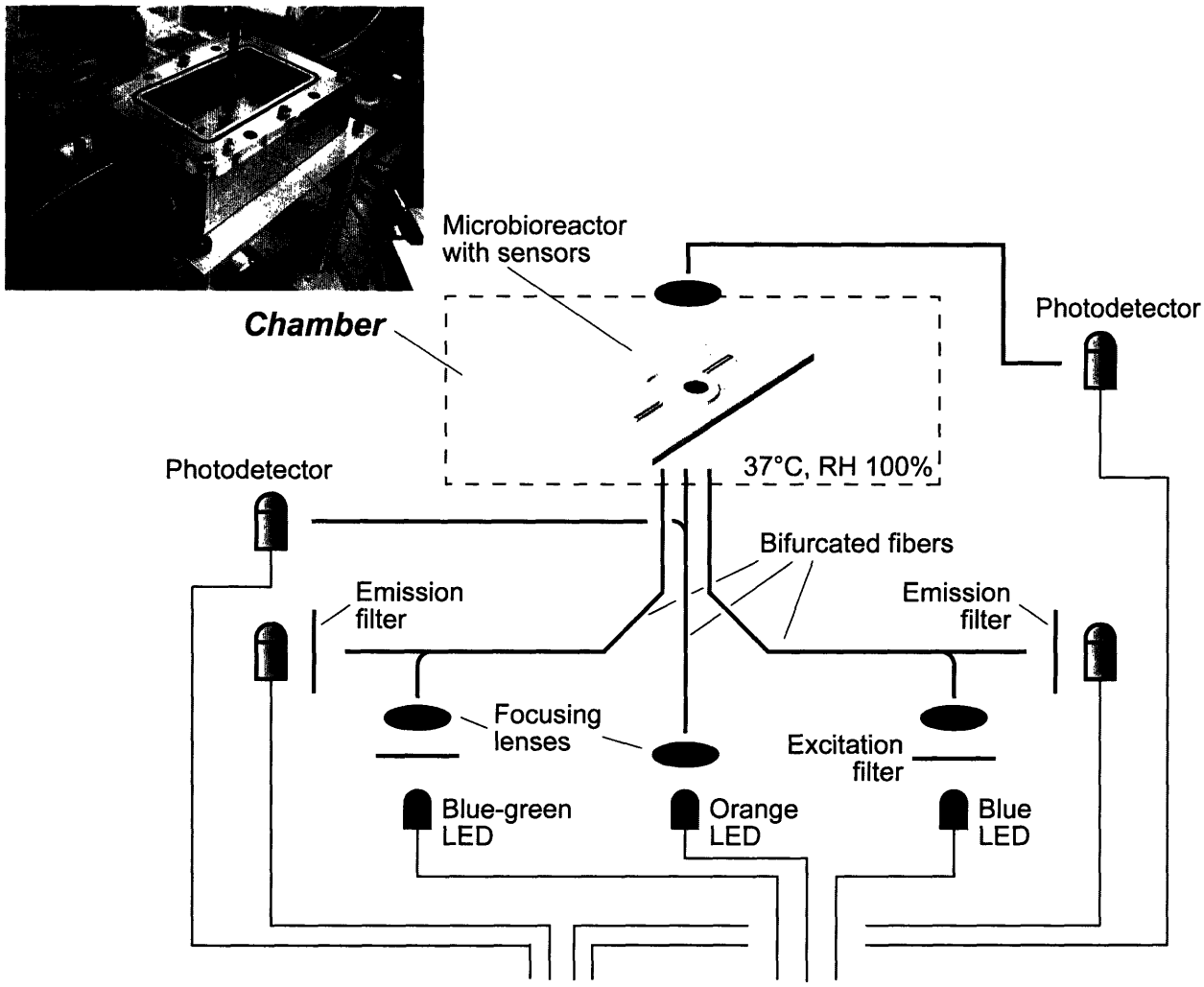

Figure 4-1. Schematic of the microfermentor and experimental set-up. After inoculation, the microbioreactor is placed inside the chamber. The chamber is kept at 100% humidity and 37°C. Three optical fibers carry three different wavelengths of light to the bottom of the microbioreactor for the three measurements: OD, DO, and pH. Photodetectors collect the transmitted or emitted light and send it to a lock-in amplifier where the signal is detected and analyzed.

In this equation I_{signal} is the intensity of the signal and $I_{reference}$ is the intensity of the first measurement for a given experiment. The multiplication factor of 33.33 in Equation 4-1 is used to normalize the data for the pathlength in the microbioreactor of 300 μm, which enables direct comparisons with results from conventional cuvettes with pathlengths of 1 cm. This adjustment is only strictly valid if the absorption and light scattering by the cell culture are in the linear

region. A calibration of optical density measurements in the microbioreactor was performed using serial dilutions of an *E. coli* culture grown to OD ~ 7. Optical density measurements of diluted cultures were made in a 300 μm-deep microbioreactor using a Spectronic 20 Genesys spectrophotometer (Spectronic Instruments Inc., Rochster, NY). The calibration data (Figure 4-2) produced a linear fit with a slope close to one.

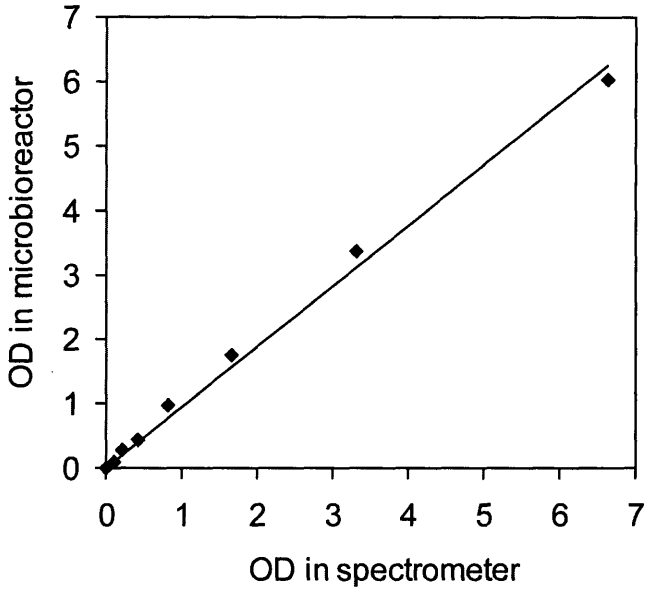

Figure 4-2. Calibration curve for optical density measurements in a microbioreactor. A dilution series of *E. coli* cells was used to compare direct measurements in a spectrophotometer with pathlength-adjusted measurements in the microbioreactor. Optical density was measured at 600 nm in both systems. Optical density in the microbioreactor was scaled to a pathlength of 1 cm from 300 μm.

Inoculation of the microbioreactor via the channels was carried out outside of the chamber using a needle and syringe. Following inoculation, the microbioreactor was secured to the base of the chamber. Open reservoirs of water were placed inside the chamber to provide humidity. Maintaining high humidity minimized evaporative losses through the PDMS membrane. The chamber was then closed and real-time data collection initiated. Sterility was maintained through

the addition of the antibiotic kanamycin to the growth medium. Additional details of the microbioreactor and its set-up are described by Zanzotto et al.[118] Triplicate fermentations of *E. coli* grown in LB and DM in 50 μℓ microbioreactors with on-line measurements of OD_{600}, DO, and pH are shown in Figure 4-3.

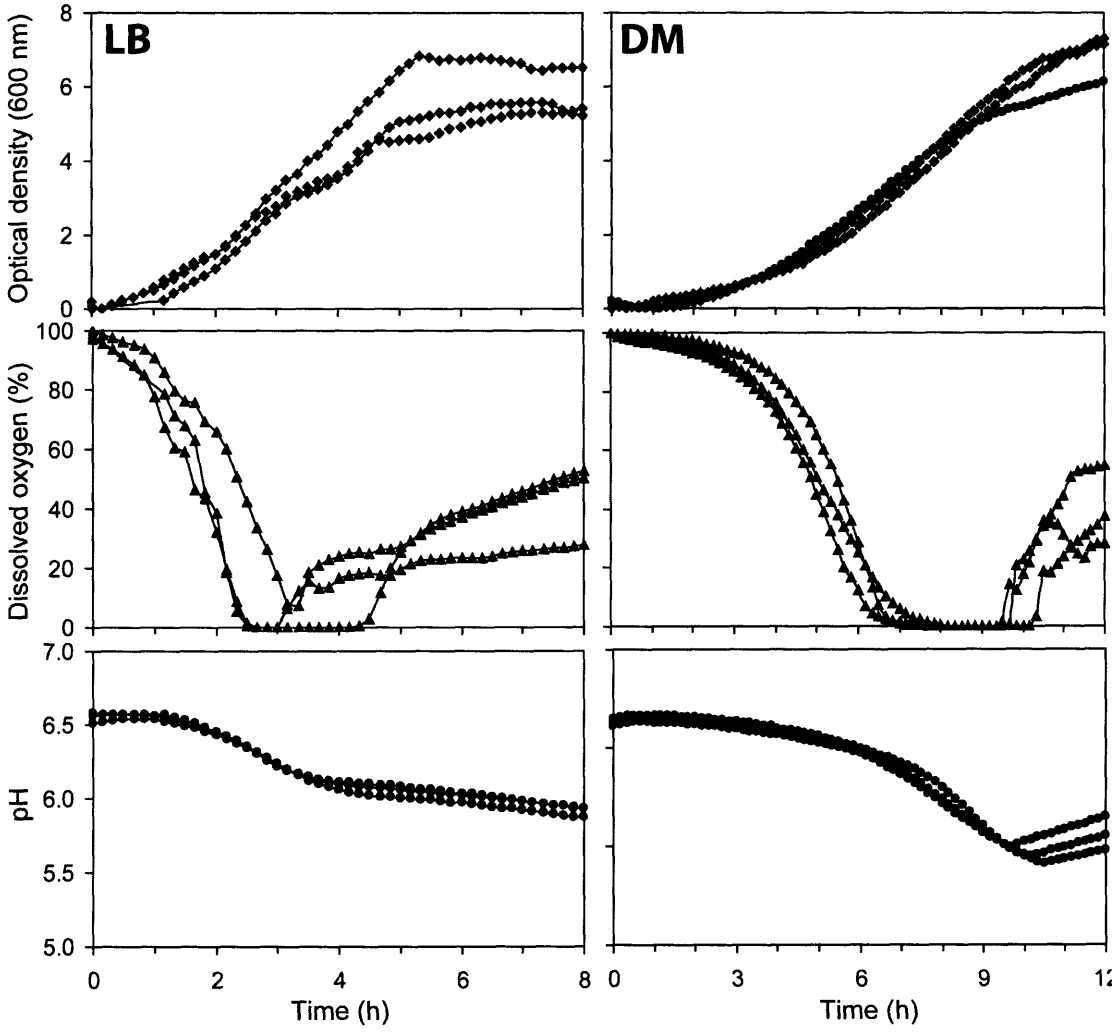

Figure 4-3. Fermentations *(n=3)* of *E. coli* grown in 50 μℓ microbioreactors in LB (left panels) and DM (right panels). The fermentations were performed on different days.

4.2.3. Total RNA isolation

Total RNA was isolated from three independent 50 μℓ fermentations in LB and DM. To isolate total RNA from these small volumes of culture we developed the following procedure: cells were harvested during exponential growth phase when they reached an OD_{600} of about 1.0, typically at a population density of 2-4 x 10^9 cells/mℓ culture fluid. Thus the number of cells recovered from 50 μℓ was 1-2 x 10^8 cells. To harvest cell cultures, the incubation chamber was opened and the culture withdrawn from the microbioreactor in its entirety with a 200 μℓ pipette. The culture was then transferred immediately to 1.5 mℓ Eppendorf tubes containing two volumes of RNAprotect Bacteria (Qiagen, Valencia, CA) for RNA stabilization. After 5 minutes of incubation at room temperature, the cells were precipitated by centrifugation, resuspended in 200 μℓ of TE (10 mM tris-HCl, 1 mM EDTA, pH 8.0) containing 15 mg/mℓ of lysozyme and incubated for 20 minutes at room temperature on a Nutator (Becton Dickinson, Parsippany, NJ) for gentle mixing. The cells were then transferred to 2 mℓ tubes (Sarstedt, Newton, NC) containing 50 mg of acid-washed 0.1 mm zirconia/silica beads (Biospec Products Inc. Bartesville, OK) and lysed in a FastPrep FP120 (Qbiogene, Carlsbad, CA) for 90 seconds at maximum speed. We found that we consistently obtained higher yields and better RNA quality if we performed a combination of enzymatic and mechanical cell disruption. Total RNA isolation was performed using an RNeasy kit (Qiagen) by loading the lysed sample, without the beads, directly onto RNeasy columns and then following the manufacturer's protocol. The concentration and quality of the purified RNA was assessed by the determination of the OD 260/280 ratio and analysis on an Agilent 2100 Bioanalyzer (Palo Alto, CA). RNA samples were stored at –80°C. The average yield of total RNA from 50 μℓ of *E .coli* culture grown in LB or DM to an OD_{600} of about 1 was approximately 3 μg and 1 μg, respectively.

4.2.4. Microarray hybridizations and analysis

DNA microarrays were printed at the MIT BioMicro Center (Cambridge, MA) with a BioRobotics MicroGrid Two printer (Genomic Solutions, Ann Arbor, MI) on Corning GAPS slides (Acton, MA) with a 50mers oligo set (MWG-Biotech Inc, High Point, NC) composed of 4,288 gene specific oligonucleotide probes representing the complete *E. coli* (K12) genome.

Microarray hybridizations were performed with the GeniconRLS two color array detection system (Invitrogen), based on RLS technology. From each fermentation, 500 ng of total RNA were used to generate cDNA labeled with Biotin-16-dUTP (Enzo Life Sciences, Inc., Framingdale, NY) for LB samples, and Fluorescin-12-dUTP (Roche Diagnostics, Indianapolis, IN) for DM samples. Direct labeling was performed with the LabelStar Kit (Qiagen) using a modified protocol as follows.

For each of the biotin-labeled reactions the labeling mix contained the following components: 5 $\mu\ell$ 10x Buffer, 5 $\mu\ell$ dNTP-Mix H, 1 $\mu\ell$ biotin-labeled dUTP, 1 $\mu\ell$ random DNA hexamers (Roche Diagnostics), 0.5 $\mu\ell$ RNase inhibitor, 2.5 $\mu\ell$ LabelStar Reverse Transcriptase, 15 $\mu\ell$ RNase-free water, and 20 $\mu\ell$ denatured RNA template. The fluorescein-labeled mixes were prepared as described for the biotin-labeled mixes except that 2 $\mu\ell$ of fluorescein-labeled dUTP and 14 $\mu\ell$ of RNase-free water were used. dNTP mixes contained 0.5 mM each of dATP, dCTP, dGTP and 0.04 mM dTTP. RNA templates were denatured before cDNA labeling by adding 2 $\mu\ell$ of denaturation solution to 18 $\mu\ell$ of RNA sample, followed by incubation for 5 minutes at 65°C in a water bath with subsequent cooling on ice.

Labeling mixes were incubated for 2 hours at 37°C in a thermocycler with a hot lid. One microliter of dTTP (20 mM) was then added to each labeling mix, and incubation at 37°C was continued for another hour. Reactions were then stopped with the addition of 2 $\mu\ell$ of stop

solution LS (Invitrogen). Purification of labeled cDNA was performed immediately using the LabelStar Kit (Qiagen). Purification of labeled cDNA was performed as directed in the protocol with the difference that each of the six samples was purified independently and that in the final step of the purification, each column was eluted twice with 50 μℓ of EB (Qiagen). Each 100 μℓ labeled cDNA sample was then diluted with 400 μℓ of RNase-free water. Next, one labeled cDNA sample generated from an LB culture and one labeled cDNA sample generated from a DM culture were pooled and concentrated to 12 μℓ with a Microcon Y-30 0.5 mℓ column (Millipore, Bedford, MA) as directed by the manufacturer.

Before array hybridizations were performed, microarray slides were baked in an oven at 80°C for 2 hours. After cooling, the slides were cross-linked with UV light in a Stratalinker 2400 (Stratagene, La Jolla, CA) at 300 mJ. Prehybridization was performed as directed by the manufacturer's protocol by incubating microarray slides for 30 minutes at 42°C in a polypropylene slide mailer filled with 25 mℓ of pre-hybridization solution, washed twice in deionized water at room temperature and dried with a stream of filtered nitrogen gas.

We performed 3 co-hybridizations, each comparing an LB versus a DM fermentation on a single array (Figure 4-4). For array hybridization, the 25 μℓ hybridization mix contained 12.5 μℓ of hybridization solution pre-heated to 42°C, 0.5 μℓ of hybridization blocker (salmon sperm DNA, 10 mg/mℓ), and 12 μℓ of labeled target cDNA (biotin and fluorescein-labeled cDNA). We used a smaller volume than the one recommended in the protocol since we used lifter slips (Erie Scientific, Portsmouth, NH) of smaller dimensions (24x24 mm). Hybridization mixes were incubated at 95°C for 5 minutes. Before hybridization, the lifterslips were first washed with deionized water, then with 70% ethanol, and finally dried with a stream of filtered nitrogen gas. The lifterslips were then placed over the arrays and the hot (95°C) hybridization mix was added

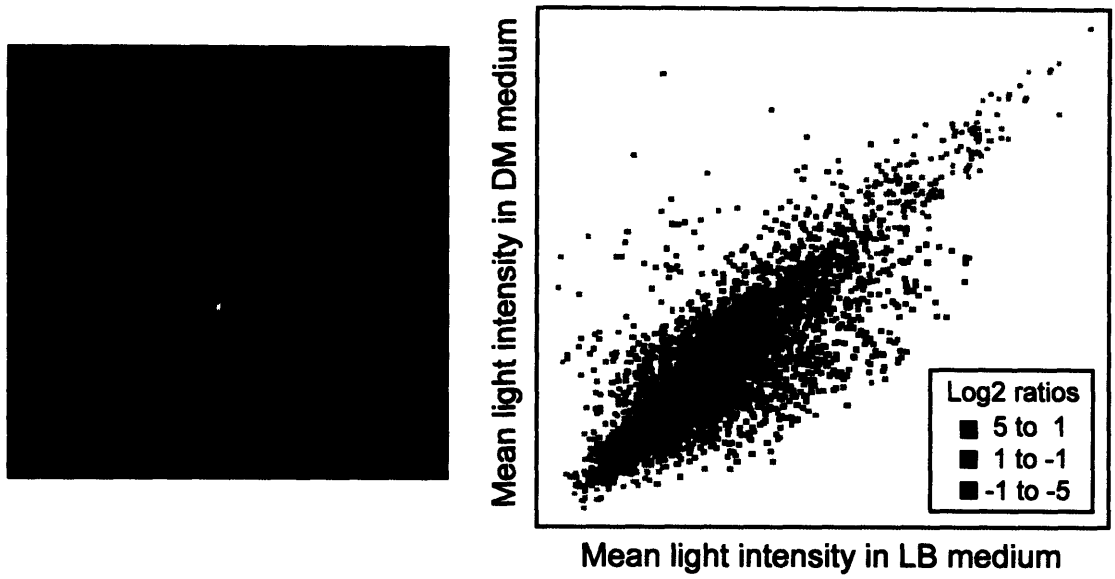

Figure 4-4. *E. coli* microarrays (left) hybridized with cDNA obtained from 500 ng of total RNA from cultures grown in 50 μℓ microbioreactors in DM (green) and LB (red). Normalized mean spot intensities *(n=3)* of the two growth conditions were plotted against each other (right) and the log2 ratios of DM (green) over LB (red) intensities were binned to identify genes upregulated more than two-fold.

to one of the free edges of the lifterslip to entirely cover the array area by capillary action. The slides were placed in ArrayIt hybridization cassettes (TeleChem International, Sunnyvale, CA) together with 250 μℓ of water for humidity control, and placed overnight in a 42°C incubator. Post-hybridization washes were performed as directed. Microarray slides were then blocked in 25 mℓ of blocking solution (Invitrogen) for 2 minutes at room temperature. The slides were then placed on a wet paper towel and put inside a plastic container, which functioned as a hydration chamber. Each array was covered with 45 μℓ of the RLS Particle Mix, which was composed of 15 μℓ AntiBiotin RLS Particle Au (gold), 15 μℓ AntiFluorescein RLS Particle Ag (silver), and 15 μℓ RLS Particle Diluent. Lifterslips were washed and dried as described above and carefully lowered over the array area. Microarray slides were then incubated in the Hydration Chamber for 1 hour. The RLS particle wash was performed as directed with wash solutions using a squirt

bottle and a slide mailer. Following final washes in a glass tank with deionized water, the slides were dried with a stream of filtered nitrogen gas and archived in 25 mℓ of archiving solution (Invitrogen) and dried for about 2 hours in a laminar flow hood.

To determine spot intensities, microarray slides were scanned in a GSD-501 RLS Detection and Imaging Instrument (Invitrogen) and image data were analyzed using MolecularWare software (Cambridge, MA).

For each array, the intensity ratio of each ORF-specific spot was obtained using the intensity-dependent non-linear normalization LOWESS[137,138] on the ratios of the two channels. The two growth conditions were compared by determining the log2 ratios of the mean light intensies across the three arrays. Intensity ratios were calculated using defined medium as numerator and LB as denominator. Differential gene expression was considered significant if the log2 ratio of DM intensity over LB intensity for each ORF was greater than 1 or lower than -1. The complete set of data was deposited and can be viewed on the NCBI Gene Expression Omnibus web site (http://www.ncbi.nlm.nih.gov/geo/, accession number GSE1981).

For gene annotation, *E. coli* sequences were compared to proteins in the cluster of orthologous group (COG) database[139] using the BLASTP sequence similarity search program.[140] Assignment to a particular COG group was made by transferring the COG function of the top alignment to the *E. coli* protein. This allowed high-throughput annotation of gene function.

4.3. Results

To investigate gene-expression level cellular behavior in the miniaturized 50 μℓ bioreactors of Zanzotto et al.,[118] we carried out fermentation studies in two media, one a defined minimal medium (DM), the other a rich medium (LB) (Figure 4-3). It is known that *E. coli* grows faster in

rich than in minimal media[141] and in our studies our strain grew with average generation times of about 28 and 48 minutes in LB and DM, respectively. Cells for RNA isolation were harvested when the cultures reached an OD_{600} of about 1. At this OD, the average pH of both media was about 6.6 and the dissolved oxygen concentration of the fermentation medium was on average 60-80 % in DM and 40-60 % in LB (Figure 4-3), defining 100% as the oxygen concentration of saturated medium in equilibrium with air.

For assessment of gene expression profiles in *E. coli* cultures grown in the two growth conditions, we identified upregulated genes by taking the log2 ratio of the mean spot intensities of DM over LB (Figure 4-4). Table 4-1 summarizes the number of upregulated genes annotated in functional groups and classes in the two growth conditions. The total number of upregulated genes in the two media was 507, of which 232 were specifically upregulated in DM and 275 in LB (Table 4-1). Results indicate that when *E. coli* was grown in DM, a larger number of "Metabolism" genes were upregulated, while when the culture was grown in LB, more "Cellular processes" and "Information storage and processing" genes were upregulated.

These results were expected since *E. coli* growing on glucose as sole carbon and energy source must generate *de novo* building blocks (i.e. amino acids, vitamins, nucleosides, etc.) for macromolecular synthesis. In LB, *E. coli* grows more rapidly since the building blocks for macromolecular synthesis are provided by yeast extract and tryptone, and more regulatory genes are expected to be upregulated.[142] A complete list of the upregulated genes is given in Table 4-2.

Table 4-1. Numbers of upregulated genes in *E. coli* growing in defined minimal medium (DM) and LB[a].

Function group	Function class	Medium	
		DM	LB
Metabolism	Amino acid transport and metabolism	48	10
	Carbohydrate transport and metabolism	19	20
	Coenzyme metabolism	2	4
	Energy production and conversion	25	6
	Lipid metabolism	--	4
	Nucleic acid transport and metabolism	2	5
Cellular processes	Cell division and chromosome partitioning	--	1
	Cell envelope biogenesis, outer membrane	7	7
	Cell motility and secretion	1	16
	Defense mechanisms	--	3
	Inorganic ion transport and metabolism	13	13
	Posttranslational modification, protein turnover	5	3
	Signal transduction mechanisms	5	5
Information storage and processing	DNA replication, recombination, and repair	8	10
	Transcription	11	22
	Translation, ribosomal structure and biogenesis	2	3
Poorly characterized	Function unknown	84	143
TOTAL		**232**	**275**

[a]Functional annotation was performed by comparing *E. coli* sequences to proteins of the cluster of orthologous group (COG) database using the BLASTP sequence similarity search program. Assignment to a particular COG group and class was made by transferring the COG function of the top alignment to each *E. coli* protein. Genes were considered upregulated when the log2 ratio of the mean spot intensities was greater than 1 or lower than -1.

Table 4-2. Differential gene expression profile of the functional group "Metabolism" in *E. coli* growing in defined minimal minimum (DM) and LB.

Gene ID	Gene Product	Log2 (DM/LB)	Gene ID	Gene Product	Log2 (DM/LB)
Amino acid transport and metabolism			**Amino acid metabolism contd.**		
proX	transport system for glycine and proline	5.8	*speE*	spermidine synthase	1.0
leuB	3-isopropylmalate dehydrogenase	4.2	*yfcK_2*	putative peptidase	1.0
thrB	homoserine kinase	3.6	*phnC*	ATP-binding component of phosphonate transport	1.0
proV	transport system for glycine, betaine and proline	3.5	*ilvB*	acetolactate synthase I,valine-sensitive	1.0
oppA	oligopeptide transport; periplasmic binding protein	3.4	*leuA*	2-isopropylmalate synthase	1.0
dppA	dipeptide transport protein	3.3	*poxB*	pyruvate oxidase	1.0
leuC	3-isopropylmalate isomerase (dehydratase)	3.1	*ygfK*	putative oxidoreductase, Fe-S subunit	1.0
metE	tetrahydropteroyltriglutamate methyltransferase	3.1	*xasA*	acid sensitivity protein, putative transporter	-2.3
gltD	glutamate synthase, small subunit	2.9	*tnaA*	tryptophanase	-2.0
asd	aspartate-semialdehyde dehydrogenase	2.9	*gltK*	glutamate/aspartate transport system permease	-1.8
ddpA	putative hemin-binding lipoprotein	2.4	*ydgR*	putative transport protein	-1.7
thrC	threonine synthase	2.3	*yhaP*	putative L-serine dehydratase	-1.6
gltB	glutamate synthase, large subunit	2.3	*potH*	putrescine transport protein; permease	-1.4
hisC	histidinol-phosphate aminotransferase	2.3	*yhfX*	Predicted amino acid racemase	-1.2
livJ	high-affinity amino acid transport system	2.2	*tdcB*	threonine dehydratase, catabolic	-1.2
gadB	glutamate decarboxylase isozymes	2.2	*ptrB*	protease II	-1.2
proW	transport system for glycine and proline	2.1	*sdaB*	L-serine dehydratase (deaminase), L-SD2	-1.0
trpC_1	N-(5-phosphoribosyl)anthranilate isomerase	1.8			
cysM	cysteine synthase B, O-acetylserine sulfhydrolase B	1.7	**Coenzyme metabolism**		
cysD	ATP:sulfurylase , subunit 2	1.6	*folE*	GTP cyclohydrolase I	1.5
trpC_1	N-(5-phosphoribosyl)anthranilate isomerase	1.5	*bioD*	dethiobiotin synthetase	1.4
ygjI	putative oxidoreductase	1.4	*abgT*	putative pump protein (transport)	-1.8
aroL	shikimate kinase II	1.4	*ubiA*	4-hydroxybenzoate-octaprenyltransferase	-1.5
hisF	imidazole glycerol phosphate synthase subunit	1.4	*ubiX*	3-octaprenyl-4-hydroxybenzoate carboxy-lyase	-1.5
hisI_1	phosphoribosyl-amp cyclohydrolase	1.4	*moaA*	molybdopterin biosynthesis, protein A	-1.1
leuD	isopropylmalate isomerase subunit	1.4			
gatD	galactitol-1-phosphate dehydrogenase	1.4	***Nucleic acid transport and metabolism (F)***		
ddpF	ATP-binding component of a transport system	1.4	*cmk*	cytidylate kinase	2.1
ilvN	acetolactate synthase I, valine sensitive	1.3	*purF*	amidophosphoribosyltransferase	1.2
cysH	3'-phosphoadenosine 5'-phosphosulfate reductase	1.3	*guaA*	GMP synthetase (glutamine-hydrolyzing)	-2.0
thrA	aspartokinase I, homoserine dehydrogenase I	1.3	*dgt*	deoxyguanosine triphosphate triphosphohydrolase	-1.5
livG	ATP-binding component of amino acid transport system	1.2	*purH*	phosphoribosylcarboxamideformyltransferase	-1.1
serA	D-3-phosphoglycerate dehydrogenase	1.2	*guaB*	IMP dehydrogenase	-1.1
aroC	chorismate synthase	1.2	*pyrI*	aspartate carbamoyltransferase, regulatory subunit	-1.1
ilvD	dihydroxyacid dehydratase	1.1			
trpB	tryptophan synthase, beta protein	1.1	**Lipid metabolism**		
aroG	arabinoheptulosonate-7-phosphate synthase	1.1	*atoE*	short chain fatty acid transporter	-2.6
aroF	arabinoheptulosonate-7-phosphate synthase	1.1	*ynjF*	putative cytochrome oxidase	-2.4
cysA	sulfate permease A protein	1.1	*idnO*	5-keto-D-gluconate 5-reductase	-1.2
aegA_2	putative oxidoreductase, Fe-S subunit	1.1	*entA*	2,3-dihydro-2,3-dihydroxybenzoate dehydrogenase	-1.2
glnH	periplasmic glutamine-binding protein; permease	1.1			

Table 2 (continued). Differential gene expression profile of the functional group "Metabolism" in *E. coli* growing in defined minimal minimum (DM) and LB.

Gene ID	Gene Product	Log2 (DM/LB)	Gene ID	Gene Product	Log2 (DM/LB)
Carbohydrate transport and metabolism			**Carbohydrate metabolism contd.**		
gatA	galactitol-specific of phosphotransferase system	4.2	*malG*	part of maltose permease, inner membrane	-1.1
gatZ	putative tagatose 6-phosphate kinase 1	3.5	*gmhA*	phosphoheptose isomerase	-1.0
gatY	tagatose-bisphosphate aldolase 1	3.0	*lacY*	galactoside permease (M protein)	-1.0
ZgapC	glyceraldehyde 3-phosphate dehydrogenase C	2.6			
yicM	putative transport protein	2.5	**Energy production and conversion**		
gapC	glyceraldehyde-3-phosphate dehydrogenase	2.4	*aceB*	malate synthase A	4.8
gatY	tagatose-bisphosphate aldolase 1	1.9	*aceA*	isocitrate lyase	3.5
otsA	trehalose-6-phosphate synthase	1.8	*yodB*	putative cytochrome	2.6
rbsB	D-ribose periplasmic binding protein	1.7	*sucC*	succinyl-CoA synthetase, beta subunit	2.4
pykF	pyruvate kinase I (formerly F), fructose stimulated	1.5	*narJ*	nitrate reductase 1, delta subunit	2.3
gatC	PTS system galactitol-specific enzyme IIC	1.4	*narG*	nitrate reductase 1, alpha subunit	2.0
glgX	part of glycogen operon, a glycosyl hydrolase	1.4	*sdhA_1*	succinate dehydrogenase, flavoprotein subunit	1.7
glgC	glucose-1-phosphate adenylyltransferase	1.3	*nuoB*	NADH dehydrogenase I chain B	1.6
uxaC	uronate isomerase	1.3	*pntA*	pyridine nucleotide transhydrogenase, alpha subunit	1.5
ptxA	putative PTS system enzyme II A component	1.3	*nuoE*	NADH dehydrogenase I chain E	1.5
alsC	putative transport system permease protein	1.3	*SdhA_2*	succinate dehydrogenase, flavoprotein subunit	1.3
malK	transport system for maltose	1.1	*fdx*	[2FE-2S] ferredoxin, electron carrer protein	1.3
ycjR	putative transient receptor potential locus	1.1	*nuoG*	NADH dehydrogenase I chain G	1.3
talA	transaldolase A	1.0	*ybiC*	putative dehydrogenase	1.3
agaD	PTS system, N-acetylglucosamine enzyme IID	-2.6	*hyfI*	hydrogenase 4 Fe-S subunit	1.2
xapB	xanthosine permease	-2.2	*glcB*	malate synthase G	1.2
shiA	putative transport protein, shikimate	-2.0	*fdhD*	affects formate dehydrogenase-N	1.2
uidB	glucuronide permease	-1.7	*nuoI*	NADH dehydrogenase I chain I	1.2
frvX	frv operon protein	-1.7	*gltA*	citrate synthase	1.2
agaW	PTS system N-acetylgalactosameine-specific IIC	-1.7	*sucD*	succinyl-CoA synthetase, alpha subunit	1.2
mglC	methyl-galactoside transport and galactose taxis	-1.6	*hyfF*	hydrogenase 4 membrane subunit	1.2
ptsG	PTS system, glucose-specific IIBC component	-1.5	*prpC*	putative citrate synthase; propionate metabolism	1.2
rhaT	rhamnose transport	-1.4	*nuoH*	NADH dehydrogenase I chain H	1.1
ybhC	putative pectinesterase	-1.3	*sdhD*	succinate dehydrogenase, hydrophobic subunit	1.1
agaC	PTS system N-acetylgalactosamine-specific IIC	-1.3	*ydgN*	putative membrane protein	1.0
yfeV_2	putative PTS enzyme II	-1.3	*ybiW*	putative formate acetyltransferase	-1.6
fucI	L-fucose isomerase	-1.3	*ydeP*	putative oxidoreductase, major subunit	-1.4
ebgA	evolved beta-D-galactosidase, gene	-1.2	*lldP*	L-lactate permease	-1.3
gntP	gluconate transport system permease 3	-1.2	*cydA*	cytochrome d terminal oxidase, polypeptide subunit I	-1.1
xylE	xylose-proton symport	-1.2	*araB*	L-ribulokinase	-1.1
galP	galactose-proton symport of transport system	-1.1	*hyfD*	hydrogenase 4 membrane subunit	-1.0

Table 4-3. Differential gene expression profile of the functional group "Cellular processes" in *E. coli* growing in defined minimal minimum (DM) and LB.

Gene ID	Gene Product	Log2 (DM/LB)
Cell envelope biogenesis, outer membrane		
yedS	putative outer membrane protein	2.5
dniR	transcriptional regulator for nitrite reductase	2.4
spr	putative lipoprotein	1.6
murG	UDP-N-acetylglucosamine	1.2
nlpD	lipoprotein	1.1
b1980	ADP-heptose:LPS heptosyltransferase	1.1
yaiP	polysaccharide metabolism	-2.1
rhsC	protein in rhs element	-1.7
mreD	rod shape-determining protein	-1.7
rhsE	rhsE protein in rhs element	-1.6
rfbC	dTDP-6-deoxy-D-glucose-3,5 epimerase	-1.3
kdsB	CTP:CMP-3-D-manno-octulosonate transferase	-1.1
Cell motility and secretion		
flhA	flagellar biosynthesis	2.0
fliC	flagellar biosynthesis; flagellin	-2.5
tar	methyl-accepting chemotaxis protein II	-2.2
motB	enables flagellar motor rotation	-2.1
yqiH	P pilus assembly protein, chaperone PapD	-1.6
ycbT	homolog of Salmonella FimH protein	-1.5
fliA	flagellar biosynthesis	-1.4
cheA	sensory transducer kinase	-1.4
ppdD	prelipin peptidase dependent protein	-1.4
flgE	flagellar biosynthesis, hook protein	-1.3
cheZ	chemotactic response; CheY protein phophatase	-1.2
fliN	flagellar biosynthesis, component of motor switch	-1.2
yehD	P pilus assembly protein, pilin FimA	-1.2
fliS	flagellar biosynthesis; repressor of (RflA activity)	-1.2
flgA	flagellar biosynthesis; periplasmic P ring	-1.1
flgC	flagellar biosynthesis,basal-body rod	-1.1
flgK	flagellar biosynthesis, hook-filament	-1.1
cheY	chemotaxis regulator	-1.0
Signal transduction mechanisms		
glnL	histidine protein kinase sensor for GlnG regulator	1.6
ybcZ	putative 2-component sensor protein	1.4
ypdA	putative sensor protein	1.2
phoQ	sensor protein PhoQ	1.2
ygeV	putative transcriptional regulator	1.2
yjiY	putative carbon starvation protein	-2.1
ybdQ	universal stress protein UspA	-1.6
yeiL	cAMP-binding proteins - catabolite gene activator	-1.3
fimZ	fimbrial Z protein; probable signal transducer	-1.1
barA	sensor-regulator, activates OmpR by phophorylation	-1.0
Cell division and chromosome partitioning		
sulA	suppressor of lon; inhibits cell division	-1.0
Defense mechanisms		
bacA	bacitracin resistance	-1.9
mcrC	component of McrBC restriction system	-1.1
dinF	DNA-damage-inducible protein F	-1.0
Inorganic ion transport and metabolism		
cysJ	sulfite reductase (NADPH)	1.6
oppB	oligopeptide transport permease protein	1.6
dps	global regulator, starvation conditions	1.5
oppC	homolog of Salmonella transport permease	1.4
cutCm	copper homeostasis protein	1.4
yejE	putative transport system permease protein	1.4
cysC	adenosine 5'-phosphosulfate kinase	1.3
cysP	thiosulfate binding protein	1.3
phnM	phosphonate metabolism	1.2
cysWm	sulfate transport system permease W protein	1.2
yoaE_2	putative transport protein	1.1
nikB	transport of nickel, membrane protein	-2.0
focB	probable formate transporter (formate channel 2)	-1.8
nikC	transport of nickel, membrane protein	-1.8
kdpB	ATPase of high-affinity potassium transport system	-1.7
yliD	putative transport system permease protein	-1.7
nirCm	nitrite reductase activity	-1.5
tolQ	inner membrane protein, membrane-spanning	-1.5
dppB	dipeptide transport system permease protein 1	-1.5
yliC	putative transport system permease protein	-1.3
emrE	methylviologen resistance	-1.3
ccmD	heme exporter protein C	-1.2
yieL	putative xylanase	-1.1
fecB	citrate-dependent iron transport	-1.1
znuA	putative adhesin	1.1
ybhI	putative membrane pump protein	1.1
Posttranslational modification, protein turnover		
slpA	FKBX-type peptidyl-prolyl cis-trans isomerase	1.5
nrdH	glutaredoxin-like protein; hydrogen donor	1.5
hslJ	heat shock protein hslJ	1.4
grxB	glutaredoxin 2	1.1
ybeW	putative dnaK protein	1.0
sirA	regulator of disulfide bond formation	-1.3
groL	GroEL, chaperone Hsp60, heat shock protein	-1.2
yqjG	putative transferase	-1.0

Table 4-4. Differential gene expression profile of the functional group "Information storage and processing" in *E. coli* growing in defined minimal minimum (DM) and LB.

Gene ID	Gene Product	Log2 (DM/LB)	Gene ID	Gene Product	Log2 (DM/LB)
Transcription			**Transcription contd.**		
cspG	homolog of Salmonella cold shock protein	3.5	*ygjJ*	transcription regulator containing HTH domain	-1.1
feaR	regulatory protein for 2-phenylethylamine catabolism	2.4	*yegW*	putative transcriptional regulator	-1.1
b1770	putative DEOR-type transcriptional regulator	2.1	*lexA*	regulator for SOS(lexA) regulon	-1.0
rpoS	RNA polymerase, sigma S (sigma38) factor	1.7	*rhaR*	positive regulator for rhaRS operon	-1.0
yrbL	orf, hypothetical protein	1.6	*nusG*	component in transcription antitermination	-1.0
cspH	cold shock-like protein; cold shock protein	1.6			
dsdC	D-serine dehydratase transcriptional activator	1.5	**DNA replication, recombination, and repair**		
nusA	transcription pausing; L factor	1.5	*yi91b*	IS911 hypothetical protein (IS911B)	1.9
rnc	RNase III, ds RNA	1.4	*trs5_1*	IS5 transposases	1.4
narP	nitrate/nitrite response regulator (sensor NarQ)	1.3	*ycaJ*	putative polynucleotide enzyme	1.3
torR	response transcriptional regulator for torA	1.2	*dinJ*	damage-inducible protein J	1.2
ygeV	putative transcriptional regulator	1.2	*recR*	recombination and repair	1.2
uhpA	positive activator of uhpT transcription	1.1	*rnhB*	RNAse HII, degrades RNA of DNA-RNA hybrids	1.1
psiF	induced by phosphate starvation	1.1	*dnaX*	DNA polymerase III, tau and gamma subunits	1.1
ygeP	orf, hypothetical protein	1.1	*dnaQ*	DNA polymerase III, epsilon subunit	1.1
ygiR	orf, hypothetical protein	1.0	*b0105*	transposase and inactivated derivatives	-2.5
ylcA	putative 2-component transcriptional regulator	1.0	*fimB*	regulator for fimA	-2.2
hcaR	transcriptional activator of hca cluster	-2.6	*b2596*	transposase and inactivated derivatives	-2.0
ygiU	transcription regulator containing HTH domain	-2.1	*b1788*	transposase	-1.9
ydeO	putative ARAC-type regulatory protein	-1.8	*lit*	phage T4 late gene expression	-1.8
yghW	transcription regulator containing HTH domain	-1.8	*ynjG*	orf, hypothetical protein	-1.7
ypdB	putative 2-component transcriptional regulator	-1.7	*intA*	prophage CP4-57 integrase	-1.6
cadC	transcriptional activator of cad operon	-1.7	*sbmC*	SbmC protein	-1.6
yqeI	putative sensory transducer	-1.6	*nfi*	endonuclease V (deoxyinosine 3'endoduclease)	-1.5
ygiZ	transcription regulator containing HTH domain	-1.6	*b0309*	transposase and inactivated derivatives	-1.4
ydiP	putative ARAC-type regulatory protein	-1.6	*b1903*	transposase	-1.4
iclR	repressor of aceBA operon	-1.6	*b2191*	transposase and inactivated derivatives	-1.4
ybaD	predicted transcriptional regulator	-1.5	*alkB*	DNA repair system specific for alkylated DNA	-1.2
yjcT	putative NAGC-like transcriptional regulator	-1.5	*hupB-r*	DNA-binding protein HU-beta, NS1 (HU-1)	-1.2
fliA	flagellar biosynthesis	-1.4	*recG*	DNA helicase, resolution of Holliday junctions	-1.2
b2635	predicted transmembrane transcriptional regulator	-1.4	*recN*	protein used in recombination and DNA repair	-1.1
hcaR-r	transcriptional activator of hca cluster	-1.4	*b0165*	transposase and inactivated derivatives	-1.1
perR	putative transcriptional regulator LYSR-type	-1.3	*recA*	DNA strand exchange and renaturation	-1.1
yhcO	barstar, RNAse (barnase) inhibitor	-1.3	*ycfH*	Mg-dependent DNase	-1.0
nhaR	transcriptional activator of nhaA	-1.3	*seqA*	negative modulator of initiation of replication	-1.0
gntR	regulator of gluconate (gnt) operon	-1.2			
yiaG	predicted transcriptional regulator	-1.2	**Translation, ribosomal structure and biogenesis**		
ykgD	putative ARAC-type regulatory protein	-1.2	*tsf*	protein chain elongation factor EF-Ts	1.4
ycjW	putative LACI-type transcriptional regulator	-1.2	*rsuA*	16S pseudouridylate 516 synthase	1.1
pssR	regulator of pssA	-1.2	*smpA*	small membrane protein A	-1.6
fimZ	fimbrial Z protein; probable signal transducer	-1.1	*lysU*	lysine tRNA synthetase; heat shock protein	-1.5
paaX	phenylacetic acid-responsive transcriptional repressor	-1.1	*rplS*	50S ribosomal subunit protein L19	-1.1

The total number of upregulated genes in the functional group "Metabolism", in *E. coli* growing in DM versus LB, was 96 and 49 respectively, and the major differences between the two growth conditions were in the two functional classes "Amino acid transport and metabolism" and "Energy production and conversion". Specifically, in DM, 48 "Amino acid transport and metabolism" genes were upregulated, including genes involved in the synthesis of all of the 20 amino acids found in proteins (Table 4-2). Three genes for proline biosynthesis (*proVWX*) were strongly upregulated, with *proX* showing the most significant increase in this functional class. Other genes that were highly upregulated in DM are *leuB* (responsible, along with *leuACD*, for leucine biosynthesis), the three genes of the *thrABC* operon for threonine biosynthesis, four genes (*aroCFGL*) for the synthesis of chorismate (a central intermediate in aromatic amino acid biosynthesis), and seven genes (*cysACDHJMP*) for the synthesis and metabolism of cysteine.

In LB medium only 10 genes in the functional class "Amino acid transport and metabolism" were upregulated, with no genes involved in amino aid biosynthesis and four genes involved in amino acid degradation: *sdaB* and *yhaP* (glycine), *tnaA* (tryptophan) and *tdcB* (threonine) (Table 4-2).

In the functional classes "Carbohydrate transport and metabolism" and "Energy production and conversion" a higher number of genes were upregulated in DM than in LB (Table 4-2). In *E. coli* growing in DM these genes are involved in acetate utilization and the glyoxylate shunt (*aceA*, *aceB* and *gltA*), in the tricarboxylic acid cycle, e.g. citrate synthetase (*sdhAD*) and succinyl-CoA synthetase (*sucCD*), and the NADH dehydrogenase genes (*nuoBEGHI*) involved in oxidative phosphorylation and ubiquinone biosynthesis. Additional genes upregulated in *E. coli* growing in DM are involved in galacitol and tagatose transport and metabolism

(*gatACDYZ*) and in glycolysis, such as glyceraldehyde 3-phosphate dehydrogenase (*gapC* 1 and 2) and pyruvate kinase (*pykF*).

During growth in LB, the most upregulated genes from the two functional classes "Carbohydrate transport and metabolism" and "Energy production and conversion" were those involved in the expression of the PTS protein N-acetyl glucosamine (*agaCDW*) and another protein of the PTS system that is glucose specific (*ptsG*) .

E. coli growing in LB had a higher number of upregulated genes in the functional group "Cellular processes" than cells growing in DM (Table 4-1). The major differences in this functional group were in the functional class "Cell motility and secretion" where *E. coli* growing in LB exhibited 17 upregulated genes (Table 4-3), with eight of these involved in the flagellum assembly (*fliACNS and flgACEK*) and five involved in chemotaxis (*cheAYZ*, *tar,* and *motB*), indicating that the strain growing in rich medium at an OD of 1 is actively motile.

As expected, *E. coli* in LB showed higher expression of genes from the group "Information storage and processing" than when grown in DM (Table 4-1). *E. coli* divides more rapidly in LB than in DM (Figure 4-3) and it is known that fast growing cultures synthesize proteins at a higher rate than slow-growing populations.[142-144] Of the 35 "Information" genes upregulated in LB medium, the majority (22 genes) belong to the "Transcription" class (Table 4-1). More strongly expressed were *hcaR* (Table 4-4), a transcriptional regulator of the LysR family that controls the *hca* cluster for propionate catabolism,[145] and *iclR*, a repressor of the *aceBA* operon that mediates acetate utilization. Accordingly, the *aceBA* genes were strongly upregulated in *E. coli* grown in DM (Table 4-2).

In DM, *rpoS*, which encodes the RNA polymerase sigma subunit regulating many cellular responses to environmental stress,[146,147] was strongly expressed (Table 4-4), which is in

agreement with the reports of Tao et al.[135] and Wei et al.[136] This suggests that RpoS regulation may be important not only during the transition between the exponential and stationary phases, but also in early and late logarithmic phase. Other genes that exhibited upregulation in DM were *narP*, a nitrate/nitrite response regulator that belongs to the LuxR/UhpA family of the two-component regulatory system controlling the expression of several genes involved in anaerobic fermentation and respiration,[148] and *uhpA* of the two-component regulatory system UhpB/UhpA, involved in the uptake of hexose phosphates.[149]

4.4. Discussion

Rapid screening for microorganisms exhibiting specific patterns of gene expression and protein production is critical for progress in microbiology, biotechnology, and the pharmaceutical industry. We used a novel microbioreactor platform that is scalable and has the advantage of providing real-time data on bacterial growth parameters for OD_{600}, DO, and pH. *E. coli* cultures grown in this microbioreactor exhibited growth patterns that are comparable to bench-scale 500 mℓ bioreactors.[118] Microbioreactors have the potential to provide much of the data and functionality that a large bioreactor system does while offering the advantages of scale for high-throughput processes. Microbioreactors could become especially valuable since recent advances in molecular biology have made it possible to create large numbers of evolved biocatalysts, new pathway designs, and a variety of unique biological organisms from diverse sources. It is likely that microbioreactors with integrated sensors and actuators will be the driving force behind research in high-throughput screening for general biological research.

Our aim was to determine whether the microbioreactor platform we had previously described can be used, not only to grow potentially large numbers of microbial strains to study their physiology, but to link this real-time information to global gene-expression analysis. To this end,

we performed microarray analysis on 500 ng of total RNA from *Escherichia coli* cultures grown in LB medium and in minimal medium in an instrumented 50 μℓ bioreactor, using the RLS system for cDNA labeling. Two previous studies[135,136] have performed microarray analysis on *E. coli* strain MG1655 grown in rich and minimal media. In both of those cases bacterial cultures were grown in 50 mℓ batch cultures in 250 mℓ Erlenmeyer flasks. For microarray analysis the two studies used different methods: Tao et al.[135] used 1 μg of total RNA with 32P-dCTP to label cDNA and nylon DNA arrays; Wei et al.[136] used 6 μg of total RNA with Cy3 and Cy5 fluorophores to label cDNA, and printed microarrays with PCR amplified ORFs.

These studies reached similar general conclusions, indicating that in *E. coli* grown in minimal medium metabolism genes such as those for amino acid biosynthesis and energy production and conversion are upregulated, while in cultures grown in LB, genes involved in translation and ribosome structure and biogenesis are upregulated. These results confirm general predictions that bacteria grown in minimal media must generate the monomers needed to build macromolecules *de novo*, while in rich media that support more rapid growth they must assemble an increased number of *de novo* ribosomes and translation factors.

In our miniaturized system we found that *E. coli* grown in minimal medium, with glucose as sole carbon and energy sources, upregulated a large number of amino acid biosynthesis and energy production and conversion genes. Paralleling the two large-scale studies described above, threonine, phenylalanine, leucine, serine, tryptophan, isoleucine/valine and histidine biosynthesis genes were over-expressed. Other similarities included the overexpression of *aceAB*, involved in acetate metabolism, and of *rpoS*, a global gene expression regulator. Several additional genes that were upregulated in minimal medium in our microbioreactors were also upregulated in minimal medium in at least one of the two studies mentioned.

Conversely, we found some differences with reported results[135,136] in the gene expression profiles of *E. coli* cultures grown in LB. One was the clear upregulation of genes for chemotaxis and motility in our system. This result was, however, expected since *E. coli* is motile in LB but not in minimal medium due to catabolite repression by glucose (sole carbon source) in the medium.[150] Also, in our study we did not observe large differences in the gene expression of the translational apparatus and ribosomal structure and biogenesis between cells grown in LB versus DM. This dissimilarity with the studies mentioned may be attributable to differences in growth and analytical conditions such as media composition, phase of physiological growth at which cells were harvested, type of microarray platform used, etc. They could also be due to the cDNA labeling system that we used. At the time of our studies the RLS system had proven to be sufficiently sensitive to obtain gene expression profiles of human genes[132] and we were among the first to apply it to bacterial cultures. In a more recent study, the RLS system was used to efficiently detect bacterial cultures down to 10^5 cells.[134] We found some variability between our replicates and were also not able to confirm all our results in dye-swap experiments (data not shown). We believe this may be due to the fact that we were using much more complex arrays than Francois et al.[134] who tested a limited number of ORFs and used a single RLS label (gold). The RLS system may require optimization to perform global gene expression analysis. Nevertheless, it has proven useful in our proof of concept study of cDNA arrays from small-volume bacterial cultures.

In summary, we have shown that microbioreactors can be used to reproducibly grow bacterial cultures, we have developed protocols to isolate high-quality total RNA from small volumes of cultures grown in microbioreactors, and we have performed differential gene expression analysis in *E. coli* grown in two different conditions in microbioreactors equipped

with real-time monitoring of growth parameters. *E. coli* generally exhibited gene expression profiles that were predicted for growth under the conditions tested, in essential agreement with data from thousand-fold larger culture volumes.

The ability to obtain reliable data from 50 $\mu\ell$ cultures demonstrates that, in the future, rapid screening of metabolic and genomic data will be possible with the use of scalable microbioreactor platforms and improved technology that increases the sensitivity of microarrays.

Chapter 5. Modeling of a Glucose Sensor Based on Glucose Oxidase

5.1. Introduction

We model a potential glucose sensor for *in situ* use in the microbioreactor to determine the feasibility of developing and testing such a sensor in the laboratory. Significant interest in glucose monitoring exists in the fields of bioprocessing and medicine.[151-153] In bioprocessing, control of glucose levels in fermentation medium is crucial in both fed-batch and continuous systems when glucose is used as the carbon source. Effective control requires the ability to monitor glucose levels quickly and accurately. In addition, knowledge of glucose consumption is needed to close the carbon balance as well as for metabolic studies and medium optimization, making glucose monitoring crucial for batch systems as well. In the field of medicine, interest in glucose monitoring is spurred by the high incidence of diabetes in the population. Diabetes affects the body's ability to metabolize glucose by interfering with the synthesis (Type I diabetes) or action (Type II diabetes) of insulin, the hormone required by cells to take up glucose from the blood. Individuals with diabetes must closely monitor their blood glucose levels throughout the day to keep them within an acceptable range.

A number of different techniques for monitoring glucose have been presented in the literature. Among these are polarimetry,[154,155] optical absorption (particularly in the near-IR),[156,157] Raman scattering,[158,159] fluorescence techniques using fluorescence resonance energy transfer (FRET) that employ competition assays between glucose and labeled glucose analogs,[160,161] glucose-specific fluorescent probes, reversible reactions using glucose-binding functional groups,[162,163] and techniques that employ the enzyme glucose oxidase (GOD) as a

catalyst in a redox reaction involving glucose. The majority of glucose sensors currently on the market for both medical and bioprocessing applications employ this last method.

The glucose oxidase enzyme catalyzes the conversion of β-D-glucose and oxygen to D-gluconic acid and hydrogen peroxide (Figure 5-1). This reaction has been used to monitor glucose indirectly by measuring either oxygen depletion or hydrogen peroxide production. Both optical[164-167] and electrochemical[168-170] methods of detection have been demonstrated.

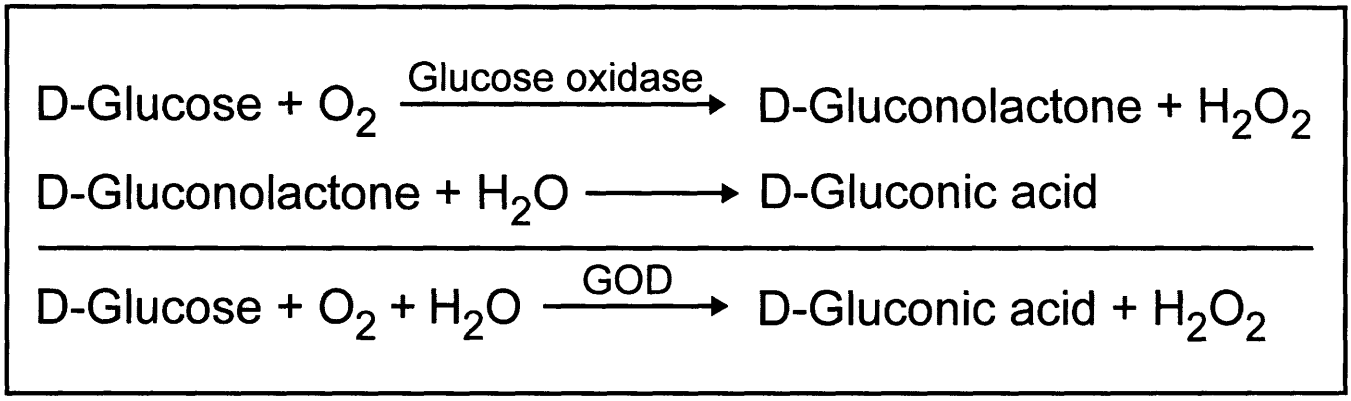

Figure 5-1. Glucose oxidation reaction catalyzed by the enzyme glucose oxidase (GOD).

A sensor based on the glucose oxidase reaction was selected for the current study because of its simplicity, ease in miniaturization, and integration potential. Optical monitoring of oxygen was attractive since we have previously demonstrated the ability to monitor oxygen *in situ* using fluorescence lifetime measurements.

Although glucose concentrations used in industrial fermentations can be as high as 100 g/ℓ, a typical glucose concentration used in the microbioreactor has been 10 g/ℓ. A glucose sensor for the microbioreactor should therefore be able to measure concentrations in the range 0-10 g/ℓ. Required response times for the glucose sensor vary depending on the application. In the case

where glucose levels are controlled, the response time of the sensor should be less than 1 minute, particularly if low glucose levels are to be maintained. If glucose is being monitored but not controlled, the sensor response time can be somewhat higher, and the needed performance will depend on the rate of glucose uptake. In general, faster-growing cultures which use glucose more quickly would need a faster response time. A response time of five minutes or less should be sufficient for most applications.

5.2. Description of Glucose Oxidase Sensor

The structure of sensors that utilize glucose oxidase to measure glucose levels generally consist of at least two layers. The first layer is the material in which the glucose oxidase is immobilized. Various materials can be used for this purpose including sol-gel,[167,171] polyacrylamide hydrogel,[168] and polyvinyl alcohol hydrogel.[170] The second layer separates the immobilized enzyme from the glucose-containing medium and serves two major purposes. The first is to protect the GOD (Figure 5-2) from the constituents of the medium that could inactivate the enzyme or foul the surface of the hydrogel. The second is to control the rates of diffusion of oxygen and glucose to the glucose oxidase. The presence of excess oxygen relative to glucose is necessary for the operation of a glucose sensor based on glucose oxidase, otherwise the rate and extent of reaction will not be indicative of the glucose level. It is therefore critical that this layer be selective for oxygen. In addition, the properties of this layer (water content, diffusivity and solubility of species) control the overall performance of the sensor as measured by the time constant, analytical range, and sensitivity, through control not only of the ratio of oxygen to glucose that reaches the enzyme but also the rate of transport of these species.

A multi-layer glucose sensor was proposed for the current study (Figure 5-2). The base of the sensor was the optical oxygen sensor described in Chapter Two. Above this, polyvinyl alcohol

(PVA) hydrogel was selected for the immobilization layer. Finally, a polyurethane (PU) layer acted as an oxygen-selective membrane. Polyurethane was selected because of its biocompatibility and the ability to tune its properties through synthesis. The height of the medium above the sensor is the same as the height of the microbioreactor well (300 μm as described in Chapter Two).

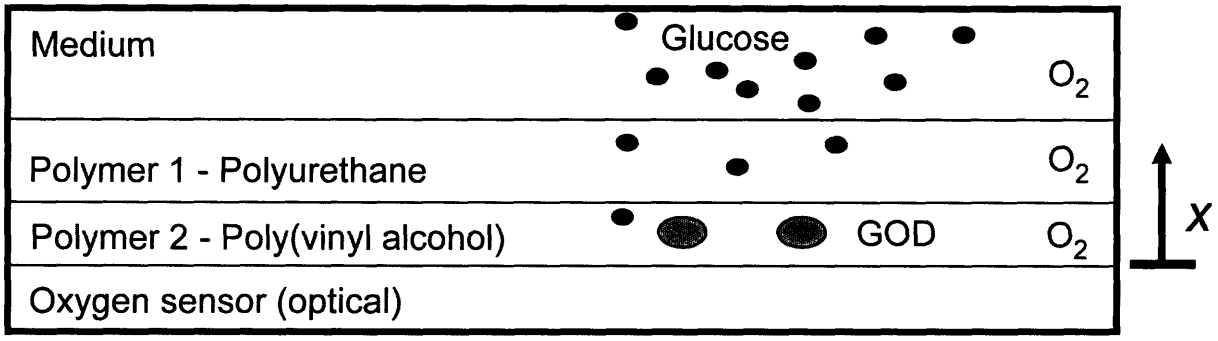

Figure 5-2. Schematic of a glucose sensor based on glucose oxidase. Glucose and oxygen from the medium diffuse through the PU layer and enter the PVA layer, where glucose oxidase is immobilized. In this layer the two undergo a reaction catalyzed by the GOD enzyme. The resulting depletion in the local oxygen concentration is monitored by the optical oxygen sensor. The axis used for simulations is indicated by x.

A one-dimensional model of the sensor was developed. Diffusion of each species (oxygen and glucose) in each layer is governed by Equation 5-1. The reaction of oxygen and glucose within the PVA layer is governed by Michaelis-Menten kinetics[172] (Equation 5-2).

$$\frac{\partial C}{\partial t} = D\frac{\partial^2 C}{\partial x^2} - R_V \qquad (5\text{-}1)$$

$$R_V = \frac{v_{\max} C}{K_m + C} \qquad (5\text{-}2)$$

Initially, it is assumed that oxygen is fully saturating all of the layers, while the concentration of glucose in the two polymers is zero. The initial concentration of glucose in the medium is defined for each simulation. Interfacial boundary conditions used for each species are equated flux with a difference in solubility defined by a partition coefficient. No reaction occurs in either the medium or the polyurethane layer. The reaction in the polyvinyl alcohol layer occurs with a one-to-one stoichiometric ratio, that is, moles of glucose and oxygen are depleted at an equal rate as indicated in the reaction equation. All simulations were carried out using FEMLAB simulation software.

Values for the properties of the medium (approximated as water due to the relatively low glucose concentrations under consideration), the two polymer layers, and the glucose oxidase enzyme were obtained from the literature (Table 5-1). In cases where multiple references are listed, the value used in simulations is within the range reported by the literature. The solubility of glucose in the two polymer layers was approximated as being proportional to their water content, as described in the literature.[173-176] As a result, glucose partition coefficients are dependent on the percentage water pickup of the polyurethane layer, which is different for each polymer formulation considered.[173,174] The water content of the polyvinyl alcohol layer is taken to be 90% for all simulations.[175,176] Likewise, the solubility of oxygen in PVA is proportional to the water content.[177,178] The glucose oxidase Michaelis-Menten constant, K_m, depends on several factors including temperature, pH, whether the enzyme is free or immobilized, and whether the reaction is operating under glucose- or oxygen-limited conditions.[170] As a result, the apparent K_m will change throughout the course of an experiment as the conditions in the medium and the concentrations of the reactants change. A mid-range value for K_m was therefore selected, and the approximation was made that this value would remain constant throughout the simulation.[179]

Table 5-1. List of parameters used to model a GOD sensor operating in a microbioreactor.

Parameter	Definition	Value	Reference
$D_{O2\text{-}water}$	Diffusivity of O_2 in water	2.5 x 10^{-5} cm^2/s	[80]
$D_{O2\text{-}PU}$	Diffusivity of O_2 in PU	Variable	[173,174]
$D_{O2\text{-}PVA}$	Diffusivity of O_2 in PVA	7 x 10^{-6} cm^2/s	[178,180,181]
$S_{O2\text{-}water}$	Solubility of O_2 in water	7.36 mg/ℓ	[80]
$S_{O2\text{-}PU}$	Solubility of O_2 in PU	0.45 $cm^3(STP)/cm^3 \cdot atm$	[182]
$S_{O2\text{-}PVA}$	Solubility of O_2 in PVA	Proportional to water content (90%)	[177,178]
$K_{O2\text{-}water/PU}$	Partition coefficient of O_2 between water and PU	0.0541	Calculated
$K_{O2\text{-}PU/PVA}$	Partition coefficient of O_2 between PU and PVA	20.53	Calculated
$D_{glucose\text{-}water}$	Diffusivity of glucose in water	6.8 x 10^{-6} cm^2/s	[175,183]
$D_{glucose\text{-}PU}$	Diffusivity of glucose in PU	Variable	[173,174]
$D_{glucose\text{-}PVA}$	Diffusivity of glucose in PVA	2 x 10^{-6} cm^2/s	[175-177,180,184]
$S_{glu\text{-}water}$	Solubility of glucose in water	165 g glucose/100 g water	[86]
$S_{glu\text{-}PU}$	Solubility of glucose in PU	Proportional to water content	[173,174]
$S_{glu\text{-}PVA}$	Solubility of glucose in PVA	Proportional to water content	[175]
$K_{glu\text{-}water/PU}$	Partition coefficient of glucose between water and PU	Variable – based on PU water content	[173,174]
$K_{glu\text{-}PVA/water}$	Partition coefficient of glucose between PVA and water	0.9	[175,176]
v_{max}	Maximum reaction rate	8.8 $mol/m^3 \cdot s$	[170]
K_m	Michaelis-Menten constant	50 mM	[179]
t_{water}	Thickness of medium layer	300 μm	Assigned
t_{PU}	Thickness of PU layer	50 μm	Assigned
t_{PVA}	Thickness of PVA layer	100 μm	Assigned

In addition to the properties of the PU layer, three parameters in the model were adjustable: the thickness of the two polymer layers and the concentration of enzyme immobilized in the PVA hydrogel, which determined the maximum rate of reaction. A reasonable value was used for the thickness of each polymer layer, given typical values found in the literature and the dimensions of the microbioreactor as described in Chapter Two. The value of v_{max}, the maximum catalytic rate of the glucose oxidase enzyme, is a product of the specific activity of the enzyme and the concentration used. It was calculated from the specific activity of a container of

laboratory-grade enzyme and concentrations of enzyme typically cited in the literature.[170] A sensitivity analysis of these assigned values in which their effect on the sensor performance is examined will be described later in this chapter.

5.3. Model of Large, Well-Stirred System

5.3.1. Generation of calibration curves

The first case that was examined is the case of the large, well-stirred system. In this system it is assumed that no gradient exists within the medium layer for the concentration of either glucose or oxygen. Furthermore, it is assumed that the medium layer is fully saturated with oxygen throughout the time course of the simulation, and that the concentration of glucose in the medium likewise remains constant at its initial value. This would be the case in a system where the volume of medium is very large compared to the size of the sensor, so that the amount of glucose that is depleted as the enzyme-catalyzed reaction proceeds does not significantly deplete the total amount of glucose within the system.

The objective was to model the transient behavior of the system and determine if a steady-state occurred in which the oxygen concentration at the surface of the oxygen sensor was constant for a given glucose concentration. A theoretical calibration curve for the sensor could then be constructed by running simulations at several different glucose concentrations.

Two patents were selected that described the synthesis, molecular structure, and properties of various polyurethane-based polymers created for the purpose of acting as a selection layer in glucose sensors (Table 5-2).[173,174] These polymers differ in the diffusivity of both glucose and oxygen through them, as well as the ratio of the two diffusivities. The ability to control these parameters is critical in the development of glucose sensors adaptable to different environments.

These particular polymers were developed to be highly permeable to oxygen and relatively impermeable to glucose in response to the oxygen-deficient environment in which they would be operating (i.e. the epidermis). Because the glucose level in a typical bioreactor (1-100 g/ℓ) is one or two orders of magnitude higher than that found in blood (~ 1 g/ℓ), a very low rate of glucose diffusion to the enzyme is also required for our application, making these polymers highly attractive.

The so-called "Polymer 2" from the MiniMed patent[174] was selected for the initial simulations. As expected, concentration gradients of glucose (Figure 5-3) and oxygen (Figure 5-4) across the two polymer layers can be seen. Curves of oxygen concentration at the oxygen sensor surface were obtained by running simulations with different medium glucose concentrations (Figure 5-5). The simulated steady-state oxygen concentrations were used to draw a theoretical calibration curve for this polymer (Figure 5-6).

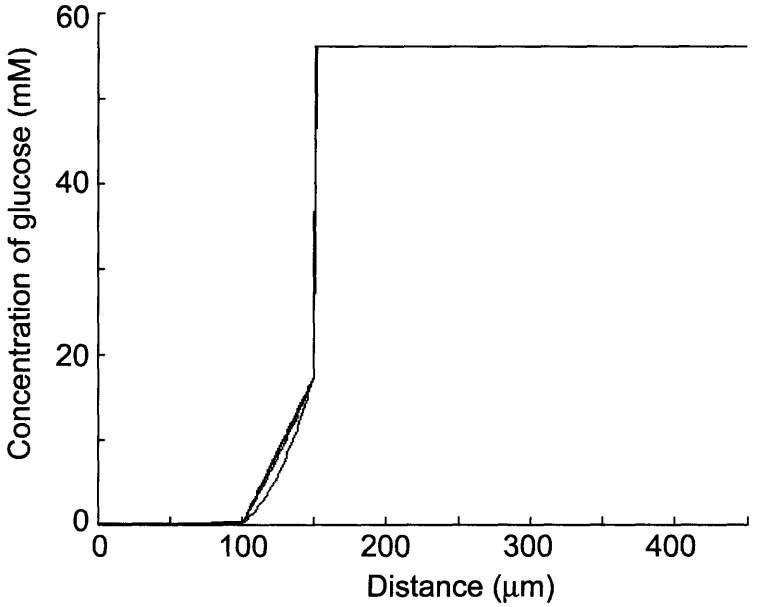

Figure 5-3. Glucose profile in sensor layers using MiniMed Polymer 2. Simulation is for 15 minutes at 1 minute intervals with a glucose concentration of 10 g/ℓ.

Table 5-2. Formulations of patent polymers to be used as a selection layer in a glucose sensor based on the oxidation of glucose in the presence of glucose oxidase.

(a) MiniMed patent[174]

Polymer	Diisocyanate	Hydrophilic Diol	Aliphatic Diol	Siloxane
1	1-6 Hexamethylene	PEG 600 20%	DEG 60%	Aminopropyl 20%
2	Isophorone	PEG 600 20%	DEG 50%	Aminopropyl 30%
3	1-6 Hexamethylene	PEG 600 50%	None	Aminopropyl 50%
4	1-6 Hexamethylene	PEG 600 40%	None	Aminopropyl 60%
5	1-6 Hexamethylene	PEG 600 60%	None	Aminopropyl 40%

PEG – polyethylene glycol
DEG – diethylene glycol

(b) Eli Lilly patent[173]

Polymer	Diisocyanate	Glycol (M)	PEO (Molecular weight)	Type
1	HMDI (0.048)	Ethylene (0.040)	600 (0.008)	Bulk
2	HMDI (0.048)	Diethylene (0.040)	600 (0.008)	Dimethylformamide
3	HMDI (0.048)	Diethylene (0.040)	1500 (0.008)	Bulk
4	HMDI (0.054)	Diethylene (0.048)	1000 (0.006)	Bulk
5	HMDI (0.052)	Diethylene (0.048)	600 (0.004)	Bulk
6	HMDI (0.052)	Diethylene (0.048)	1000 (0.004)	Bulk
7	HMDI (0.045)	Diethylene (0.042)	1500 (0.003)	Bulk
8	HMDI (0.048)	Diethylene (0.042)	600 (0.006)	Bulk

HMDI – hexamethylene-1,6-diisocyanate
PEO – polyethylene oxide
DMF - dimethylformamide

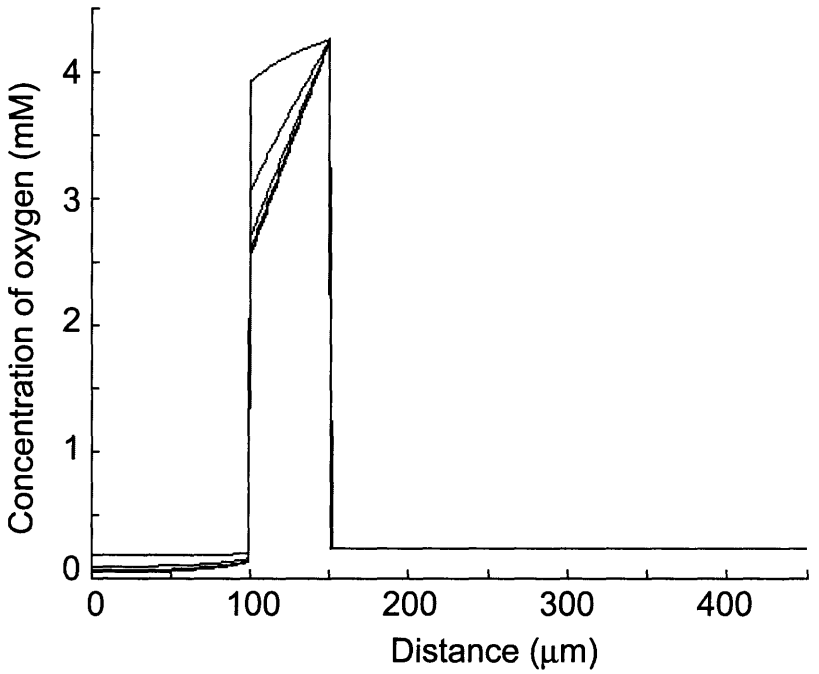

Figure 5-4. Oxygen profile in sensor layers using MiniMed Polymer 2. Simulation is for 15 minutes at 1 minute intervals with a glucose concentration of 10 g/ℓ.

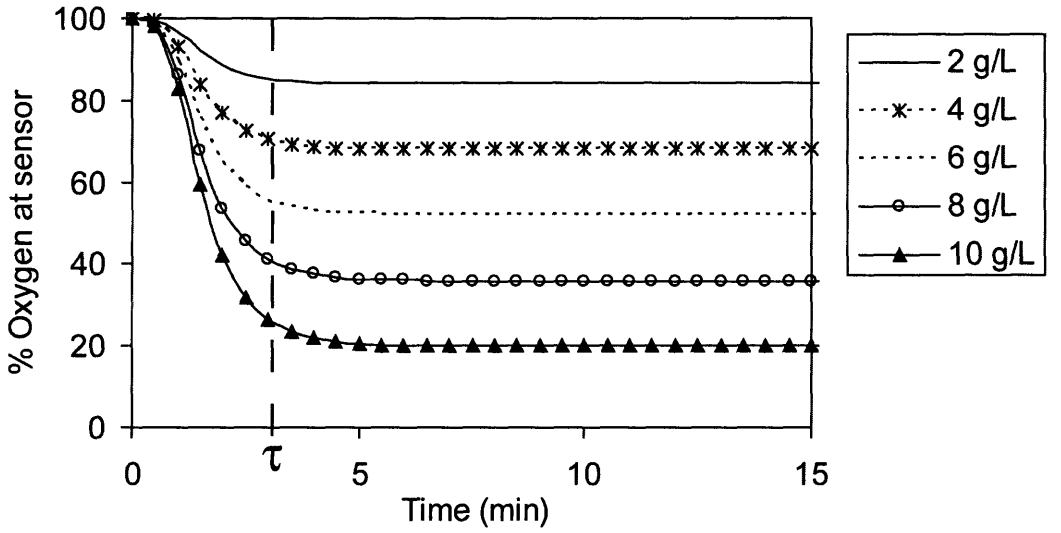

Figure 5-5. Simulations of steady-state oxygen concentration at the sensor surface using MiniMed Polymer 2. The time required to reach 90% of the final signal is defined as the time constant τ.

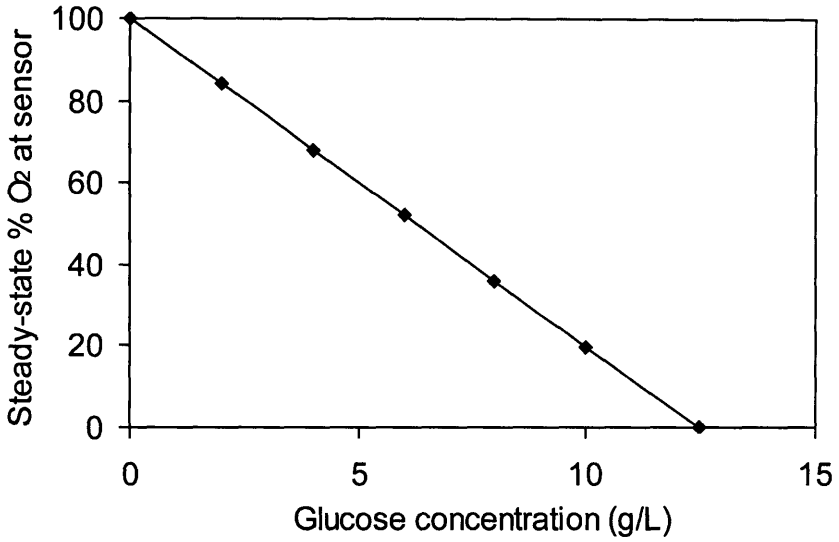

Figure 5-6. Predicted calibration curve of steady-state oxygen concentration at the oxygen sensor as a function of glucose concentration in the medium using MiniMed Polymer 2 as a selection polymer.

5.3.2. Comparison of patent polymers

A calibration curve was drawn for every patent polymer using the same procedure as for Polymer 2 (Figure 5-7 and Figure 5-8). A time constant (τ) for each sensor was calculated as the time required to reach 90% of the steady-state signal (Table 5-3). For these calculations, it is assumed that the response of the oxygen sensor is immediate, that is, the time constant of the real sensor would also need to take into account the time delay in the oxygen sensor output. The analytical range of each polymer was taken as the glucose concentration at which the oxygen concentration at the oxygen sensor surface reached zero. The sensitivity was calculated from the slope of each calibration curve and is expressed as % oxygen change per g/ℓ of glucose.

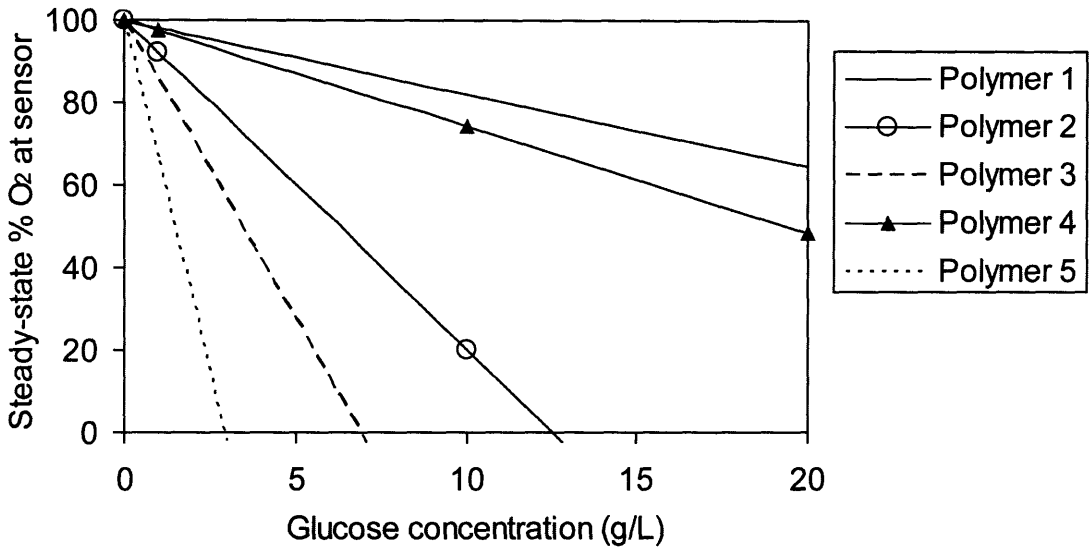

Figure 5-7. Simulated calibration curves for all MiniMed polymers.

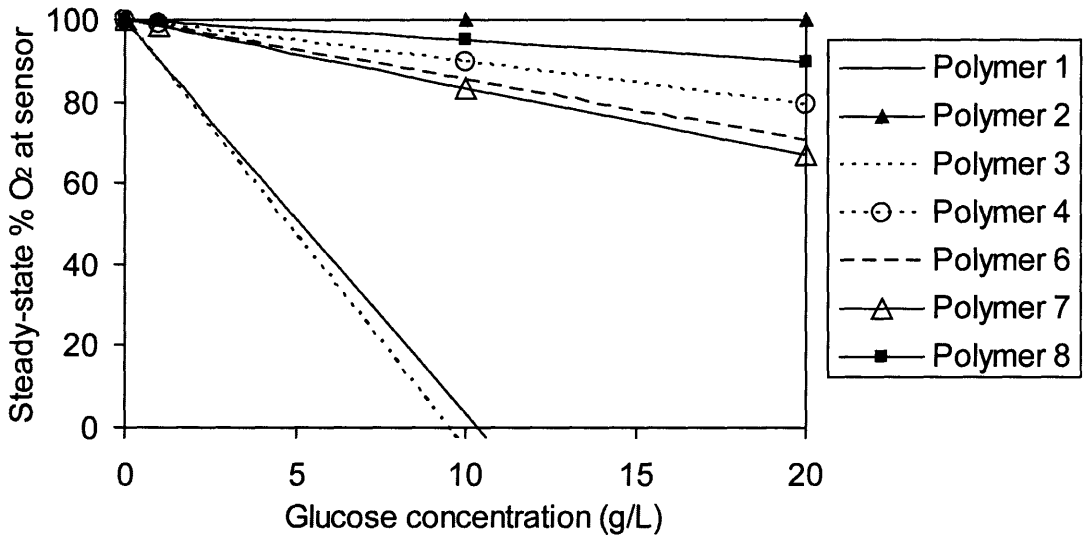

Figure 5-8. Simulated calibration curves for all Eli Lilly polymers.

Table 5-3. Measured and calculated properties of patent polymers to be used as a selection layer in a glucose sensor based on the oxidation of glucose in the presence of glucose oxidase.

(a) MiniMed patent[174]

Polymer	Water Pickup %	D_{O2} x 10^{-6} cm^2/s	$D_{Glucose}$ x 10^{-9} cm^2/s	$D_{O2}/D_{Glucose}$	τ (min)	Sensitivity (%/[g/L])	Range (g/L)
1	28.5	1.21	18.5	65	*7*	*1.7*	*56*
2	31.3	0.57	55.7	10	*3*	*8*	*12*
3	44	1.50	105	14	*1.5*	*14*	*7*
4	57	1.22	13.5	90	*9.5*	*3*	*39*
5	71	1.45	155	9	*1*	*34*	*3*

Based on simulations

(b) Eli Lilly patent[173]

Polymer	Water Pickup %	D_{O2} x 10^{-6} cm^2/s	$D_{Glucose}$ x 10^{-9} cm^2/s	$D_{O2}/D_{Glucose}$	τ (min)	Sensitivity (%/[g/L])	Range (g/L)
1	22.0	5.50	174	32	*1*	*10*	*10*
2	24.5	8.83	2.33	3790	*57*	*0.02*	*5360*
3	56.0	6.93	76.0	91	*2*	*10*	*10*
4	21.8	4.59	18.1	254	*7*	*1*	*100*
5	9.4	3.87	•	–	–	–	–
6	15.0	5.72	38.5	149	*3.5*	*1.5*	*69*
7	13.4	4.83	47.8	101	*3*	*1.6*	*61*
8	20.0	16	11	145	*11*	*0.5*	*200*

• = Impermeable
Based on simulations

It is apparent that changing the properties of the polyurethane layer can have a significant impact on the properties of the glucose sensor (Table 5-3). For example, the diffusivity of glucose through the PU layer impacts the time constant of the sensor, high diffusivities resulting in low time constants and vice versa (Figure 5-9). However, while a fast response is desirable, a high rate of glucose diffusion to the enzyme limits the range over which the sensor can be used because the large number of glucose molecules entering the PVA result in a high reaction rate, which in turn uses up the available oxygen. The trade-off is that the steep slope of the calibration

curve gives higher sensitivity. Ideally, the useable range of the sensor should be optimized to extend over the necessary range for the conditions under which it will be operating while still providing a reasonable response time. In this way maximum sensitivity and a low time constant will be achieved. These criteria were used to select a polymer for further study.

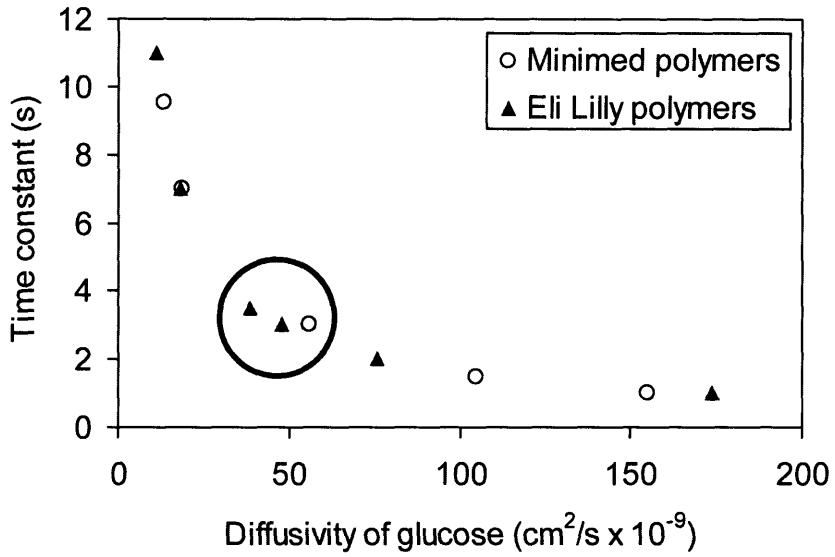

Figure 5-9. Time constants of all sensors as a function of the diffusivity of glucose through the PU layer.

Medium in the microbioreactor typically contains 10 g/ℓ of glucose. This range was therefore used as a minimum requirement for the selection of a suitable polymer for further studies, with the intention of extending it later to 20 g/ℓ to increase application flexibility and provide a reserve. Five polymers cover this range while providing a time response of five minutes or less (the maximum response time allowable for glucose sensing without control). These are Polymer 2 from MiniMed and Polymers 1, 3, 6, and 7 from Eli Lilly. Polymers 6 and 7 were eliminated because of their large range, which results in very low sensitivity. The three

remaining polymers lie in a cluster in Figure 5-9. Polymer 2 from MiniMed was finally selected because its range extends slightly beyond 10 g/ℓ, and could probably be extended beyond that in later optimization simulations.

5.4. Modeling of Small, Unstirred System with Oxygen Saturation

To further examine the potential performance of the glucose sensor, the assumption of a large, well-stirred medium was lifted with respect to glucose. In these simulations, the volume of medium in contact with the sensor was modeled to correspond to the typical volume in the microbioreactor. In addition, a glucose gradient was allowed to form as glucose diffused through, and was consumed within, the polymer layers. This assumption was approximate since a one-dimensional model was used. In reality, the entire bottom of the microbioreactor chamber would not be covered by the glucose sensor, so that the current simulation represents a worst-case scenario. However, the sensor would have to be relatively large in order to generate sufficient signal, so the assumption is valid. For these simulations, oxygen was still assumed to be saturating the medium without depletion.

It can be seen that when the large, well-stirred assumption is lifted, the concentration of glucose in the medium decreases significantly over time (Figure 5-10). That is, the measurement is altering the variable to be measured. Furthermore, this prevents the oxygen concentration at the oxygen sensor surface from reaching a steady-state, and oxygen actually begins to recover as glucose in the medium is depleted (Figure 5-11 and Figure 5-12).

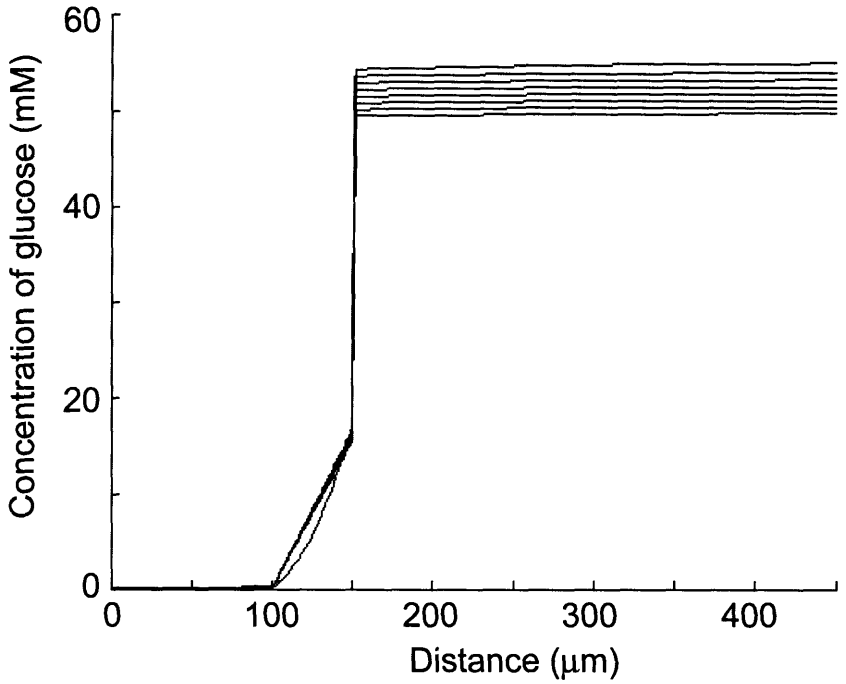

Figure 5-10. Glucose profile in the sensor layers using MiniMed Polymer 2 as a selection polymer when no stirring of the medium occurs. Oxygen is still considered to be fully saturating the medium. Simulation is for 15 minutes at 2 minute intervals with a glucose concentration of 10 g/ℓ.

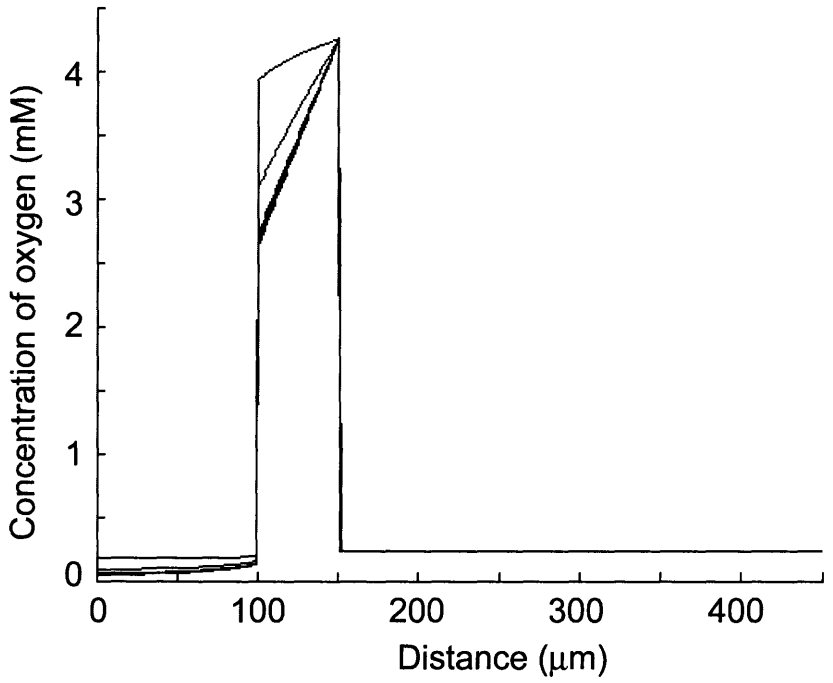

Figure 5-11. Oxygen profile in the sensor layers using MiniMed Polymer 2 as a selection polymer when no stirring of the medium occurs. Oxygen is still considered to be fully saturating the medium. Simulation is for 15 minutes at 1 minute intervals with a glucose concentration of 10 g/ℓ.

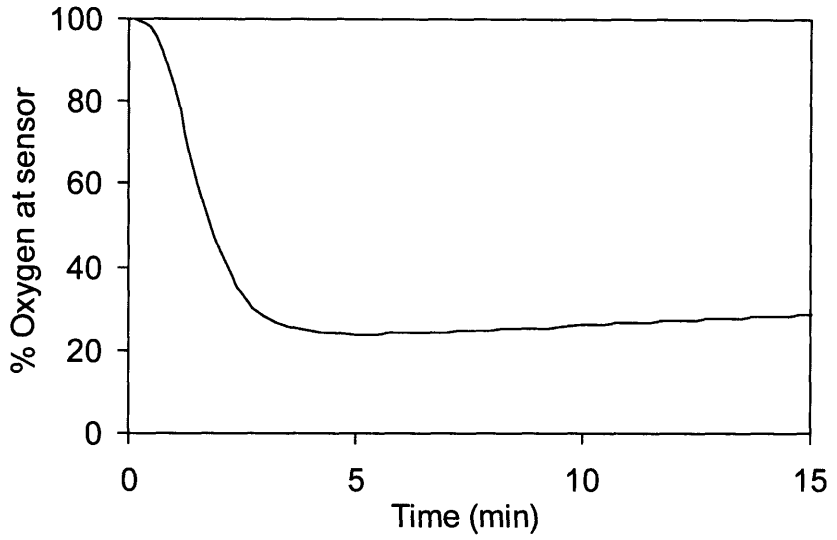

Figure 5-12. Oxygen profile at the oxygen sensor surface using MiniMed Polymer 2 as a selection polymer when no stirring of the medium occurs. Oxygen is still considered to be fully saturating the medium.

5.5. Modeling of Small, Unstirred System without Oxygen Saturation

To further investigate the performance of the glucose sensor under operating conditions, the condition of oxygen saturation of the medium was removed. For this simulation, oxygen was assumed to be diffusing into the medium from the contacting gas above. The initial condition used was a fully-saturated medium, and the boundary condition at the top of the medium layer equated the oxygen concentration with the solubility of oxygen in water. This simplification ignored the PDMS membrane through which oxygen must diffuse in experiments. However, because it was previously shown that the low solubility of oxygen in water is the primary limitation to oxygenation, the assumption is valid.

When the concentration of oxygen at the surface of the oxygen sensor is plotted over time (Figure 5-13), it is apparent that oxygen is depleted within a few minutes at this location. This is limiting for two reasons. First, oxygen must always be in excess within the PVA so that glucose

is the limiting reagent. Second, a sufficient oxygen level in the medium is vital for cell growth. The oxygen demand of the sensor is clearly too high since sufficient oxygen would not remain available. Finally, two variables to be measured – cell growth and glucose concentration – are confounded due to their interdependence on the oxygen level of the medium. Thus, neither process is occurring independently of the other.

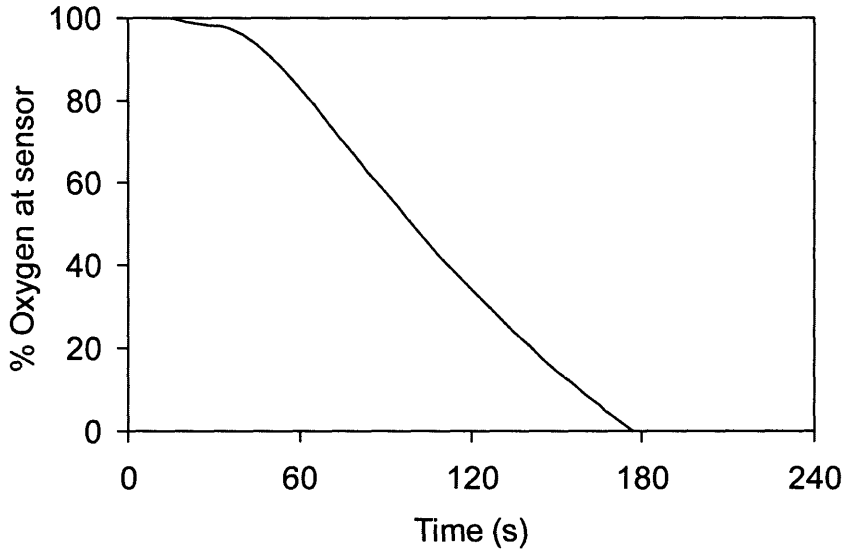

Figure 5-13. Simulated time course of oxygen concentration at the oxygen sensor surface when oxygen is no longer assumed to be saturating the medium. MiniMed Polymer 2 is used as the selection polymer, and the medium is modeled as unstirred.

5.6. Sensitivity Analysis and Optimization of Selected Polymer

In this section of the work, a sensitivity analysis of MiniMed Polymer 2 was carried out to understand the effect of the controllable parameters v_{max}, PU thickness, and PVA thickness on the properties of the resulting sensor. Each parameter was varied ± 50%, and a simulation using the original large, well-stirred assumption was carried out (Figure 5-14).

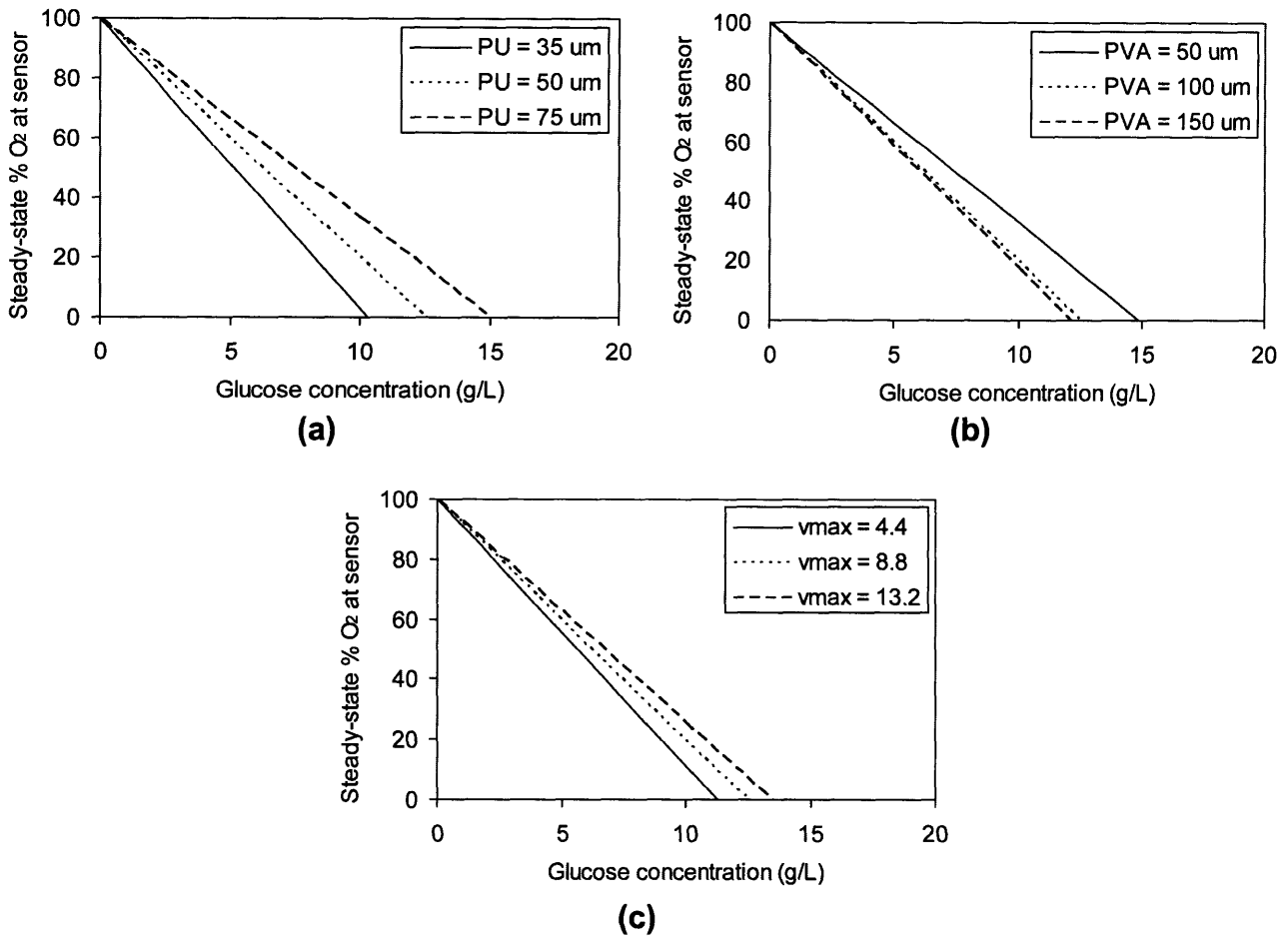

Figure 5-14. Sensitivity to changes in controllable parameters for MiniMed Polymer 2 with large, well-stirred assumption. (a) thickness of the polyurethane (PU) layer, (b) thickness of the polyvinyl alcohol (PVA) layer, (c) v_{max}.

As a second step, an attempt was made to optimize Polymer 2 to cover a wider range of glucose concentrations. The goal was to increase the analytical range to approximately 20 g/ℓ of glucose in the medium, a more realistic glucose level in bench-scale fermentation. The identified trends in sensitivity that increased the analytical range of the sensor were a thicker PU layer, a thinner PVA layer, and a higher v_{max}. A full factorial experimental design (Table 5-4) was used to model the combined effects of changes in these variables (Figure 5-15).

Table 5-4. MiniMed polymer 2 optimization conditions.

Combination	Thickness of PU (μm)	Thickness of PVA (μm)	vmax (cm^2/s)
Original	**50**	**100**	**8.8**
1	**50**	50	13.2
2	75	50	**8.8**
3	75	**100**	13.2
4	75	50	13.2

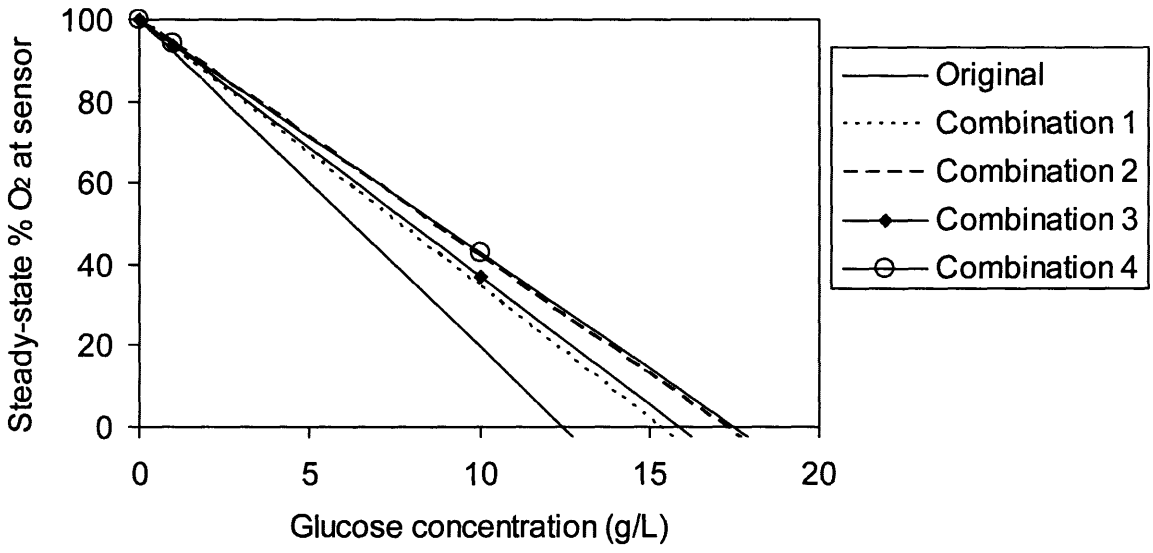

Figure 5-15. Optimization of MiniMed Polymer 2 with large, well-stirred assumption.

It can be seen that changing the controllable parameters allows us to predictably manipulate the properties of the resulting sensor. In particular, by adjusting v_{max} and the thickness of the two polymer layers it is possible to extend the analytical range of the sensor to approximately 17 g/ℓ. Additional adjustments could easily be made to further extend the range.

5.7. Conclusion

We investigated a potential glucose sensor for use in the microbioreactor. The multilayer glucose sensor was based on the enzyme glucose oxidase, and operated on the principle that oxygen depletion as measured by an optical oxygen sensor could be correlated to the glucose concentration in the medium. We carried out simulations of diffusion and reaction in the system using three sets of assumptions to determine feasibility. First, we assumed that the medium was large and well-stirred, and that oxygen was continuously saturating the medium. Under these conditions it was possible to draw theoretical calibration curves for potential sensor formulations. Second, we removed the 'large' assumption and allowed the glucose in the medium to be consumed as it underwent reaction within the sensor. Under this assumption the glucose concentration in the medium was seen to decrease and calibration curves could not be drawn because the oxygen concentration never achieved a steady-state. Finally, we removed the assumption of oxygen saturation within the medium. Simulations showed that under these conditions all oxygen within the medium was quickly depleted.

The simulations carried out to model the proposed sensor demonstrate that this method is unsuitable for our application. Specifically, the volume of the microbioreactor is small enough that the glucose consumption experienced during sensor operation causes a significant drop in the glucose level in the medium. This deprives cells of glucose substrate, changes the variable to measured, and prevents a measurement from being made due to the lack of a steady-state achievable at the PVA/oxygen sensor interface. In addition, the oxygen depletion that occurs in the medium deprives cells of oxygen substrate as well as preventing a measurement from being made, since oxygen must remain in excess for the sensor reading to be meaningful.

To effectively monitor glucose within the microbioreactor, alternative methods will need to

be explored. In particular, methods that do not consume either glucose or oxygen must be considered. Other optical methods, such as Raman spectroscopy, may be more appropriate. In particular, the colorimetric method of Asher[163] appears promising. This method employs colloidal crystal arrays (CCA) embedded within hydrogels. The hydrogels contain functional groups that bind glucose reversibly, and swell and shrink in response to their glucose content. This change in size causes a shift in the lattice constant of the CCA, which in turn causes a shift in the Bragg diffraction. The method is appealing for its appropriateness to the size of our microbioreactor and to the relative simplicity of the sensing setup required to make measurements.

Chapter 6. Conclusions and Recommendations for Future Work

6.1. Conclusions

This thesis has demonstrated the feasibility of culturing bacterial cells in microliter volumes and of obtaining reproducible results similar to those shown at larger scales. A microbioreactor designed to provide sufficient oxygen to a growing culture was fabricated out of PDMS and glass. Models were developed to understand oxygen transport and consumption, as well as the kinetics of growth, within the microbioreactor. Sensors were integrated to measure the important growth parameters optical density (OD), dissolved oxygen (DO), and pH. Based on these measurements, reproducibility was established and comparisons to bench-scale bioreactors were made. It was demonstrated that the behavior of bacteria at the two scales was very similar. It was further demonstrated that off-line analysis could be carried out by serial sacrifice of microbioreactors operating under identical conditions. Additional sensing capabilities in the form of *in situ* measurements for luminescence and fluorescence were demonstrated, and a potential glucose sensor was modeled to explore feasibility.

Once reproducibility in fabrication, experimental protocol, and experimental results were established, the microbioreactor was used for several applications. The ability to monitor luminescence and fluorescence on-line enabled the use of bacterial reporter strains to characterize the bioreactor environment. The ability to reproducibly sacrifice microbioreactors mid-run was exploited to demonstrate the feasibility of linking microbioreactors to genome-wide expression studies using DNA microarrays. The potential of the microbioreactor for investigating different growth conditions was confirmed by comparing bacterial growth, as evaluated by the measured parameters, under conditions of different medium and oxygen concentration. It was

shown that statistical differences could be observed, and that these differences are similar to those observed at a larger scale.

Chapter Two demonstrated the operation of a batch microbioreactor with a volume as low as 5 $\mu\ell$ containing integrated, automated sensors for the measurement of OD, DO, and pH. The microbioreactor was fabricated out of PDMS, with glass serving as the base and a PDMS membrane allowing culture aeration. The high surface area-to-volume ratio, and the high permeability of PDMS to oxygen, allowed the culture to be well-aerated despite the lack of active mixing. We showed that results from the microbioreactor are reproducible in both complex medium (LB) and defined medium. We also demonstrated that we are able to understand the oxygen transfer characteristics of the microbioreactor, and that by assuming Monod growth of the bacteria with oxygen as the limiting nutrient, we can effectively model growth and predict oxygen consumption during a fermentation. We also showed that it is possible to sequentially sacrifice microbioreactors that are running in parallel to carry out off-line analysis using traditional techniques. This was demonstrated by using HPLC to measure glucose consumption and organic acid production during a bacterial fermentation. Finally, we showed that results obtained from the microbioreactor correspond closely with results obtained in bench-scale volumes under similar conditions, as determined by the measured growth parameters as well as total and viable cell counts and observed cell morphology.

Chapter Three presented methods for *in situ* measurements of bioluminescence and fluorescence from bacterial cultures grown in 50 $\mu\ell$ instrumented microbioreactors. Results from the microbioreactors were compared to results obtained from conventional 500 mℓ batch bioreactors and/or shake flasks. Experiments were conducted with reporter strains of *E. coli* in which the *luxCDABE* or *gfp* operon was fused to a promoter that was either expressed

constitutively or that responded to oxygen limitation. We used an anaerobiosis-sensitive *E. coli* strain to indicate the condition of oxygen depletion, and compared the response to a growth situation in which oxygen limitation does not occur to demonstrate the feasibility of using reporter strains as environmental markers. We also examined the reproducibility of the luminescence response and compared it to the reproducibility achieved with off-line measurements from a bench-scale system. We found that the unique geometry of the microbioreactor may provide an advantage over larger systems for light measurement. Due to the short path length through the bioreactor body, light extinction effects by the cells may be minimized, enabling direct measurements.

Chapter Four presented a comparison of global gene expression analysis using 500 ng of total RNA from *E. coli* cultures grown in rich or defined minimal medium in 50 μℓ bioreactors. Total RNA was isolated from microbioreactor-grown cells during the early exponential growth phase from three independent fermentations in rich medium and three independent fermentations in defined medium. cDNA labeling for microarray hybridizations was performed with the Genicon RLS dual-color array detection system. Printed microarray chips contained probes for 4,288 open reading frames (ORFs) representing the entire *E. coli* chromosome. From these experiments we found that 232 genes were expressed at significantly higher levels when cells were grown on defined glucose medium, including genes involved in amino acid biosynthesis, central metabolism and regulatory functions. Two hundred seventy-five genes were expressed at a significantly higher level when cells were grown in rich medium, including genes involved in the translational apparatus and the motility apparatus. In general, changes in gene expression observed under these conditions were similar to those observed in thousand-fold larger cultures.

Chapter Five describes simulations for a proposed glucose sensor that could be used for

in situ measurements of glucose concentration. The sensor is based on the reaction of glucose and oxygen in the presence of the enzyme catalyst glucose oxidase. Optical transduction based on the decrease in oxygen concentration at the surface of an oxygen sensor was proposed as the method of measurement. A multi-layer design was used, in which both glucose and oxygen had to diffuse through a polyurethane (PU) layer to reach the reaction layer where glucose oxidase was immobilized in polyvinyl alcohol (PVA). The PU served as a selection membrane while at the same time protecting the immobilized enzyme. Reaction within the PVA layer followed Michaelis-Menten kinetics. Several different polyurethanes with different physical and transport characteristics were used to determine feasibility and for performance optimization of the sensor under typical operating conditions in the microbioreactor. We found that the proposed glucose sensor was unsuitable for our application. Specifically, the amount of glucose and oxygen consumed in the reaction is too large compared to the amount available in the small volume of the microbioreactor.

6.2. Outlook and Recommendations for Future Work

During the initial stages of this work, one of the major tasks was to decide how the microbioreactor would fit into the current screening and bioprocess development flow. At that time it was unclear where the greatest impact could be made, and for what applications the microbioreactor was most appropriate. Two categories were defined: screening and scale-up. Screening required many parallel, reproducible experiments, while scale-up additionally required the duplication of large-scale bioreactor conditions at the miniaturized scale, such that the microbioreactor could be used to predict cellular behavior in significantly larger volumes.

With the completion of this thesis, we can begin to answer some of these questions. The results we have presented demonstrate that in its current incarnation, the microbioreactor is a

feasible screening tool for many applications such as environmental sensing and genome-wide expression profiling. Sufficient reproducibility and 'normal' behavior have been demonstrated to support this conclusion. On the other hand, the applicability of the microbioreactor to scale-up has not yet been explored. It is promising that the microbioreactor effectively mimics the growth in the Sixfors bioreactors as reflected by the measured growth parameters (OD, DO, and pH). However, the Sixfors are known to have weak stirring with resulting poor oxygen transfer characteristics. It is therefore unclear whether the similarities that we have documented can be extended to larger bioreactors, or those having very different mixing or oxygen-transfer characteristics. An obvious difference is the lack of mixing in the microbioreactor, which eliminates the effects of shear stress on the cells. To explore these issues, it will be necessary to develop microbioreactors that can more closely mimic large-scale bioreactors, such as with the inclusion of active mixing.[185] In current industrial scale-up efforts transfer functions are established since exact duplication at significantly different size scales is not possible. Similar relationships will need to be developed to enable the microbioreactor to be used as a tool in process scale-up.

Potential limitations that exist *a priori* for the application of the microbioreactor to process scale-up, even with the inclusion of active mixing, are the absence of bubbles, the achievability of high cell densities, and the extent of mixing. First, bubbles have been shown to have an effect on cellular growth in large-scale bioreactors, particularly through the cell damage they cause when bubbles burst at the liquid surface, generating very high strain rates. Since aeration through bubbling is impractical at a small scale, the emulation of this characteristic is unlikely. Second, it is not clear that the very high cell densities frequently encountered in industrial bioprocesses can be attained in microbioreactors, even when oxygen transfer is increased through active mixing.

Third, a major factor in bioprocessing is the dead zones that exist in a bioreactor as a result of imperfect mixing. These zones are characterized by low concentrations of nutrients, especially oxygen. As the bacteria move through the bioreactor as a result of stirring, they are constantly moving through areas differing in substrate concentration. This has been shown to have a deleterious effect on growth and production. By comparison, it may be difficult to simulate these pockets of widely-differing concentrations in a microbioreactor. One way to overcome this third limitation could be to take advantage of the precise control over the microbioreactor environment that is possible through an understanding of growth and transport. Different bioreactor zones could be established and studied in individual microbioreactors, and a compartmentalized approach taken to building a model of a full-size bioreactor. This approach would have an advantage over current scale-up methods, which are also limited by the difficulty of exact replication of conditions within single bioreactors of different shapes and sizes.

Another area in which future work can focus is true fluidic multiplexing of multiple microbioreactors. This is a necessary step if economies of scale-out in the form of reduced labor and time are to be fully realized. Fluidic integration is especially critical for continuous culture applications, such as a microchemostat.[186] One strategy that has been explored is a system that allows multiple (four or eight) microbioreactors to operate simultaneously with on-line parameter measurements by allowing the measurement arm, which holds the optical fibers, to move from bioreactor to bioreactor between readings.[185] Such a system makes it possible to perform a greater number of experiments, but currently has the limitation that effort and complexity continue to scale with the number of devices. An alternative strategy under investigation is the use of PDMS to form multiple bioreactor chambers and to perform peristaltic mixing.[187] Although the fluidics still exist primarily as external tubing interconnects, the

fabrication of a disposable cassette with the potential for additional integration is a step toward a multiplexed platform.

A large impact with increased fluidic integration could also be made by streamlining the incubation and preculture stages, both of which are time and labor-intensive. The ability to go from inoculation with cells from a plate to a completed fermentation run on a single device would greatly reduce both the effort involved in preparing and running fermentations, as well as the sources of error associated with current transfers between stages.

One feature of the microbioreactor that we modeled but never used to our benefit is the ability to obtain and maintain a gradient. In the present study it was the oxygen gradient that we considered, but with proper design considerations and different concentrations of the desired species on either side of the microbioreactor, other controlled gradients could be established. These gradients could be used to explore cell behavior such as chemotaxis,[188,189] or simply to culture cells that require gradients to survive, such as the magnetosomes.[190] Magnetotactic bacteria have the ability to orient and migrate along geomagnetic field lines as a result of intracellular magnetic structures. They are found in highest abundance at oxic/anoxic transition zones in freshwater and marine habitats, and they have been especially difficult to isolate and cultivate in the laboratory because of their dependence on chemical and redox gradients, which have been difficult to mimic. The microbioreactor of the present work could potentially be a valuable tool for the study of organisms such as these.

Lastly, our results from the luminescence and fluorescence studies suggest that the design and configuration of the microbioreactor may allow direct, on-line reading of emitted light unhampered by the inner filter effect, which may thus be more reliable and reproducible than error-prone measurements obtained off-line. One area in which this ability could have a great

impact is that of genome-wide expression profiling. Currently, samples must be removed at set time points, and the data for each analyzed using a separate DNA microarray. The ability to monitor the expression of a gene (and, with parallel scale-out, potentially all of the genes for a given cell) in real-time, would obviate the need for discrete analysis at different times and provide a true dynamic picture of cellular gene expression.

References

[1] Buckland, B. C. & M. D. Lilly. in *Bioprocessing* (ed. Stephanopolous, G.) 7-73 (VCH Publishers Inc., New York, 1993).

[2] Schmid, R. D. & R. Hammelehle. *Pocket Guide to Biotechnology and Genetic Engineering* (Wiley-VCH, 2003).

[3] Swarz, J. R. Advances in *Escherichia coli* production of therapeutic proteins. *Current Opinion in Biotechnology* **12**, 195-201 (2001).

[4] Baneyx, F. Recombinant protein expression in *Escherichia coli*. *Current Opinion in Biotechnology* **10**, 411-421 (1999).

[5] Parekh, S., V. A. Vinci & R. J. Strobel. Improvement of microbial strains and fermentation processes. *Applied Microbiology and Biotechnology* **54**, 287-301 (2000).

[6] Chiang, S. J. Strain improvement for fermentation and biocatalysis processes by genetic engineering technology. *Journal of Industrial Microbiology & Biotechnology* **31**, 99-108 (2004).

[7] Rhodius, V., T. K. Van Dyk, C. Gross & R. A. LaRossa. Impact of genomic technologies on studies of bacterial gene expression. *Annual Review of Microbiology* **56**, 599-624 (2002).

[8] Baeumner, A. J. Biosensors for environmental pollutants and food contaminants. *Analytical and Bioanalytical Chemistry* **377**, 434-445 (2003).

[9] March, J. C., G. Rao & W. E. Bentley. Biotechnological applications of green fluorescent protein. *Applied Microbiology and Biotechnology* **62**, 303-315 (2003).

[10] Jansson, J. K. Marker and reporter genes: illuminating tools for environmental microbiologists. *Current Opinion in Microbiology* **6**, 310-316 (2003).

[11] Andreescu, S. & O. A. Sadik. Trends and challenges in biochemical sensors for clinical and environmental monitoring. *Pure and Applied Chemistry* **76**, 861-878 (2004).

[12] Naylor, L. H. Reporter gene technology: the future looks bright. *Biochemical Pharmacology* **58**, 749-757 (1999).

[13] Van Dyk, T. K. et al. Rapid and sensitive pollutant detection by induction of heat shock gene-bioluminescence gene fusions. *Applied and Environmental Microbiology* **60**, 1414-1420 (1994).

[14] Rupani, S. P. et al. Characterization of the stress response of a bioluminescent biological sensor in batch and continuous cultures. *Biotechnology Progress* **12**, 387-392 (1996).

[15] Bechor, O., D. R. Smulski, T. K. Van Dyk, R. A. LaRossa & S. Belkin. Recombinant microorganisms as environmental biosensors: pollutants detection by *Escherichia coli* bearing *fabA '':: lux* fusions. *Journal of Biotechnology* **94**, 125-132 (2002).

[16] Rozen, Y., T. K. Van Dyk, R. A. LaRossa & S. Belkin. Seawater activation of *Escherichia coli* gene promoter elements: Dominance of *rpoS* control. *Microbial Ecology* **42**, 635-643 (2001).

[17] Cha, H. J., R. Srivastava, V. M. Vakharia, G. Rao & W. E. Bentley. Green fluorescent protein as a noninvasive stress probe in resting *Escherichia coli* cells. *Applied and Environmental Microbiology* **65**, 409-414 (1999).

[18] Funabashi, H. et al. Non-destructive monitoring of *rpoS* promoter activity as stress marker for evaluating cellular physiological status. *Journal of Biotechnology* **95**, 85-93 (2002).

[19] Lu, C., W. E. Bentley & G. Rao. Comparisons of oxidative stress response genes in

aerobic *Escherichia coli* fermentations. *Biotechnology and Bioengineering* **83**, 864-870 (2003).

[20] Seo, J. H., D. G. Kang & H. J. Cha. Comparison of cellular stress levels and green-fluorescent-protein expression in several *Escherichia coli* strains. *Biotechnology and Applied Biochemistry* **37**, 103-107 (2003).

[21] Buckland, B. C., D. K. Robinson & M. Chartrain. Biocatalysis for pharmaceuticals - status and prospects for a key technology. *Metabolic Engineering* **2**, 42-48 (1999).

[22] Shanks, J. V. & G. Stephanopoulos. Biochemical engineering - bridging the gap between gene and product. *Current Opinion in Biotechnology* **11**, 169-170 (2000).

[23] Jasny, B. R. & D. Kennedy. The human genome. *Science* **291**, 1153-1153 (2001).

[24] John, G. T., I. Klimant, C. Wittmann & E. Heinzle. Integrated optical sensing of dissolved oxygen in microtiter plates: A novel tool for microbial cultivation. *Biotechnology and Bioengineering* **81**, 829-836 (2003).

[25] Stitt, D. T., M. S. Nagar, T. A. Haq & M. R. Timmins. Determination of growth rate of microorganisms in broth from oxygen-sensitive fluorescence plate reader measurements. *BioTechniques* **32**, 684, 686, 688-689 (2002).

[26] John, G. T., D. Goelling, I. Klimant, H. Schneider & E. Heinzle. pH-sensing 96-well microtitre plates for the characterization of acid production by dairy starter cultures. *Journal of Dairy Research* **70**, 327-333 (2003).

[27] Anderlei, T. & J. Buchs. Device for sterile online measurement of the oxygen transfer rate in shaking flasks. *Biochemical Engineering Journal* **7**, 157-162 (2001).

[28] Tolosa, L., Y. Kostov, P. Harms & G. Rao. Noninvasive measurement of dissolved oxygen in shake flasks. *Biotechnology and Bioengineering* **80**, 594-597 (2002).

[29] Gupta, A. & G. Rao. A study of oxygen transfer in shake flasks using a non-invasive oxygen sensor. *Biotechnology and Bioengineering* **84**, 351-358 (2003).

[30] Wittmann, C., H. M. Kim, G. John & E. Heinzle. Characterization and application of an optical sensor for quantification of dissolved O_2 in shake-flasks. *Biotechnology Letters* **25**, 377-380 (2003).

[31] Weuster-Botz, D., J. Altenbach-Rehm & M. Arnold. Parallel substrate feeding and pH-control in shaking-flasks. *Biochemical Engineering Journal* **7**, 163-170 (2001).

[32] Kelley, B. D., T.-W. Chiou, M. Rosenberg & D. I. C. Wang. in *Bioprocessing* (ed. Stephanopolous, G.) 23-38 (VCH Publishers Inc., New York, 1993).

[33] Petersen, K. E. Silicon as a mechanical material. *Proceedings of the IEEE* **70**, 420-457 (1982).

[34] Trimmer, W. *Micromechanics and MEMS: classic and seminal papers to 1990* (IEEE Press, New York, 1997).

[35] Voldman, J., M. L. Gray & M. A. Schmidt. Microfabrication in biology and medicine. *Annual Review of Biomedical Engineering* **1**, 401-425 (1999).

[36] Voldman, J. BioMEMS: Building with cells. *Nature materials* **2**, 433-434 (2003).

[37] Jensen, K. F. Microreaction engineering - is small better? *Chemical Engineering Science* **56**, 293-303 (2001).

[38] Laurell, T., J. Nilsson, K. Jensen, D. J. Harrison & J. P. Kutter. in *Micro Total Analysis Systems 2004* (The Royal Society of Chemistry, Malmo, Sweden, 2004).

[39] Anderson, J. R. et al. Fabrication of topologically complex three-dimensional microfluidic systems in PDMS by rapid prototyping. *Analytical Chemistry* **72**, 3158-3164 (2000).

[40] Xia, Y. N. & G. M. Whitesides. Soft lithography. *Annual Review of Materials Science* **28**, 153-184 (1998).
[41] Qin, D., Y. N. Xia & G. M. Whitesides. Rapid prototyping of complex structures with feature sizes larger than 20 μm. *Advanced Materials* **8**, 917-& (1996).
[42] Duffy, D. C., J. C. McDonald, O. J. A. Schueller & G. M. Whitesides. Rapid prototyping of microfluidic systems in poly(dimethylsiloxane). *Analytical Chemistry* **70**, 4974-4984 (1998).
[43] Jackman, R. J., D. C. Duffy, O. Cherniavskaya & G. M. Whitesides. Using elastomeric membranes as dry resists and for dry lift-off. *Langmuir* **15**, 2973-2984 (1999).
[44] Twork, J. V. & A. M. Yacynych (eds.) *Sensors in Bioprocess Control* (Marcel Dekker, Inc., New York and Basel, 1990).
[45] Lindemann, C., S. Marose, H. O. Nielsen & T. Scheper. 2-dimensional fluorescence spectroscopy for on-line bioprocess monitoring. *Sensors and Actuators B-Chemical* **51**, 273-277 (1998).
[46] Schugerl, K. Progress in monitoring, modeling and control of bioprocesses during the last 20 years. *Journal of Biotechnology* **85**, 149-173 (2001).
[47] Scragg, A. H. (ed.) *Bioreactors in Biotechnology* (Ellis Horwood Limited, Chichester, England, 1991).
[48] Lee, J. N., X. Jiang, D. Ryan & G. M. Whitesides. Compatibility of mammalian cells on surfaces of poly(dimethylsiloxane). *Langmuir* **20**, 11684-11691 (2004).
[49] van Kooten, T. G., J. F. Whitesides & A. F. von Recum. Influence of silicone (PDMS) surface texture on human skin fibroblast proliferation as determined by cell cycle analysis. *Journal of Biomedical Materials Research* **43**, 1-14 (1998).
[50] Folch, A. & M. Toner. Cellular micropatterns on biocompatible materials. *Biotechnology Progress* **14**, 388-392 (1998).
[51] Park, J. H., K. D. Park & Y. H. Bae. PDMS-based polyurethanes with MPEG grafts: synthesis, characterization and platelet adhesion study. *Biomaterials* **20**, 943-953 (1999).
[52] Aunins, J. G. & H.-J. Henzler. in *Bioprocessing* (ed. Stephanopolous, G.) 219-281 (VCH Publishers Inc., New York, 1993).
[53] Stanier, R. Y., M. Doudoroff & E. A. Adelberg. *The Microbial World* (Prentice-Hall Inc., Englewood Cliffs, N.J., 1970).
[54] Bacon, J. R. & J. N. Demas. Determination of oxygen concentrations by luminescence quenching of a polymer-immobilized transition-metal complex. *Analytical Chemistry* **59**, 2780-2785 (1987).
[55] Klimant, I. & O. S. Wolfbeis. Oxygen-sensitive luminescent materials based on silicone-soluble ruthenium diimine complexes. *Analytical Chemistry* **67**, 3160-3166 (1995).
[56] Demas, J. N., B. A. DeGraff & P. B. Coleman. Oxygen sensors based on luminescence quenching. *Analytical Chemistry* **71**, 793A-800A (1999).
[57] Bailey, J. E. & D. F. Ollis. *Biochemical Engineering Fundamentals* (McGraw-Hill, Inc., 1986).
[58] Kosch, U., I. Klimant, T. Werner & O. S. Wolfbeis. Strategies to design pH optodes with luminescence decay times in the microsecond time regime. *Analytical Chemistry* **70**, 3892-3897 (1998).
[59] Lin, J. Recent development and applications of optical and fiber-optic pH sensors. *Trac-Trends in Analytical Chemistry* **19**, 541-552 (2000).
[60] Norris, J. R. & D. W. Ribbons. *Methods in Microbiology* (Academic Press, New York,

1970).
[61] Debouck, C. & P. N. Goodfellow. DNA microarrays in drug discovery and development. *Nature Genetics* **21**, 48-50 (1999).
[62] Bodrossy, L. & A. Sessitsch. Oligonucleotide microarrays in microbial diagnostics. *Current Opinion in Microbiology* **7**, 245-254 (2004).
[63] Kumar, S., C. Wittmann & E. Heinzle. Minibioreactors. *Biotechnology Letters* **26**, 1-10 (2004).
[64] Kim, J. W. & Y. H. Lee. Development of microfermenter chip. *Journal of the Korean Physical Society* **33**, S462-S466 (1998).
[65] Kostov, Y., P. Harms, L. Randers-Eichhorn & G. Rao. Low-cost microbioreactor for high-throughput bioprocessing. *Biotechnology and Bioengineering* **72**, 346-352 (2001).
[66] Maharbiz, M. M., W. J. Holtz, S. Sharifzadeh, J. D. Keasling & R. T. Howe. A microfabricated electrochemical oxygen generator for high-density cell culture arrays. *Journal of Microelectromechanical Systems* **12**, 590-599 (2003).
[67] Maharbiz, M. M., W. J. Holtz, R. T. Howe & J. D. Keasling. Microbioreactor arrays with parametric control for high-throughput experimentation. *Biotechnology and Bioengineering* **85**, 376-381 (2004).
[68] Lamping, S. R., H. Zhang, B. Allen & P. A. Shamlou. Design of a prototype miniature bioreactor for high throughput automated bioprocessing. *Chemical Engineering Science* **58**, 747-758 (2003).
[69] Gram, A. Biochemical engineering and industry. *Journal of Biotechnology* **59**, 19-23 (1997).
[70] Chartrain, M., P. M. Salmon, D. K. Robinson & B. C. Buckland. Metabolic engineering and directed evolution for the production of pharmaceuticals. *Current Opinion in Biotechnology* **11**, 209-214 (2000).
[71] Merkel, T. C., V. I. Bondar, K. Nagai, B. D. Freeman & I. Pinnau. Gas sorption, diffusion, and permeation in poly(dimethylsiloxane). *Journal of Polymer Science Part B-Polymer Physics* **38**, 415-434 (2000).
[72] Demas, J. N. & B. A. DeGraff. Design and applications of highly luminescent transition metal complexes. *Analytical Chemistry* **63**, 829-837 (1991).
[73] Lakowicz, J. R. (ed.) *Principles of Fluorescence Spectroscopy* (Plenum Publishing Corporation, 1999).
[74] Carraway, E. R., J. N. Demas, B. A. DeGraff & J. R. Bacon. Photophysics and photochemistry of oxygen sensors based on luminescent transition-metal complexes. *Analytical Chemistry* **63**, 337-342 (1991).
[75] Demas, J. N., B. A. DeGraff & W. Xu. Modeling of luminescence quenching-based sensors: comparison of multisite and nonlinear gas solubility models. *Analytical Chemistry* **67**, 1377-1380 (1995).
[76] Liebsch, G., I. Klimant, C. Krause & O. S. Wolfbeis. Fluorescent imaging of pH with optical sensors using time domain dual lifetime referencing. *Analytical Chemistry* **73**, 4354-4363 (2001).
[77] Van Suijdam, J. C., N. W. F. Kossen & A. C. Joha. Model for oxygen transfer in a shake flask. *Biotechnology and Bioengineering* **20**, 1695-1709 (1978).
[78] Ausubel, F. M. et al. (eds.) *Short Protocols in Molecular Biology* (John Wiley & Sons, Inc., 1995).
[79] Monod, J. The growth of bacterial cultures. *Annual Review of Microbiology* **3**, 371-394

(1949).
[80] Perry, R. H. & D. Green (eds.) *Perry's Chemical Engineering Handbook* (R.R. Donnelley & Sons Company, 1984).
[81] Konz, J. O., J. King & C. L. Cooney. Effects of oxygen on recombinant protein expression. *Biotechnology Progress* **14**, 393-409 (1998).
[82] Verhulst, P.-F. Notice sur la loi que la population suit dans son accroissement. *Correspondance Mathematique et Physique*, 113-121 (1838).
[83] Randers-Eichhorn, L., R. A. Bartlett, D. D. Frey & G. Rao. Noninvasive oxygen measurements and mass transfer considerations in tissue culture flasks. *Biotechnology and Bioengineering* **51**, 466-478 (1996).
[84] Maier, U. & J. Buchs. Characterisation of the gas-liquid mass transfer in shaking bioreactors. *Biochemical Engineering Journal* **7**, 99-106 (2001).
[85] Hermann, R., M. Lehmann & J. Buchs. Characterization of gas-liquid mass transfer phenomena in microtiter plates. *Biotechnology and Bioengineering* **81**, 178-186 (2003).
[86] Lide, D. R. (ed.) *CRC Handbook of Chemistry and Physics* (CRC Press, 2001).
[87] Brunker, R. L. & O. R. Brown. Effects of hyperoxia on oxidized and reduced NAD and NADP concentrations in *Escherichia coli*. *Microbios* **4**, 193-203 (1971).
[88] Gottlieb, S. F. Effect of hyperbaric oxygen on microorganisms. *Annual Review of Microbiology* **25**, 111-152 (1971).
[89] Onken, U. & E. Liefke. Effect of total and partial pressure (oxygen and carbon dioxide) on aerobic microbial processes. *Advances in Biochemical Engineering/Biotechnology* **40**, 137-169 (1989).
[90] Bauer, S. & J. Shiloach. Maximal exponential growth rate and yield of *E. coli* obtainable in a bench-scale fermentor. *Biotechnology and Bioengineering* **16**, 933-941 (1974).
[91] Ge, X., Y. Kostov & G. Rao. High-stability non-invasive autoclavable naked optical CO_2 sensor. *Biosensors & Bioelectronics* **18**, 857-865 (2003).
[92] Engebrecht, J., M. Simon & M. Silverman. Measuring gene expression with light. *Science* **227**, 1345-1347 (1985).
[93] Hastings, J. W., C. J. Potrikus, S. C. Gupta, M. Kurfurst & J. C. Makemson. Biochemistry and physiology of bioluminescent bacteria. *Advances in Microbial Physiology* **26**, 235-291 (1985).
[94] Meighen, E. A. Enzymes and genes from the lux operons of bioluminescent bacteria. *Annual Review of Microbiology* **42**, 151-176 (1988).
[95] Meighen, E. A. Molecular biology of bacterial bioluminescence. *Microbiological Reviews* **55**, 123-142 (1991).
[96] Chalfie, M., Y. Tu, G. Euskirchen, W. W. Ward & D. C. Prasher. Green fluorescent protein as a marker for gene expression. *Science* **263**, 802-805 (1994).
[97] Shimomura, O., F. H. Johnson & Y. Saiga. Extraction, purification and properties of aequorin, a bioluminescent protein from the luminous *hydromedusan, Aequorea*. *Journal of Cellular and Comparative Physiology* **59**, 223-239 (1962).
[98] Morin, J. G. & J. W. Hastings. Energy transfer in a bioluminescent system. *Journal of cellular physiology* **77**, 313-318 (1971).
[99] Morise, H., O. Shimomura, F. H. Johnson & J. Winant. Intermolecular energy transfer in the bioluminescent system of *Aequorea*. *Biochemistry* **13**, 2656-2662 (1974).
[100] Selifonova, O., R. Burlage & T. Barkay. Bioluminescent sensors for detection of bioavailable mercury(II) in the environment. *Applied and Environmental Microbiology*

59, 3083-3090 (1993).

[101] Riether, K. B., M. A. Dollard & P. Billard. Assessment of heavy metal bioavailability using *Escherichia coli zntAp::lux* and *copAp::lux*-based biosensors. *Applied Microbiology and Biotechnology* **57**, 712-716 (2001).

[102] King, J. M. H. et al. Rapid, sensitive bioluminescent reporter technology for naphthalene exposure and biodegradation. *Science* **249**, 778-781 (1990).

[103] Belkin, S., D. R. Smulski, A. C. Vollmer, T. K. Van Dyk & R. A. LaRossa. Oxidative stress detection with *Escherichia coli* harboring a *katG'::lux* fusion. *Applied and Environmental Microbiology* **62**, 2252-2256 (1996).

[104] Rozen, Y., A. Nejidat, K.-H. Gartemann & S. Belkin. Specific detection of p-chlorobenzoic acid by *Escherichia coli* bearing a plasmid-borne *fcbA'::lux* fusion. *Chemosphere* **38**, 633-641 (1999).

[105] Van Dyk, T. K. et al. A genomic approach to gene fusion technology. *Proceedings of the National Academy of Sciences of the United States of America* **98**, 2555-2560 (2001).

[106] Van Dyk, T. K., B. L. Ayers, R. W. Morgan & R. A. Larossa. Constricted flux through the branched-chain amino acid biosynthetic enzyme acetolactate synthase triggers elevated expression of genes regulated by *rpoS* and internal acidification. *Journal of Bacteriology* **180**, 785-792 (1998).

[107] Kalir, S. et al. Ordering genes in a flagella pathway by analysis of expression kinetics from living bacteria. *Science* **292**, 2080-2083 (2001).

[108] Sabina, J. et al. Interfering with different steps of protein synthesis explored by transcriptional profiling of *Escherichia coli* K-12. *Journal of Bacteriology* **185**, 6158-6170 (2003).

[109] Lu, C., W. E. Bentley & G. Rao. A high-throughput approach to promoter study using green fluorescent protein. *Biotechnology Progress* **20**, 1634-1640 (2004).

[110] Gupta, R. K., S. S. Patterson, S. Ripp, M. L. Simpson & G. S. Sayler. Expression of the *Photorhabdus luminescens* lux genes (*luxA, B, C, D, and E*) in *Saccharomyces cerevisiae*. *Fems Yeast Research* **4**, 305-313 (2003).

[111] Dimster-Denk, D. et al. Comprehensive evaluation of isoprenoid biosynthesis regulation in *Saccharomyces cerevisiae* utilizing the Genome Reporter Matrix(TM). *Journal of Lipid Research* **40**, 850-860 (1999).

[112] Li, J. C., H. X. Xu, W. K. Herber, W. E. Bentley & G. Rao. Integrated bioprocessing in *Saccharomyces cerevisiae* using green fluorescent protein as a fusion partner. *Biotechnology and Bioengineering* **79**, 682-693 (2002).

[113] Hakkila, K., M. Maksimow, M. Karp & M. Virta. Reporter genes *lucFF, luxCDABE, gfp,* and *dsred* have different characteristics in whole-cell bacterial sensors. *Analytical Biochemistry* **301**, 235-242 (2002).

[114] Forsberg, A. J., G. D. Pavitt & C. F. Higgins. Use of transcriptional fusions to monitor gene-expression - a cautionary tale. *Journal of Bacteriology* **176**, 2128-2132 (1994).

[115] Van Dyk, T. K., E. J. DeRose & G. E. Gonye. LuxArray, a high-density, genomewide transcription analysis of *Escherichia coli* using bioluminescent reporter strains. *Journal of Bacteriology* **183**, 5496-5505 (2001).

[116] Gu, M. B., P. S. Dhurjati, T. K. VanDyk & R. A. LaRossa. A miniature bioreactor for sensing toxicity using recombinant bioluminescent *Escherichia coli* cells. *Biotechnology Progress* **12**, 393-397 (1996).

[117] DeLisa, M. P., J. C. Li, G. Rao, W. A. Weigand & W. E. Bentley. Monitoring GFP-

operon fusion protein expression during high cell density cultivation of *Escherichia coli* using an on-line optical sensor. *Biotechnology and Bioengineering* **65**, 54-64 (1999).

[118] Zanzotto, A. et al. A membrane-aerated microbioreactor for high-throughput bioprocessing. *Biotechnology and Bioengineering* **87**, 243-254 (2004).

[119] Van Dyk, T. K. & R. A. Rosson. in *Methods in Molecular Biology: Bioluminescence Methods and Protocols* (ed. Rosson, R. A.) 85-95 (Humana Press Inc., Totowa, NJ, 1998).

[120] Blattner, F. R. et al. The complete genome sequence of *Escherichia coli* K-12. *Science* **277**, 1453-1462 (1997).

[121] Lynch, A. S. & E. C. C. Lin. in *Escherichia coli and Salmonella: Cellular and Molecular Biology* (ed. Neidhardt, F. C.) 1526-1538 (ASM Press, Washington, D.C., 1996).

[122] Yanisch-Perron, C., J. Vieira & J. Messing. Improved M13 phage cloning vectors and host strains: nucleotide sequences of the M13mp18 and pUC19 vectors. *Gene* **33**, 103-119 (1985).

[123] Jensen, P. R. & K. Hammer. The sequence of spacers between the consensus sequences modulates the strength of prokaryotic promoters. *Applied and Environmental Microbiology* **64**, 82-87 (1998).

[124] Hayes, C. S., B. Bose & R. T. Sauer. Proline residues at the C terminus of nascent chains induce *SsrA* tagging during translation termination. *Journal of Biological Chemistry* **277**, 33825-33832 (2002).

[125] Konstantinov, K. B., P. Dhurjati, T. Van Dyk, W. Majarian & R. LaRossa. Real-time compensation of the inner filter effect in high-density bioluminescent cultures. *Biotechnology and Bioengineering* **42**, 1190-1198 (1993).

[126] Lutz, H. P. & P. L. Luisi. Correction for inner filter effects in fluorescence spectroscopy. *Helvetica Chimica Acta* **66**, 1929-1935 (1983).

[127] Parker, C. A. *Photoluminescence of Solutions* (Elsevier Publishing Company, Amsterdam, 1968).

[128] Zhang, J. K., A. K. White, H. C. Kuettner, P. Boccazzi & W. W. Metcalf. Directed mutagenesis and plasmid-based complementation in the methanogenic archaeon *Methanosarcina acetivorans* C2A demonstrated by genetic analysis of proline biosynthesis. *Journal of Bacteriology* **184**, 1449-1454 (2002).

[129] Lee, H. L. T., P. Boccazzi, N. Gorret, R. J. Ram & A. J. Sinskey. *In situ* bioprocess monitoring of *Escherichia coli* bioreactions using Raman spectroscopy. *Vibrational Spectroscopy* **35**, 131-137 (2004).

[130] Loge, F. J., D. E. Thompson & D. R. Call. PCR detection of specific pathogens in water: a risk-based analysis. *Environmental Science and Technology* **36**, 2754-2759 (2002).

[131] Call, D. R., M. K. Borucki & F. J. Loge. Detection of bacterial pathogens in environmental samples using DNA microarrays. *Journal of Microbiological Methods* **53**, 235-243 (2003).

[132] Bao, P. et al. High-sensitivity detection of DNA hybridization on microarrays using resonance light scattering. *Analytical Chemistry* **74**, 1792-1797 (2002).

[133] Yguerabide, J. & E. E. Yguerabide. Resonance light scattering particles as ultrasensitive labels for detection of analytes in a wide range of applications. *Journal of Cellular Biochemistry*, 71-81 (2001).

[134] Francois, P., M. Bento, P. Vaudaux & J. Schrenzel. Comparison of fluorescence and resonance light scattering for highly sensitive microarray detection of bacterial

pathogens. *Journal of Microbiological Methods* **55**, 755-762 (2003).
[135] Tao, H., C. Bausch, C. Richmond, F. R. Blattner & T. Conway. Functional genomics: expression analysis of *Escherichia coli* growing on minimal and rich media. *Journal of Bacteriology* **181**, 6425-6440 (1999).
[136] Wei, Y. et al. High-density microarray-mediated gene expression profiling of *Escherichia coli*. *Journal of Bacteriology* **183**, 545-556 (2001).
[137] Cleveland, W. S. & S. J. Devlin. Locally weighted regression - an approach to regression-analysis by local fitting. *Journal of the American Statistical Association* **83**, 596-610 (1988).
[138] Yang, Y. H. et al. Normalization for cDNA microarray data: a robust composite method addressing single and multiple slide systematic variation. *Nucleic Acids Research* **30**, e15/11-e15/11 (2002).
[139] Tatusov, R. L., E. V. Koonin & D. J. Lipman. A genomic perspective on protein families. *Science* **278**, 631-637 (1997).
[140] Altschul, S. F. et al. Gapped BLAST and PSI-BLAST: a new generation of protein database search programs. *Nucleic Acids Research* **25**, 3389-3402 (1997).
[141] Cooper, S. Synthesis of the cell surface during the division cycle of rod-shaped, gram-negative bacteria. *Microbiological Reviews* **55**, 649-674 (1991).
[142] Gaal, T., M. S. Bartlett, W. Ross, C. L. Turnbough, Jr. & R. L. Gourse. Transcription regulation by initiating NTP concentration: rRNA synthesis in bacteria. *Science* **278**, 2092-2097 (1997).
[143] Grunberg-Manago, M. Regulation of the expression of aminoacyl-tRNA synthetases and translation factors. *Escherichia coli Salmonella typhimurium* **2**, 1386-1409 (1987).
[144] Nomura, M. Regulation of ribosome biosynthesis in *Escherichia coli* and *Saccharomyces cerevisiae*: diversity and common principles. *Journal of Bacteriology* **181**, 6857-6864 (1999).
[145] Diaz, E., A. Ferrandez & J. L. Garcia. Characterization of the *hca* cluster encoding the dioxygenolytic pathway for initial catabolism of 3-phenylpropionic acid in *Escherichia coli* K-12. *Journal of Bacteriology* **180**, 2915-2923 (1998).
[146] Hengge-Aronis, R. Survival of hunger and stress: the role of *rpoS* in early stationary phase gene regulation in *E. coli*. *Cell* **72**, 165-168 (1993).
[147] Loewen, P. C. & R. Hengge-Aronis. The role of the sigma factor sigma S (KatF) in bacterial global regulation. *Annual Review of Microbiology* **48**, 53-80 (1994).
[148] Rabin, R. S. & V. Stewart. Dual response regulators (NarL and NarP) interact with dual sensors (NarX and NarQ) to control nitrate- and nitrite-regulated gene expression in *Escherichia coli* K-12. *Journal of Bacteriology* **175**, 3259-3268 (1993).
[149] Dahl, J. L., B. Y. Wei & R. J. Kadner. Protein phosphorylation affects binding of the *Escherichia coli* transcription activator UhpA to the *uhpT* promoter. *Journal of Biological Chemistry* **272**, 1910-1919 (1997).
[150] Silverman, M. & M. Simon. Flagellar rotation and the mechanism of bacterial motility. *Nature* **249**, 73-74 (1974).
[151] McNichols, R. J. & G. L. Cote. Optical glucose sensing in biological fluids: an overview. *Journal of Biomedical Optics* **5**, 5-16 (2000).
[152] D'Auria, S. & J. R. Lakowicz. Enzyme fluorescence as a sensing tool: new perspectives in biotechnology. *Current Opinion in Biotechnology* **12**, 99-104 (2001).
[153] Cote, G. L. & R. J. McNichols. in *Biomedical Photonics Handbook* (ed. Vo-Dinh, T.)

18/11-18/19 (CRC Press, 2003).
[154] Cote, G. L. & B. D. Cameron. Noninvasive polarimetric measurement of glucose in cell culture media. *Journal of Biomedical Optics* **2**, 275-281 (1997).
[155] Chou, C. et al. Noninvasive glucose monitoring in vivo with an optical heterodyne polarimeter. *Applied Optics* **37**, 3553-3557 (1998).
[156] Haaland, D. M., M. R. Robinson, G. W. Koepp, E. V. Thomas & R. P. Eaton. Reagentless near-infrared determination of glucose in whole blood using multivariate calibration. *Applied Spectroscopy* **46**, 1575-1578 (1992).
[157] Heise, H. M., R. Marbach, T. Koschinsky & F. A. Gries. Noninvasive blood glucose sensors based on near-infrared spectroscopy. *Artificial Organs* **18**, 439-447 (1994).
[158] Wicksted, J. P., R. J. Erckens, M. Motamedi & W. F. March. Monitoring of aqueous humor metabolites using Raman spectroscopy. *Proceedings of SPIE-The International Society for Optical Engineering* **2135**, 264-274 (1994).
[159] Berger, A. J., I. Itzkan & M. S. Feld. Feasibility of measuring blood glucose concentration by near-infrared Raman spectroscopy. *Spectrochimica Acta, Part A: Molecular and Biomolecular Spectroscopy* **53A**, 287-292 (1997).
[160] Ballerstadt, R. & J. S. Schultz. Competitive-binding assay method based on fluorescence quenching of ligands held in close proximity by a multivalent receptor. *Analytica Chimica Acta* **345**, 203-212 (1997).
[161] March, W. F., K. Ochsner & J. Horna. Intraocular lens glucose sensor. *Diabetes Technology & Therapeutics* **2**, 27-30 (2000).
[162] Alexeev, V. L. et al. High ionic strength glucose-sensing photonic crystal. *Analytical Chemistry* **75**, 2316-2323 (2003).
[163] Asher, S. A. et al. Photonic crystal carbohydrate sensors: Low ionic strength sugar sensing. *Journal of the American Chemical Society* **125**, 3322-3329 (2003).
[164] Werner, W., H. G. Rey & H. Wielinger. Properties of a new chromogen for the determination of glucose in blood according to the GOD/POD method. *Fresenius' Zeitschrift fuer Analytische Chemie* **252**, 224-228 (1970).
[165] Bergmeyer, H. U., M. Grassl & H.-E. Walter. in *Methods of Enzymatic Analysis* (eds. Bergmeyer, H. U., Bergmeyer, J. & Grassl, M.) (Verlag Chemie, Weinheim, 1983).
[166] Trettnak, W., M. J. Leiner & O. S. Wolfbeis. Optical sensors. Part 34. Fibre optic glucose biosensor with an oxygen optrode as the transducer. *Analyst* **113**, 1519-1523 (1988).
[167] Wolfbeis, O. S., I. Oehme, N. Papkovskaya & I. Klimant. Sol-gel based glucose biosensors employing optical oxygen transducers, and a method for compensating for variable oxygen background. *Biosensors & Bioelectronics* **15**, 69-76 (2000).
[168] Gao, C. et al. in *2nd Annual International IEEE-EMBS Special Topic Conference on Microtechnologies in Medicine and Biology* (eds. Andre, D. & David, B.) 223-226 (Madison, Wisconsin ,USA, 2002).
[169] Ward, W. K. et al. A new amperometric glucose microsensor: in vitro and short-term in vivo evaluation. *Biosensors & Bioelectronics* **17**, 181-189 (2002).
[170] Zimmermann, S., D. Fienbork, A. W. Flounders & D. Liepmann. In-device enzyme immobilization: wafer-level fabrication of an integrated glucose sensor. *Sensors and Actuators, B: Chemical* **B99**, 163-173 (2004).
[171] Kuenzelmann, U. & H. Boettcher. Biosensor properties of glucose oxidase immobilized within SiO_2 gels. *Sensors and Actuators, B: Chemical* **B39**, 222-228 (1997).
[172] Gibson, Q. H., B. E. Swoboda & V. Massey. Kinetics and mechanism of action of

glucose oxidase. *Journal of Biological Chemistry* **239**, 3927-3934 (1964).
[173] Allen, D. J., K. W. Johnson & R. S. Nevin. in *Eur. Pat. Appl.* 12 pp. ((Eli Lilly and Co., USA)., Ep, 1993).
[174] Van Antwerp, B. in *PCT Int. Appl.* 36 pp. ((MiniMed, Inc., USA)., Wo, 1998).
[175] Ariga, O., T. Kubo & Y. Sano. Effective diffusivity of glucose in PVA hydrogel. *Journal of Fermentation and Bioengineering* **78**, 200-201 (1994).
[176] Burczak, K., T. Fujisato, M. Hatada & Y. Ikada. Protein permeation through polymer membranes for hybrid-type artificial pancreas. *Proceedings of the Japan Academy, Series B: Physical and Biological Sciences* **67**, 83-88 (1991).
[177] Sudoh, M., T. Mukouyama, M. Katsumata, H. Aoyanagi & Y. Nakano. Transport properties of oxygen, hydrogen peroxide and glucose through membrane supports for glucose sensor. *Kagaku Kogaku Ronbunshu* **17**, 119-126 (1991).
[178] Zhang, W., M. Satoh & J. Komiyama. Permeability to oxygen and nitrogen of poly(vinyl alcohol) membranes swollen with aqueous solutions of nonvolatile substances. *Journal of Membrane Science* **31**, 147-156 (1987).
[179] Glucose Oxidase (GOD) (Roche Applied Science, 2004).
[180] Praveen, S. S., R. Hanumantha, J. M. Belovich & B. L. Davis. Novel hyaluronic acid coating for potential use in glucose sensor design. *Diabetes Technology & Therapeutics* **5**, 393-399 (2003).
[181] Renneberg, R., K. Sonomoto, S. Katoh & A. Tanaka. Oxygen diffusivity of synthetic gels derived from prepolymers. *Applied Microbiology and Biotechnology* **28**, 1-7 (1988).
[182] Chen, S.-H., K.-C. Yu, S.-L. Houng & J.-Y. Lai. Gas transport properties of HTPB based polyurethane/cosalen membrane. *Journal of Membrane Science* **173**, 99-106 (2000).
[183] Tanaka, H., M. Matsumura & I. A. Veliky. Diffusion characteristics of substrates in calcium-alginate gel beads. *Biotechnology and Bioengineering* **26**, 53-58 (1984).
[184] Young, T. H., N. K. Yao, R. F. Chang & L. W. Chen. Evaluation of asymmetric poly(vinyl alcohol) membranes for use in artificial islets. *Biomaterials* **17**, 2139-2145 (1996).
[185] Szita, N. et al. Multiplexed microbioreactor system for high-throughput bioprocess development. *Special Publication - Royal Society of Chemistry* **296**, 390-392 (2004).
[186] Zhang, Z. et al. A microchemostat-continuous cell culture in microbioreactors. *Special Publication - Royal Society of Chemistry* **297**, 231-233 (2004).
[187] Lee, H. L. T. *Ph. D. Thesis in Electrical Engineering and Computer Science* (Massachusetts Institute of Technology, Expected 2005).
[188] Jeon, N. L. et al. Generation of solution and surface gradients using microfluidic systems. *Langmuir* **16**, 8311-8316 (2000).
[189] Jeon, N. L. et al. Neutrophil chemotaxis in linear and complex gradients of interleukin-8 formed in a microfabricated device. *Nature Biotechnology* **20**, 826-830 (2002).
[190] Schuler, D. & R. B. Frankel. Bacterial magnetosomes: microbiology, biomineralization and biotechnological applications. *Applied Microbiology and Biotechnology* **52**, 464-473 (1999).

APPENDIX A. Sensor Calibrations

The calibration procedures and calibration curves for the sensors used in the microbioreactor are presented in this appendix.

A.1. Calibration of optical density measurements

E. coli was grown in a shake flask to an optical density approaching seven, and serial dilutions of the medium were carried out. Optical density measurements at 600 nm were made in a microbioreactor with a depth of 300 μm as well as a spectrophotometer (Spectronic® 20 Genesys, Spectronic Instruments Inc.). Equation A-1 was used to calculate optical density from raw transmission data from the microbioreactor. In this equation I_{signal} is the intensity of the signal and $I_{reference}$ is the intensity of the signal when pure water is inside the microbioreactor. The multiplication factor of 33.33 is a normalization for the pathlength of 300 μm in the microbioreactor which enables direct comparisons with results from conventional cuvettes with pathlengths of 1 cm.

The calibration data is shown below. A linear curve fit results in an $R^2 = 0.9941$ and a slope close to one.

$$OD = 33.33 \log_{10}\left(\frac{I_{reference}}{I_{signal}}\right) \qquad \text{(A-1)}$$

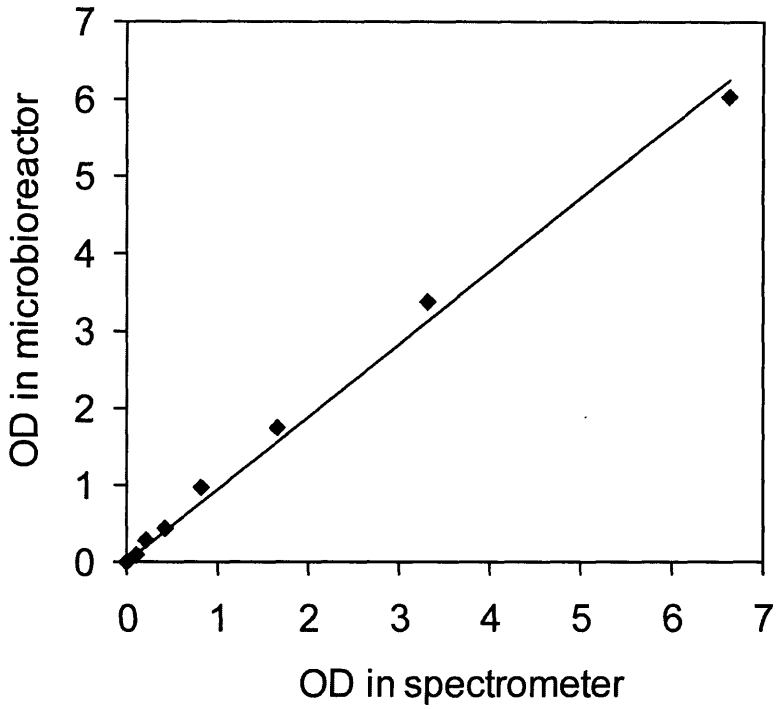

Figure A-1. Calibration curve for optical density measurements.

A.2. Calibration of dissolved oxygen sensor

Mass flow controllers for oxygen and nitrogen were used to create gas mixtures with different concentrations of oxygen, which were described as a percentage of pure oxygen. A chamber was used to flow each gas composition past the submerged sensor. Optical fibers below the sensor coupled excitation light at 505 nm to the sensor and carried the emission signal to the lock-in amplifier, where a phase shift was detected. In each case the sensor was given sufficient time to reach a steady signal. An eleven-point calibration between 0% and 100% oxygen was carried out.

The calibration data were fit to a modified Stern-Volmer equation (Equation A-2). It was found that for low oxygen concentrations, a better fit was obtained when the calibration range included in the model fit was limited to 0-21% oxygen and the experimental value for 0% was used (1-parameter fit for K_{SV}) (Figure A-2). Therefore, data from experiments with air as the contacting gas were processed using that range, and a 0% calibration was carried out for each sensor foil at the time of the experiment. Data from experiments using pure oxygen were processed using the full range of calibration (2-parameter fit for K_{SV} and ϕ_0) (Figure A-3).

$$[O_2] = \frac{1 - \dfrac{\tan\phi}{\tan\phi_0}}{K_{SV}\left(\dfrac{\tan\phi}{\tan\phi_0} - 0.11\right)} \qquad \text{(A-2)}$$

where: K_{SV} is the modified Stern-Volmer constant

ϕ is the phase shift

ϕ_0 is the phase shift at 0% dissolved oxygen

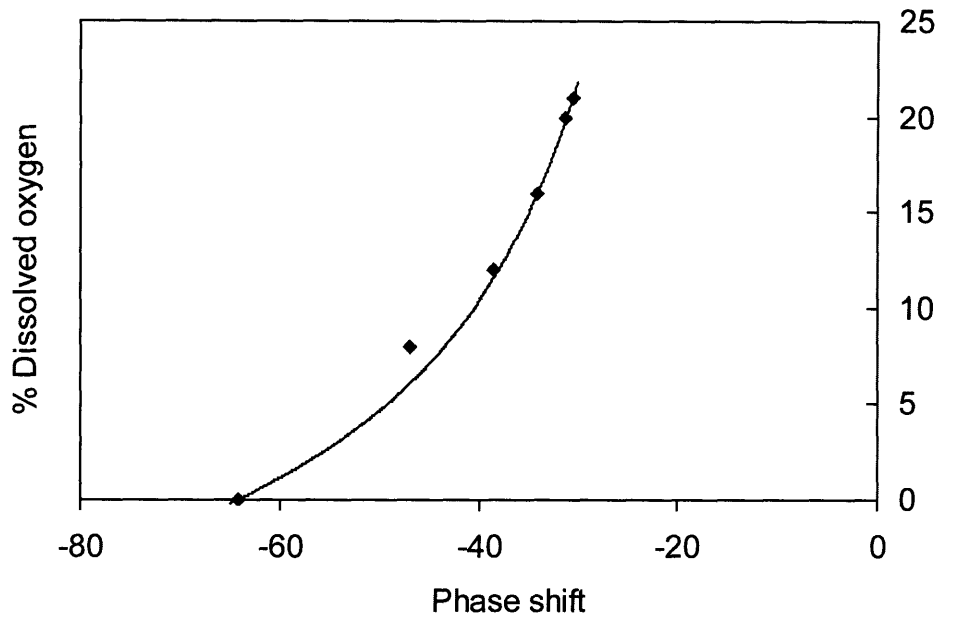

Figure A-2. Calibration of oxygen concentration range encountered when air is used as the contacting gas (0-21%). Data are fit to a 1-parameter model for each experiment.

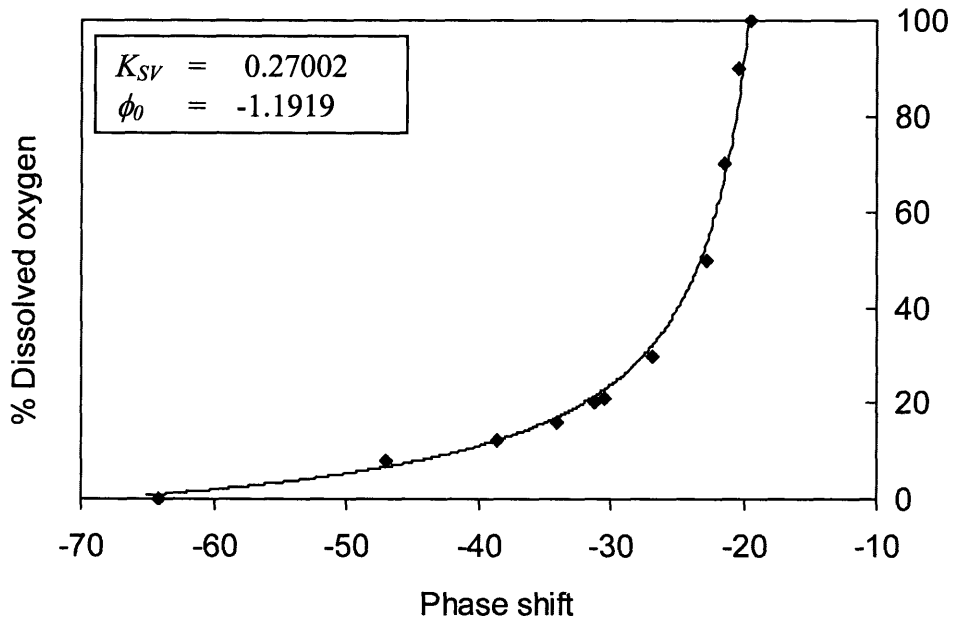

Figure A-3. Calibration of the full range of oxygen concentration (0-100%). Data are fit to a 2-parameter model.

A.3. Calibration of pH sensor

A six-point calibration was carried out between pH 4 and pH 9 using colorless buffers (VWR). Excitation light at 465 nm was coupled to the sensor using an optical fiber, and the emission signal was sent to the lock-in amplifier. The measured phase shift of the pH sensor fluorescence was correlated to the pH by fitting to the 4-parameter sigmoidal Boltzmann curve (Equation A-3).

$$Phase = \frac{\phi_{min} - \phi_{max}}{1 + e^{\left(\frac{pH - pH_0}{dpH}\right)}} + \phi_{max} \qquad \text{(A-3)}$$

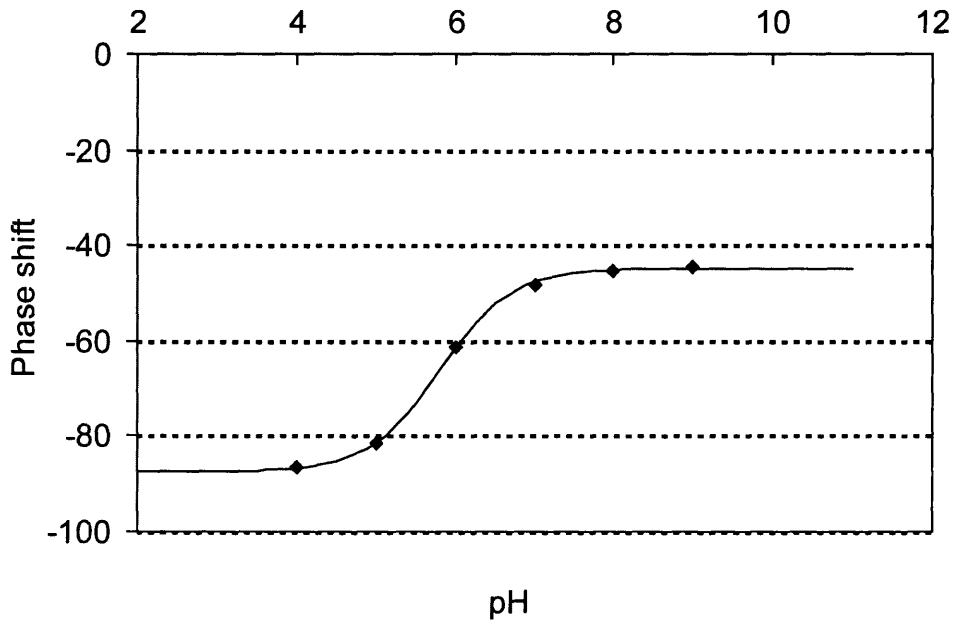

Figure A-4. Calibration of pH sensor.

APPENDIX B. Characterization of Photomultiplier Tube

This appendix presents the characterization protocols and results for the photomultiplier tube (R928, Hamamatsu) that was used in luminescence and fluorescence experiments. For all characterization procedures the current signal from the PMT was sent to a low-noise current preamplifier (Model SR570, Stanford Research Systems) operating at a sensitivity of 20 μV/A that converted the signal to a voltage that was passed to a multimeter (Fluke 45, Fluke). Data from the multimeter were logged every second using a data logger routine in LabVIEW.

Protocol 1: The signal from the multimeter was recorded with the PMT off to determine the magnitude of the instrument offset.

Protocol 2: The orange LED (Epitex L600-10V, 600nm) used for optical density measurements was turned on for 60 minutes to ensure that it had warmed-up sufficiently and generated a steady signal. The voltage to the LED was 350 mV. The cold PMT (off overnight) was then turned on suddenly, and the signal was recorded for one hour (Figure B-1).

Protocol 3: With the orange LED constantly on, the PMT was turned off for 10 minutes, then turned back on. The signal was recorded for one hour (Figure B-2).

Protocol 4: The LED was turned off for 10 minutes, after which time it was turned back on. The PMT remained on during this time, and the signal was recorded for one hour (Figure B-3).

Protocol 5: With the PMT continuously on, step changes in the LED voltage were made. The

PMT signal at each voltage was recorded for 15 minutes. The voltages used were 350 mV – 340 mV –330 mV – 340 mV – 350 mV – 360 mV (Figure B-4).

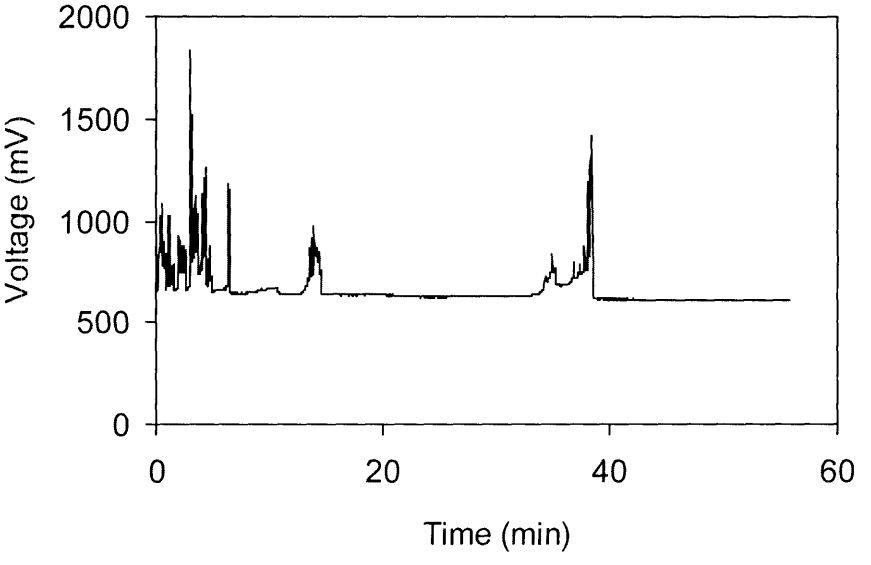

Figure B-1. PMT response when the cold PMT is turned on while the 600 nm LED is shining.

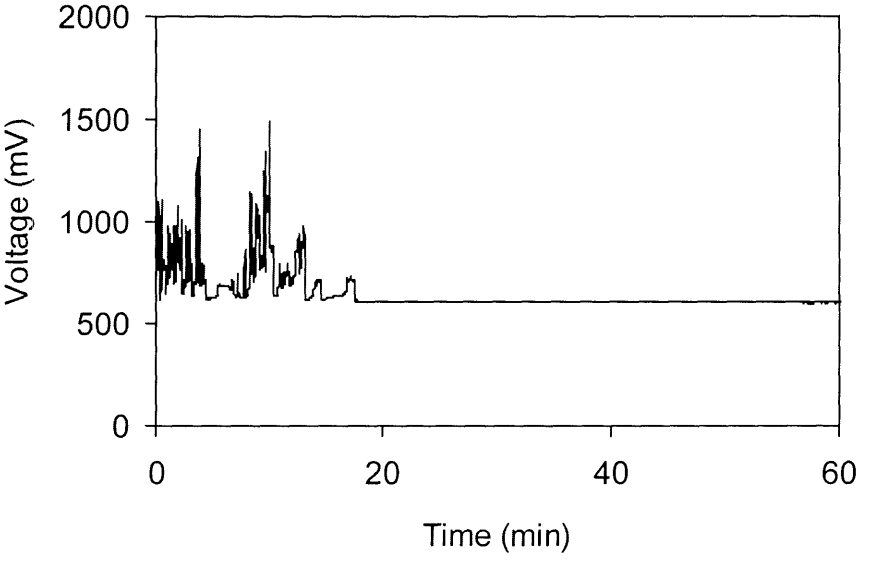

Figure B-2. PMT response when the warm PMT is turned off for 10 minutes, then turned back on while the 600 nm LED shines continuously.

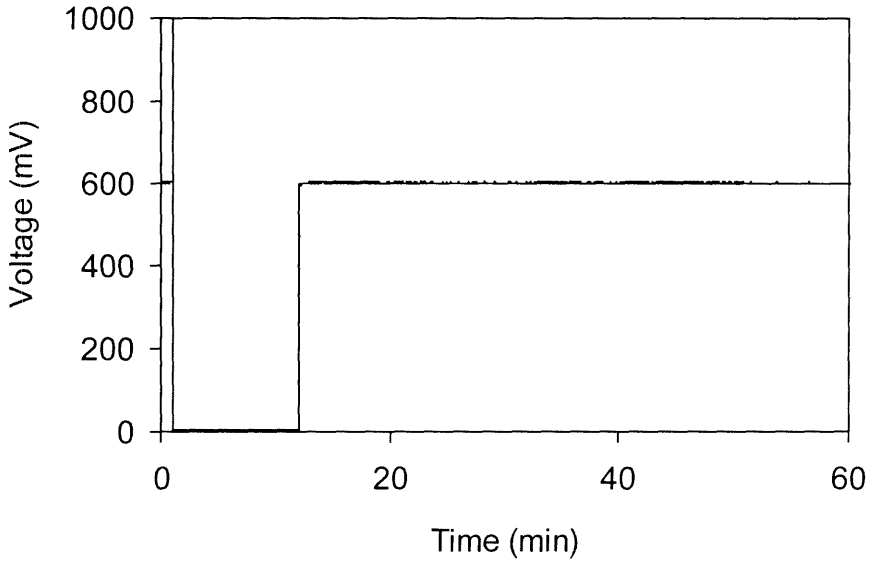

Figure B-3. PMT response when the 600 nm LED is turned off for 10 minutes, then turned back on.

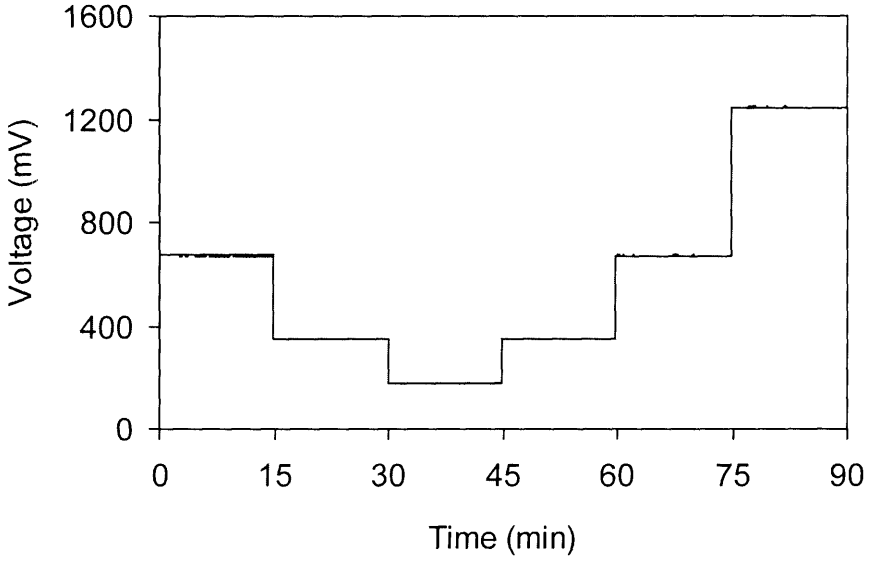

Figure B-4. PMT response to step changes in the LED voltage.

PMT characteristics when the current preamplifier is set to a sensitivity of 20 μA/V:

PMT voltage:	900 V
Anode luminous sensitivity (from Matsudaira lab):	1419 A/lm
Mean of instrument offset:	1.37 μV
Standard deviation (SD) of instrument offset:	0.12 μV
Mean of offset + dark current (dark chamber):	2.92 μV
Standard deviation of offset + dark current:	0.09 μV
Signal-to-noise of offset + dark current:	30
Anode dark current:	1.55 μV (0.03 nA)
Conversion:	1 lumen = 4×10^{15} photons/s at 555 nm
Lower detection limit of PMT (2 SDs above mean background):	100 photons/s

APPENDIX C. Protocol for Microbioreactor Fabrication

C.1. Obtaining PDMS layers

Treat wafers with silane to prevent PDMS from sticking in subsequent steps. To do so, place a few drops of silane reagent (tridecafluoro-1,1,2,2-tetrahydro octyl trichlorosilane) into a vial. Put the wafer in a petri dish and place it into a vacuum chamber together with the silane reagent in the open vial. Let the silane evaporate under vacuum for at least 2 hours. It is better to err on the side of more time rather than less. The setup can safely be left overnight, and several wafers can be treated simultaneously. After silanization is completed, remove the wafers and dispose of the vial as chemically contaminated glass.

Weigh out PDMS prepolymer and initiator (10:1) and mix in a cup. Degas the mixture under vacuum until no bubbles are visible. For consistent results during the subsequent spinning step, degassing should be carried out for a standardized period of time since the polymer immediately begins to cure and the rheological properties begin to change. A time of 30 minutes is suggested as ideal for all bubbles to be eliminated. Spin the PDMS to obtain PDMS layers of 100 μm (for the membrane) and 300 μm (for the body and base). Spinning protocol for the spinner in the KFJ laboratory:

Volume:	5 mℓ
Acceleration:	Maximum (dial turned all the way to the right)
Spinning time:	20 seconds
Rpm:	100 μm membrane - 1240
	300 μm membrane - 430

The above conditions are valid if spinning is carried out within 30 minutes of the PDMS being taken out of the degassing chamber, since the PDMS continues to thicken. After spinning,

cure the PDMS in an oven at 70°C for 2 hours.

C.2. Microbioreactor assembly

Use a razor blade to cut the PDMS into pieces of the desired size. Use the machined punches to cut round circles into the PDMS. Holes for the DO and pH sensors should be 1.1 mm in diameter. Also cut any desired channels into the PDMS body layer. Punch DO and pH sensors out of the sensor foil sheets. Sensors should be 0.9 mm in diameter.

To assemble the microbioreactor, begin by gluing the base PDMS layer to a glass cover slip using silicone adhesive (ASI 502, American Sealants, Inc.). Use tweezers to handle the PDMS. Use a wooden stick with a rolling motion to press the PDMS down. Since the coverslips are fragile, a microscope slide can be used underneath as a support during the assembly process. Once the base is glued down, the body can be added next. Use the same adhesive and again roll the PDMS layer to ensure that it is flat and in contact with the layer beneath. Next, place a small amount of vacuum grease into the opening for the two sensors (use the tip of a 30 gauge needle). Then, use tweezers to insert the two sensors (with the sensing side up) into the holes, using the end of the wooden stick to gently press the sensors down until they are even with the bottom layer. Finally, glue the membrane over the structure, using the wooden stick in an outward rolling motion to flatten and tighten the aeration membrane. Place the finished microbioreactor into a covered Petri dish containing water (the microbioreactor should not be in direct contact with the water). Use paraffin paper to close the Petri dish and leave overnight at room temperature to cure.

Appendix D. Protocols for Microbioreactor Experiments

D.1. Inoculation of bacteria

To inoculate the microbioreactor, use a 1 mℓ syringe to withdraw medium from the Falcon tube containing the inoculated culture. Attach a 23 gauge needle to the syringe. Before introducing the medium into the chamber, use a needle to pierce holes into the channels of the microbioreactor, and also place a needle into the channel opposite of the one that the medium will be injected through. This is to give air within the bioreactor a way to move out, and prevents bubbles from forming. To inject the medium, pierce the selected channel and slowly depress the plunger. Once the chamber is full and medium begins to flow out of the channels, remove the needles and use a roughened glass slide to press excess liquid from the chamber. This ensures a constant depth between experiments. Finally, use 5-minute epoxy to cover the needle holes.

D.2. Experiments in the sensing chamber without lux/gfp measurements

Once the microbioreactor is inoculated (and after 20 minutes have passed since the transfer into fresh medium was carried out), place the bioreactor into the chamber and secure it to the base with laboratory tape. Fill Falcon tube caps with water and place them in the chamber. Close the chamber and secure the screws. Use the next 10 minutes to check the LabVIEW routine and determine the appropriate sensitivity for each measurement. After 10 minutes, begin the first recorded reading. This is time zero for experiments. (This is the 20min/10min protocol, developed to improve reproducibility).

D.3. Experiments in the sensing chamber with lux/gfp measurements

D.3.1 Measurement of luminescence

For measurements of luminescence and fluorescence, all LEDs should be packaged such that no stray light enters the chamber via the connected optical fibers.

To properly warm the PMT, ensure that it has been on for several hours before an experiment is begun. To avoid damage, the PMT should be turned off while the microbioreactor is set up within the sensing chamber. Once the chamber is sealed, the PMT should be turned on immediately and left on for 20 minutes before a reading is taken. The orange LED should be left on during this time to prime the PMT. To keep the pre-experimental phase at 30 minutes, the protocol can be adapted to be 10min/20min. This leaves 20 min for the PMT to achieve a steady output signal.

Once an experiment has begun, luminescence can be monitored continuously using the data logger for the Fluke 45 multimeter. Dissolved oxygen and pH can be monitored every 10 minutes using the function generator and lock-in amplifier, as before. Care must be taken to select an LED voltage that will not damage the PMT. To monitor optical density, the orange LED is controlled by the function-generator, but read by the PMT (multimeter). The file obtained from the multimeter readings will thus contain luminescence readings interspersed with optical density data.

D.3.2 Measurement of fluorescence

The monitoring of pH is not possible with the Presens sensors because of the overlap between the excitation and emission spectra of GFP and the sensor. Therefore, do not place a pH sensor into the microbioreactor if fluorescence is to be measured. The measurement of dissolved oxygen proceeds as before. Optical density is also measured as described previously. Fluorescence is measured by exciting the GFP in the bacteria using the blue LED previously used to measure pH, with the emission measured by the PMT. Fluorescence can be measured continuously or at discrete time intervals. Optical density and dissolved oxygen are measured every 10 minutes.